DESIGN OF LASER-INDUCED-HEATING CONFIGURATIONS FOR GENERATION AND CONTROL OF UNDERWATER SOUND BEAMS

A THESIS

Presented to

The Faculty of the Division of Graduate Studies

By

Hsiao-an Hsieh

In Partial Fulfillment

of the Requirements for the Degree

Doctor of Philosophy

in the school of Mechanical Engineering

Georgia Institute of Technology

Atlanta, Georgia

March 1987

DESIGN OF LASER-INDUCED-HEATING CONFIGURATIONS FOR GENERATION AND CONTROL OF UNDERWATER SOUND BEAMS

Approved:

Dr. Allan D. Pierce, Chairman, M.E.

Dr. Jerry H. Ginsberg, M.E.

Dr. Peter H. Rogers, M.E.

Dr. Warren C. Strahle, A.E.

Dr. John M. Mills, GTRI

Date Approved by Chairman Jan 7, 1987

ACKNOWLEDGEMENTS

The author would like to express his deepest appreciation to his advisor Dr. Allan D. Pierce, for suggesting this thesis topic, for his valuable help and guidance, and for his constant support throughout the entire course of this work.

Appreciation is extended to all members of the reading committee: Dr. Jerry H. Ginsberg, Dr. John M. Mills, Dr. Peter H. Rogers, and Dr. Warren C. Strahle, especially to Dr. Rogers for his valuable suggestions.

Thanks are extended to the Office of Naval Research for sponsoring the project (Contract N00014-82-K-0399) within whose scope this research was carried out.

Sincere thanks are also extended to Mardi Cox, Michael Smith, and Kun-tien Shu for their valuable help in the preparation of the manuscript.

The author owes his greatest gratitude to his parents, Professor and Mrs. Yun-Fei Hsieh; his sisters, Hsiao-yun Hsieh and Hsiao-chao Hsieh; and his wife, Wei for their love, encouragement, and support.

TABLE OF CONTENTS

LIST OF FIGURES

SUMMARY

The dependence of laser-generated sound fields on the spatial configuation and the temporal sequencing of laser deposition of heat onto a water surface is examined analytically. An energy corollary of the thermoacoustic field equations yields a general strategy, dubbed the pumping principle, by which the optical to acoustic energy conversion efficiency can be increased. A general class of heating configurations is suggested whereby the generated underwater sound will propagate obliquely downwards within a narrow beam pattern. Such configurations correspond to the supersonic motion of a corrugated heating pattern over the water surface. Simple analytical models are developed to relate the properties of intermediate and long range sound fields to the parameters characterizing the moving heating configuration and the properties of the laser. Such models are validated by detailed numerical integration of the three-fold integral solution of the appropriate transient inhomogeneous wave equation. It is demonstrated that substantial quantitative insight regarding beam direction and Fresnel-region amplitudes can be determined from a two-dimensional model with the rate of heat deposition at any given point described by a time independent part and a part that oscillates sinusoidally with time; the latter also oscillates with the horizontal coordinate that points in the direction of the heating configuration's supersonic motion. An extended analytical model has a moving envelope superimposed on the sinusoidal pattern, with an additional envelope to simulate the beginning and ending of the heat deposition. The width of the resulting acoustic radiation pattern can be controlled by causing the configuration to move over the surface with a time-varying speed. In spite of the adverse influence of the pressure-release character of the air-water interface, it is demonstrated that comparable amplitude sound beams can be created that propagate in nearly horizontal directions.

CHAPTER I

INTRODUCTION

1.1 Scope of Present Thesis

The phenomenon of vibration generation in materials when exposed to optical radiation has been known since the time of A. G. Bell (1881). In the case of liquids, many mechanisms are now known to be responsible for optical generation of vibration and sound; examples are thermal expansion, electrostriction, surface evaporation, explosive boiling, and optical breakdown (Lyamshev 1981). Among these mechanisms, the thermal expansion effect is predominant if the total energy deposited per unit volume in the liquid is less than the latent heat of vaporization [2260 J/cm^3 for water (Bunkin et al. 1971)]. The theory of thermal generation of sound is based on the concept that the absorption of the radiation within the liquid causes a local heating and consequent expansion; the pressure gradient associated with this expansion subsequently propagates further into the liquid as sound.

There are two divergent types of research related to the topic of laser-generated sound. One is the field of laser spectroscopy (Tam 1983) in which the optically generated sound is used to study the properties of materials and also to measure certain intrinsic constants of materials. The other type involves the generation of sound that can be used to transmit information, particularly transferring acoustic signals to relatively large distances. The study in the present thesis is focused entirely on the second category.

In the past decade, many theoretical and experimental works have discussed the possibility of using laser systems to generate underwater acoustic signals. Most of this research has concentrated on sound generation by the thermal expansion mechanism.

In the traditional sense, the sound sources in sonar systems are restricted to

having direct contact with the medium which receives the sound. A major advantage of a sonar system using the optoacoustic source over a conventional one is that the energy source can be located above the ocean surface, so the hardware can be carried in an air vehicle. Furthermore, laser systems have an inherently greater flexibility for the achievement of design objectives, such as the control of the bandwidth and the propagation direction of the generated signals. This is because the effective antenna for the acoustic signal is the spatial and temporal configuration of the heat addition to the water, and the laser beam can be controlled to achieve a wide variety of such configurations.

Most of the previous experiments and analyses are based on two types of laser systems: one involves nonmoving intensity-modulated laser beams; the other involves moving laser beams over the water surface. In the latter, the movement of the laser beams is achieved with a rotating mirror system; the analysis typically assumes the beam to be moving rectilinearly with constant speed. Results from previous studies have indicated that the energy conversion (transduction) efficiency η in a typical optoacoustic system varies linearly with the power output P of the laser beam. Typical estimates of the power outputs required for transmission of a detectable underwater signal to distances of the order of a kilometer are in the Gigawatt range (Muir, Culbertson, and Clynch 1976). For a nonmoving beam, one has practically no control of the other parameters that affect η because those parameters pertain to the physical properties of water. Unless the detailed path of the laser beam and the time variation of the energy deposition are designed with considerable forethought, it is doubtful that a respectable signal amplitude could be generated and be much higher than those achieved when the beam is stationary and its intensity is modulated.

In this thesis, optoacoustic systems are analyzed where laser energy is systematically added into a traveling acoustic disturbance in a manner that fully exploits an idealized energy deposition strategem referred to as the "acoustic pumping principle." The concept involved in this principle is discussed in Chapter II.

In Chapter III, an idealized heating configuration that exploits the acoustic pumping principle is discussed. The discussion is then followed by the treatment of a two-dimensional steady-state model of heating deposition. The results from the derivation of this rather simplified model are used to make preliminary estimates concerning the sound generation performance of the heating configuration. These include the estimation of the transduction efficiency η and of various laser parameters to guarantee that signals be easily detectable at a given farfield point.

The next two chapters are devoted to a derivation, analysis, and numerical substantiation of an approximate solution for sound generated by a refined transient three-dimensional model for the heating configuration. Also presented are various estimates which are analogous to those given in Chapter III for the two-dimensional model. Chapter VI gives alternative interpretations of the analytical results and uses these interpretations to derive approximate solutions for less idealized situations. Also discussed is the effect of water waves on sound generation. Lastly, conclusions are drawn and recommendations are made in Chapter VII.

1.2 Review of Previous Work on Laser-Generated Sound

The optoacoustic effect was first observed by Bell (reported in an 1880 letter to Tainter, reprinted 1881) as pressure pulsations in a volume filled with an optically absorbing substance with high thermal expansion coefficient irradiated by an infrared radiation. He proposed the application of this effect to study the spectral absorption of light by gases and vapors. More studies of this type were carried out by Tyndall (1881) and Roentgen (1881). Eighty years later, the research in using the optoacoustics knowledge to generate fairly easily detectable sound in various media was stimulated by the invention of the laser. Early major investigators of laser-generated sound are Askar'yan et al. (1963). The authors of this paper used a ruby laser with a pulse length of 1 μs in their experiments. No acoustic measurements are reported, but they stated that the considered effects (a very vague allusion) can

increase many fold the amplitude of the pressure waves created in a liquid by a light beam incident on its surface. Other experimental investigations include one reported by Carome, Clark, and Moeller (1964). Generated acoustic disturbances were detected when focusing pulsed light beams from a ruby laser in various liquids.

The earliest papers on optoacoustic generation that succeeded in demonstrating a number of features of the effect were for some simple situations. Gournay (1966) gave analytical results for the one-dimensional problem of sound generation in a solid with the solid surface taken as either a pressure release or a rigid surface. These analytical results also fortuitously applied to liquids, and the comparison of Gournay's experimental work with his theoretical predictions succesfully established that the linear acoustic model can be adequate for certain circumstances of optical sound generation. Two years later, Hu (1968) analytically studied a spherical model for the acoustic wave generated by the rapid thermal expansion due to laser-induced heating with pulses of rectangular shape. Although Hu's derivation of the inhomogeneous wave equation was incorrect, the general form of the results remain valid. He found that the acoustic pulse in this case consists of two strong pulses — one positive and one negative — and that the two pulses are anti-symmetric on the time axis with respect to the central time between the two peaks of the pulses.

The governing equation for the simplified model of sound generation by laser beam heating is obtained from the linearized acoustic equations (Pierce 1981, p. 15) with a heat source term included in the energy equation. The resulting inhomogeneous wave equation for the pressure perturbation is given by

$$\nabla^2 p - \frac{1}{c^2}\frac{\partial^2 p}{\partial t^2} = -\frac{\beta}{c_p}\frac{\partial q}{\partial t} \qquad (1.2\text{-}1)$$

where c_p and β represent the specific heat and the coefficient of thermal expansion measured at constant pressure, respectively. A closely related equation, with particle displacement rather than perturbed pressure as the dependent variable and restricted

to the one-dimensional ideal gas case, was derived by Putnam and Dennis (1953). The three-dimensional version of the above equation for an ideal gas was derived by Chu (1955). The equation was also independently derived by Ingard (1958) and Strahle (1971). The latter analyzed the density fluctuation inside the combustion zone of a jet using the inhomogeneous wave equation with the source term given in the form appropriate to an ideal gas. The ideal gas version in the above papers differs from that given by Eq. (1.2-1) in that the factor $(\gamma-1)/c^2$ appears instead of the more general factor β/c_p. [For an ideal gas, β is $1/T$, and c_p is $\gamma R/(\gamma-1)$, while c^2 is γRT.]

The form of the inhomogeneous wave equation (1.2-1) applying for general fluids was presented by Westervelt and Larson (1973) and by Bunkin and Komissarov (1973). In the paper by Westervelt and Larson (1973), a model of an infinitely thin laser beam with a modulated intensity, located in the center of an infinitely extended fluid, and was analytically studied; expressions for the pressure perturbation, average intensity, and total acoustic power generated in the far field were derived. They suggested that a highly directional acoustic disturbance may be generated by applying the concept of a thermoacoustic array, that is, a series of laser beams being placed in line with each other. They also concluded that, based on the expression for the total acoustic power radiated, the energy conversion efficiency of such a laser-generated sound process is low. The paper by Bunkin and Komissarov (1973) reviewed the literature that had been published up to that time (American papers) on laser-generated sound, and discussed what was then known about the mechanisms.

The experimental work validating the modulated laser sound generation theory developed by Westevelt and Larson (1973) was later performed by Muir, Culbertson, and Clynch (1976); the measurements were carried out in a fresh water lake. Their experiments showed that a sound pulse was generated in a beam whose width and source level were in reasonable agreement with those of the theoretical

model. They also studied effects due to the finite shapes of light beams and the nearfield, and they suggested that these studies are useful when designing a thermoacoustic array. In their efficiency analysis, they pointed out the low efficiency feature of the thermoacoustic array and suggested that high-power laser technology may in the future be developed and then can be applied to the sound-generation process to improve efficiency.

During the period from 1971 to 1981, a large number of publications reporting research on laser-induced sound appeared in Soviet journals. The authors of these papers (see Pierce and Hsieh 1985a) include many well known physical acousticians, such as Bozhkov, Bunkin, Dunina, Karabutov, Kasoev, Kolomenskii, Lyamshev, Mikhalevich, and Naugol'nykh. The contents of most of these publications are limited to the scopes of the thermal effect and the nonlinear effect of the optical generation of sound in liquids. Reviews for papers involving these two effects are given by Lyamshev and Sedov (1981) and by Lyamshev and Naugol'nykh (1981). In addition to these reviews. Tam (1983) has listed more than 400 references on the subject of laser-induced sound with more emphasis on the topic of laser spectroscopy. Presented in the following is a survey of research in which the dominant mechanism analyzed for the laser-generated sound generation is that of the thermal effect.

The research of laser-induced sound in the scope of thermal mechanism can be further divided into two categories. In the first category the laser energy is deposited into the interior of a body of water via guiding-pipes or transparent glass walls. The second involves depositing optical energy into water through a pressure-release (free) surface. The study in the present thesis emphsizes only the second category of sound generation. The first work presented in the literature concerning impinging a beam on the free surface is found in the paper by Bunkin et al. (1971). In their reported experiments, a focused zap of infrared radiation from a CO_2 laser was made on the surface of water. Pressure wave resulted in the water due

to the recoil of the water surface when a flow of vapor ejected into the air.

One of the most significant methods of laser-generated sound from the practical standpoint involves laser intensity modulations. Bozhkov and Bunkin (1975) derived the efficiency of conversion of optical into acoustic energy based on the model of a modulated laser beam of Gaussian shape which impinges on a water surface and propagates into the water half-space. Acoustic patterns established in both the far field and near field are studied. Somewhat superceded by this paper is an experimental work by Bozhkov, bunkin, and Savranskii (1975). The experiments were performed with Nd-glass laser, modulated to give a periodic sequence of spikes at a repetition frequency of 70-80 kHz. The overall laser pulse had an energy of 20 J and a duration of 4×10^{-4}s. The beam radius a was 2 cm. The water contained dye, such that the absorption coefficient μ of the laser was 0.4 cm^{-1}.

Based on the stationary modulated beam model, many works attempted to theoretically study the influence of roughness of the liquid surface on the characteristics of the sound field. Examples of these papers include Bozhkov, Bunkin, and Gyrdev (1976); Kasoev and Lyamshev (1977); Lyamshev and Sedov (1977); Bozhkov and Gyrdev (1978); and Kasoev et al. (1979).

The production of acoustic signals by moving laser beams has become an active research topic, since the realization of the low-efficiency nature of stationary modulated laser systems. The primary feature of these moving acoustic sources is their feasibility of being moved at any arbitrary subsonic, sonic, or supersonic velocity with complete elimination of flow of the medium around the body of the radiator (Lyamshev 1981). Bozhkov, Bunkin, and Kolomenskii (1977) theoretically analyzed the disturbance created by a laser beam with monochromatically modulated intensity gliding along the surface of an opaque liquid. In the paper, a farfield expression for the pressure is derived and anlyzed. The directions of propagation of strongest acoustic perturbations are determined for various relationships between the characteristic dimensions of a source, the Mach number, and the wave vector. An

extension of this study was given later by Bozhkov and Kolomenskii (1978). Both subsonic and supersonic velocity cases were considered. Numerical estimates were made for a YAG laser (μ=0.18 cm^{-1}) and a CO_2 laser (μ=800 cm^{-1}). The authors remarked that their analysis would breakdown as the beam velocity approaches the speed of sound. In other papers (Bozhkov, Bunkin, and Kolomenskii 1978 and 1979; Kolomenskii 1979; Lyamshev and Sedov 1979a-b), theoretical studies were devoted to the farfield and the nearfield pressure pertubations due to laser radiations whose motion are limited to a finite path.

The first experimental work on the topic of sound generation with moving laser beams was reported by Bunkin et al. (1978). The acoustic signals were excited by a YAG:Nd laser which emitted "bell-shaped millisecond light pulses." The parameters of the laser were E $\simeq$ 0.2 J, T $\simeq$ 0.2 msec, a $\simeq$ 0.25 cm, and μ = 0.17 cm^{-1}. In the experiment, the authors observed a strong wave having amplitude of "hundreds of dynes per square centermeter" and consequently suggested that the sonically moving beam could be a better means for the improvement of the generation efficiency.

Since Gournay's theoretical presentation (1966) about pulsed laser generation of sound, a large number of theoretical and experimental papers has been published on the subject within the scope of the thermal mechanism. An experimental work on the investigation of pulsed sound fields excited by moving laser beams was performed by Bunkin, Malyarovskii, and Mikhalevich (1981). The laser used (YAG:Nd) is very similar to the one described above [see Bunkin et al. (1978)]. In this paper, the influence of the velocity and geometry of the beam was studied. The authors also confirmed a relationship between the sound fields of moving and stationary sources with their experiments. Theoretical studies (Kasoev and Lyamshev 1977, Lyamshev and Naugol'nykh 1976, Lyamshev and Sedov 1977, Dunina et al. 1979a-b, Egerev et al. 1979) have shown the adequacy of using a linear acoustic model to govern the real process of sound generation by laser pulses, and results from these studies are in

reasonably good agreement with the experiments (Dunina et al. 1979b, Egerev et al. 1979, Gorodetskii et al. 1978). The laser pulses reported in these experiments (Dunina et al. 1979b and Egerev et al. 1979) are reproduced in Fig. 1.1. In addition, Burmistrova (1978) introduced the method of transfer functions for extending the solution obtained for the pulsed laser case to more complex problems.

Recently, Berthelot and Busch-Vishniac (1985) have studied sound generation by intensity modulated moving laser beams. This work is, to some extent, a continuation of the earlier work by Muir, Culbertson, and Clynch (1976). In the paper by Berthelot and Busch-Vishniac (1985), it was shown that their theoretical predictions of pressure waveforms and directivity patterns using the method of convolution compare well to the experimental results in the near field and agree in the farfield limit with existing analyses in early papers (Lyamshev and Sedov 1981). The detailed experimental efforts were documented in Berthelot's Ph.D thesis (1985). The laboratory setup consists of a laser system whose intensity may be modulated, a rotating mirror, a beam synchronizer, and signal detecting and processing hardware including a hydrophone. The laser light directed at the mirror is reflected towards the water surface so that the laser beam sweeps over the water surface when the mirror rotates. The two lasers used in the experiments are ruby (0.694 μm) and Nd:Glass (1.06 μm) lasers. The former has a pulse energy (unmodulated) E of 25 J, pulse duration T of 1 msec, and $\mu = 1.5\ m^{-1}$, and the latter has E = 30 J, T = 1 msec, and $\mu = 13.7\ m^{-1}$. It is also reported that roughly 80 percents of the unmodulated optical energy is dissipated in the process of modulation and the actual pulse energy that enters the water is approximately 5 Joules. A typical laser pulse recorded in their experiment is reproduced in Fig. 1.1. The values for μ, measured independently by Muir, Culbertson, and Clynch (1976), show minor discrepancies from those collected by Mutschlecner, Burge, and Regelson (1963) and suggested by Zolotarev et al. (1969). However, the values measured by Muir, Culbertson, and Clynch (1976) should be more reliable in the sense that more improved techniques

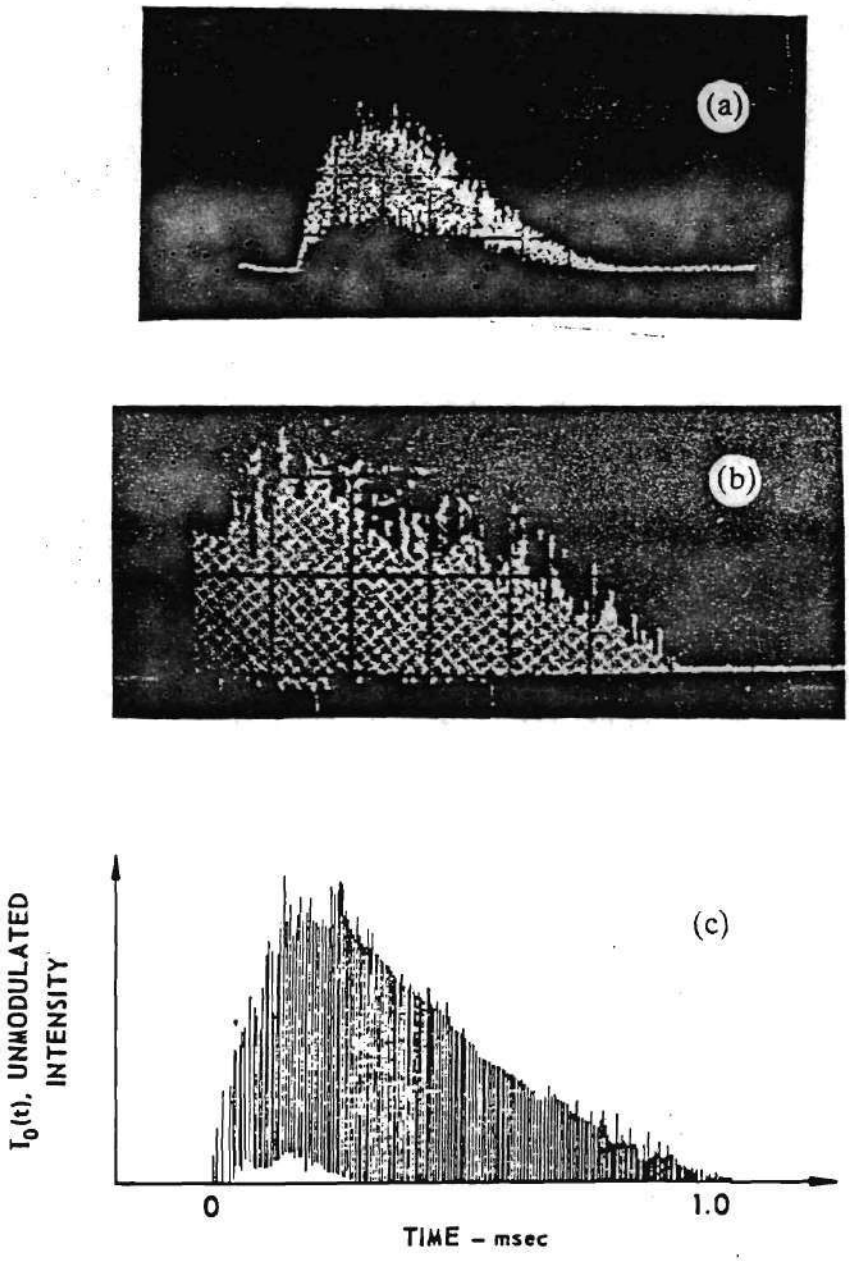

FIGURE 1.1 Examples of laser pulses reported in the previous literatures. (a)Dunina et al. 1979, (b)Egerev et al. 1979, and (c)Muir, Culbertson, and Clynch 1976 and Berthelot 1985.

and equipments were being used. Other experiments (Berthelot and Busch-Vishniac 1987a-b) are being conducted to investigate: (i) the Doppler factor contribution to pulse length and fundamental frequency, (ii) the increase in efficiency at speeds close to Mach 1, and (iii) the increase in the nearfield limit. Other recent work includes an analytical formulation (Pierce 1982a) of the sound wave generated when the laser beam is moving at constant supersonic speed in a straight line over the water surface (Pierce 1982a). The effort of the derivation was concentrated on the dominant acoustic signal that arrived with the Mach wave disturbance. It was found that relatively simple results requiring little computation could be developed for the two limiting cases when the laser beam penetration depth was either much larger or much less than the beam diameter (Pierce 1983a, Pierce and Hsieh 1984). Studies were also devoted to questions conerning the mechanisms by which laser beams generated sound and of the general correctness of the inhomogeneous wave equation that had been introduced into the thermoacoustics literature by Chu (1955) and into the optoacoustics literature by Westervelt and Larson (1973) and by Bunkin and Komissarov (1973). Experimental results (Hunter, Jones, and Malbrough 1981, Hunter et al. 1981) were brought to attention that suggested this equation was not wholly correct, especially for pure water at 4°C. This has led to the development of a theory (Pierce 1982b, 1983b, and Pierce and Hsieh 1987) that would resolve the reported discrepancy. Also, a fresh derivation of the inhomogeneous equation (Pierce 1983c and 1985) was carried out to study the importance of the role thermal conductivity plays in the optical to acoustic energy conversion process. The result clarified that the thermal conduction was indeed important in the immediate vicinity of the laser heated region, but that the acoustic pressure received at moderate to large distances was for most circumstances of interest substantially independent of the thermal conduction.

Preliminary accounts of the present research were given in abstracts published in the Journal of the Acoustical Society of America (Hsieh and Pierce 1984a-b, 1985,

and 1986; Pierce and Hsieh 1985b) and in a paper (Pierce and Hsieh 1986) presented at the ICA Associated Underwater Acoustics Conference in Halifax during the summer of 1986.

CHAPTER II

ACOUSTIC PUMPING PRINCIPLE AND TRANSDUCTION EFFICIENCY

2.1 Equations of Linear Acoustics

One of the equations governing small amplitude acoustic disturbances in a fluid can be derived from the equation of state which regards the density $\rho = \rho(p,s)$ as being a function of two state variables. The density perturbation $\rho' = (\rho - \rho_o)$ (with the subscript 'o' denoting the ambient state) is then given by the first order expansion of the right side of the equation. Using the definitions $c_p = T(\partial s/\partial T)_p$, $c^2 = (\partial p/\partial \rho)_s$, and $\beta = \rho[\partial(1/\rho)/\partial T]_p$ (representing the specific heat at constant pressure, the speed of sound squared, and the coefficient of thermal expansion, respectively), the coefficients $(\partial \rho/\partial p)_s$ and $(\partial \rho/\partial s)_p$ in the first order terms can be conveniently replaced so that an explicit expression linearly relating the perturbed state variables ρ', p' and s' is

$$\rho' = c^{-2} p' - (\rho \beta T/c_p)_o s' \tag{2.1-1}$$

The remaining linear equations come from the mass continuity equation, Euler's equation, and the energy equation including the energy generation within the body of water through which the laser beam penetrates. The corresponding three linear equations are

$$\frac{\partial \rho'}{\partial t} + \rho_o \nabla \cdot \mathbf{v}' = 0 \tag{2.1-2a}$$

$$\rho_o \frac{\partial \mathbf{v}'}{\partial t} = - \nabla p' \tag{2.1-2b}$$

$$\rho_o T_o \frac{\partial s'}{\partial t} = q \tag{2.1-2c}$$

In the last equation the parameter q is the time rate at which thermal energy per unit volume is added to the water by the laser. Here, the effect of heat conduction and viscosity are neglected in the considerations, which is valid if the constraints (Pierce 1985)

$$\mu/\rho_o c\lambda << 1 \tag{2.1-3a}$$

$$\kappa/\rho_o c_p c\lambda << 1 \tag{2.1-3b}$$

are met, where the symbols μ, κ, and λ, represent the viscosity (either the bulk or the shear viscosity), thermal conductivity, and the representative acoustic wavelength, respectively. [For typical values of μ ($\simeq 1\text{x}10^{-3}$ kg/m·s) and κ ($\simeq 0.6$ W/m°K) for water (Pierce 1981, p. 514) and in most cases of interest, these restrictions are extremely weak.]

For convenience in the following discussion, the primes are omitted in the symbols representing the perturbed state variables.

To further simplify the model, we reduce the number of dependent variables (p, **v**, ρ, and s). The variables p and **v** are retained because of their importance in acoustics, while ρ and s are eliminated from Eqs. (2.1-1), (2.1-2a), and (2.1-2c). What comes out of this manipulation is a modified mass conservation-generation equation

$$\frac{1}{c^2}\frac{\partial p}{\partial t} + \rho_o \nabla \cdot \mathbf{v} = \frac{\beta}{c_p} q \tag{2.1-4}$$

in which the term $(\beta/c_p)q$ is identified as an apparent mass source. For a given ambient state, the coefficients $1/c^2$, (β/c_p), ρ_o, etc., in Eqs. (2.1-1) through (2.1-4) can be regarded as numerical constants.

2.2 The Energy Conservation-Generation Corollary

In defining the acoustic energy generation of a particular source, one often finds it convenient to obtain an acoustic energy corollary (Pierce 1981, p. 36)

(appropriate to the solutions of the linear acoustic equations only) which resembles a statement of energy conservation of an acoustic field. To derive it, one takes the dot product of $\mathbf{v}$ with Eq. (2.1-2b), i.e.,

$$\mathbf{v}\cdot(\rho_o\frac{\partial \mathbf{v}}{\partial t}) = -\mathbf{v}\cdot\nabla p$$

$$= -\nabla\cdot(p\mathbf{v}) + p\nabla\cdot\mathbf{v}$$

$$= -\nabla\cdot(p\mathbf{v}) + (\beta/\rho_o c_p)\, pq - \rho_o^{-1}c^{-2}\, p(\partial p/\partial t) \qquad (2.2\text{-}1)$$

Here the indicated mathematical steps follow from a vector identity and from the above-mentioned modified mass conservation-generation equation (2.1-4). The term on the left can alternately be written as $(\partial/\partial t)(\frac{1}{2}\rho_o v^2)$. Using a similar identity

$$\rho_o^{-1}c^{-2}\, p(\partial p/\partial t) = (\partial/\partial t)(\tfrac{1}{2}p^2/\rho_o c^2)$$

Eq. (2.2-1) can be re-expressed as

$$\frac{\partial w}{\partial t} + \nabla\cdot\mathbf{I} = \frac{\beta}{\rho_o c_p}\, pq \qquad (2.2\text{-}2)$$

where

$$w = \tfrac{1}{2}\rho_o v^2 + \tfrac{1}{2}p^2/\rho_o c^2 \qquad (2.2\text{-}3a)$$

$$\mathbf{I} = p\mathbf{v} \qquad (2.2\text{-}3b)$$

The two terms $\frac{1}{2}\rho_o v^2$ and $\frac{1}{2}p^2/\rho_o c^2$ contained in Eq. (2.2-3a) can be interpreted as the acoustic kinetic- and potential-energy density, and w, the sum of the two, can be thought of as being the total acoustic energy density. The vector $\mathbf{I}$ is referred to as the acoustic power flux. Therefore, the term $(\beta/\rho_o c_p)pq$ on the right side of Eq. (2.2-2) can be considered as the rate of acoustic energy generated per unit volume by the laser beam.

2.3 Optical-Acoustical Energy Transduction Efficiency

The energy interpretation of Eq. (2.2-2) is apparent when both sides are integrated over a pertinent control volume V and over a relevant time frame, so that an application of Gauss's theorem yields

$$\iiint_V w\, dV + \int_{t_o}^{t} \iint_S \mathbf{I}\cdot\mathbf{n}\, dS\, dt = \frac{\beta}{\rho_o c_p} \int_{t_o}^{t} \iiint_V p\, q\, dV\, dt \qquad (2.3\text{-}1)$$

Here, the control volume V is taken to be the space (in the water) over which the heat is deposited and S is defined as the surface enclosing V. The symbol **n** defines the unit outward normal vector of the surface S, and t_o is the time at which the heating process starts.

By inspecting Eq. (2.3-1) from a energy standpoint, we can see that the first term represents the net increase in total acoustic energy within the control volume V over a time $t - t_o$. In the identical duration of time, the second term represents the aggregate amount of net energy (acoustic energy) that has radiated out of the control volume through the surface S. If one considers the integral being carried out over a sufficiently long period of time, the first term will become zero because w within the control volume must go back to zero eventually. The second term is accordingly the total acoustic energy that has propagated out of the control volume. Therefore, we conclude that the term on the right side is the net amount of deposited thermal energy converted to sound.

Since the magnitude of the parameter q indicates the rate of the laser's optical energy (the part that is transmitted through the water surface) per unit volume deposited to the water, the total deposited laser energy up to time t is given by the integral of q over the volume within which q is nonzero and over time from t_o to t. This consideration, in conjunction with the preceeding discussion on the acoustic energy generation [Eq. (2.3-1)], leads to a definition for the optical-acoustic energy transduction efficiency $\eta(t)$ which takes the form

$$\eta(t) = \frac{\beta}{\rho_o c_p} \frac{\int_{t_o}^{t} \iiint_V p\, q\, dV\, dt}{\int_{t_o}^{t} \iiint_V q\, dV\, dt} \qquad (2.3\text{-}2)$$

Equation (2.3-2) guides strategies of judiciously placing heat energy at selective locations in the water for increasing η. This idea is the topic of the following section.

2.4 The Acoustic Pumping Principle

We have seen above [Eqs. (2.2-2) through (2.3-2)] that the transduction efficiency, as well as the amount of energy converted from heat to sound, depends on a product of the deposited heat q and the local acoustic pressure p at the same instant. To study this in detail, we look at the integral containing $(\beta/\rho_o c_p)pq$ in Eq. (2.3-1) and write $q = q_o + q'$ where q' is the fluctuating part of q. If the sign of pq' is allowed to alternate, the magnitude of the integral over the integration domain will be smaller compared to the case of pq' retaining one sign over the domain. In particular, we would like to keep the term $(\beta/\rho_o c_p)pq'$ positive in dealing with the problem of improving η.

The fact that the quantity $(\beta/\rho_o c_p)pq'$ should be kept positive can be best illustrated by an analogy in which the amplitude of a conservative pendulum system (the amplitude is associated with the total energy contained in the system) is to be gradually pumped up by successive application of an external force **F**. Let us assume the direction of **F** is constant and is always tangential in a clockwise manner when viewed from one side of the pendulum (this assumption is analogous to the fact that q is always non-negative). The product of **F** and the instantaneous tangential velocity **V** is negative when the directions of the two vectors are against each other. We learn that a negative sense of the product implies that energy (or power) is drawn from the system, which is against our intention of increasing the total energy. If an input of energy to the system is going to increase the amplitude, **F** must be applied to the

pendulum at instances when the direction of **V** coincides with that of **F**; under such circumstance the sign of the product $\mathbf{F} \cdot \mathbf{V}$ is positive.

Regarding Eq. (2.2-2), it is now easy to see that a negative value of $(\beta / \rho_o c_p)pq$ in fact represents an instantaneous acoustic energy "dissipation" rather than the desired energy generation. This "dissipation" effect is elsewhere known as the anti-sound, or the sound-kill-sound effect. Therefore, without insight regarding the above energy consideration, the result of randomly adding heat to the water could possibly be destructive: a previously existing signal could be made to disappear! For all practical temperatures in the ocean (above 0°C), the sign of the factor $\beta / \rho_o c_p$ is positive. [The β for seawater is never negative for temperatures above 0°C (Pierce 1981, p. 34).] Since the parameter q (directly related to laser power) is non-negative, the heat should ideally be added to places where the currently existing acoustic pressure is positive. The greatest rate of acoustic energy increase is obtained when this positive acoustic pressure is a local maximum. For ease of referral, this concept is dubbed the acoustic pumping principle.

A strategy is therefore developed based on the pumping principle determining where and when to place the heat to achieve the maximum possible η. One should first create an acoustic disturbance and then systematically pump up its amplitude by always adding heat to the travelling wave crest (the location where the pressure perturbation has a local maximum). Accomplishing this requires the knowledge of exactly where the initially generated wave crest will be located at all subsequent instances during the heating process. An example of this strategy is illustrated in Fig. 2.1. Represented here is a two-dimensional model in which the heat deposition resembles a thin slab of concentrated electromagnetic energy with an infinite dimension in the y direction (into the paper). This light-slab is formed from the splitting of a broadened laser beam impinging on the water surface. The slab makes an angle θ_S with the vertical in the x-z plane. Vertical is indicated by the z axis; the z axis points downward. The heating pattern (namely the light-slab) is made to move

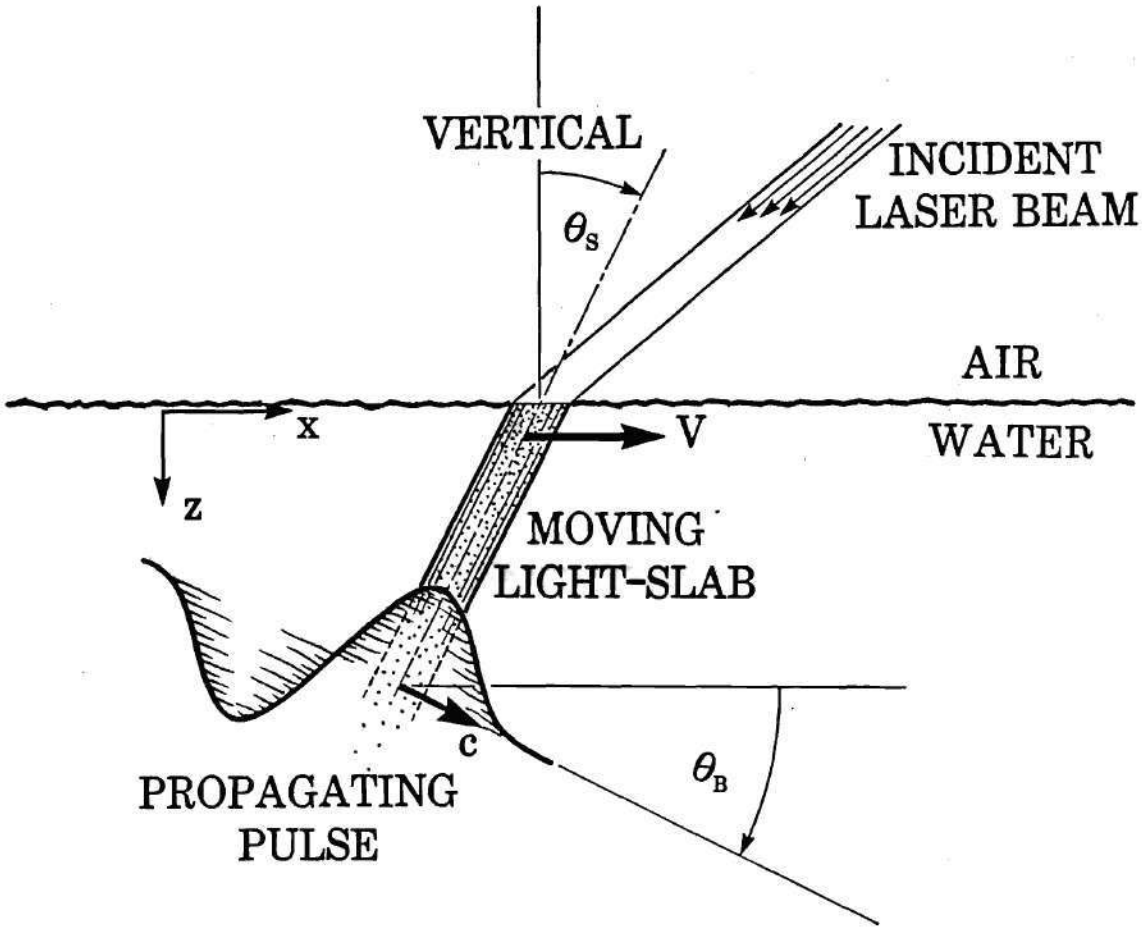

FIGURE 2.1 Concepts associated with obliquely propagating sound pulse generated by of moving a broadened laser beam on the surface at velocity $V=c/\cos\theta_B$. The condition $\theta_S=\theta_B$ maximizes the acoustic energy pumping effect when penetration depth of the light beam is sufficiently large compared with an acoustic wavelength.

towards the x direction at a speed $V = c/\cos\theta_B$. Consequently, a planar pulse is created and propagates with the speed of sound c obliquely downward into the water at an angle θ_B with the horizontal. To comply with the statement of the pumping principle, the slant angle θ_S is ideally equal to θ_B, so that heat energy contained in the light-slab in the subsequent action may accurately track the wave crest of the created pulse. [In Sec. 3.2.3, we explore to what extent it is important for θ_S to be equal to θ_B.]

2.5 Upper Bound for η — the Thermal Mechanism

An upper bound for $\eta(t)$ can be obtained from Eq. (2.3-2). First, we define p_{max} as the maximum attained accoustic pressure in the field resulting from the source pumping process, such that

$$p_{max} = \max [p_{pumping}(x,y,z,t)] \tag{2.5-1}$$

where $p_{pumping}(x,y,z,t)$ is the perturbed pressure distribution in the field at any time t as a consequence of placing heat judiciously according to the pumping principle. Then, we can argue, that because the inequality

$$\int_{t_o}^{t_f} \iiint_V p\, q\, dV\, dt \le p_{max} \int_{t_o}^{t_f} \iiint_V q\, dV\, dt \tag{2.5-2}$$

is true for all q(x,y,z,t), the upper limit for η is given by

$$\eta_{max} = \frac{\beta}{\rho_o c_p}\, p_{max} \tag{2.5-3}$$

This result might possibly be used in a systematic study for answering the question posed by Muir, Culbertson, and Clynch (1976) as to what is the upper bound for the transduction efficiency in dealing with the thermal mechanism of sound generation.

2.6 Transduction Efficiency for Sound Generation with Stationary Modulated Laser Beams

No simple derivations of the transduction efficiency η are found in the literature for sound generation with a stationary modulated laser beam (SMLB) when the beam penetration length is larger than the beam diameter, with the beam diameter not necessarily large, and when the beam penetrates the water through a free surface. The intention here is to obtain such an expression for η so that it can serve as a reference when assessing the efficiency which may be achieved when one uses other heating configurations. For the applications mentioned in the first chapter, incorporation of the presence of a free surface in the derivation is appropriate. This derivation is presented as follows.

The geometry of the problem to be solved is shown in Fig. 2.2. The laser beam enters the water vertically downwards as indicated by the positive z direction. The pressure perturbation at the point $\mathbf{x}=(x,y,z)$ satisfying the inhomogeneous wave equation (1.2-1) with the source term taken to be consistent with the present SMLB case can be studied in the context of the Green's function method (Pierce 1981, pp. 164-165). With conscious incorporation of the pressure release boundary condition through the method of images, this perturbation is expressed as the triple integral

$$p = \frac{\beta}{4\pi c_p} (\partial/\partial t) \iiint \frac{q(\mathbf{x}_o,\, t-R/c)}{R} \operatorname{sign}(z_o)\, dV_o \qquad (2.6\text{-}1)$$

where $R = |\mathbf{x}-\mathbf{x}_o|$, and where the volume V_o over which the triple integration is to be performed is defined as the unbounded free space.

The intensity of the beam is modulated in time with a constant angular frequency ω, such that the instantaneous laser power entering the water is given by $P_{laser}(1+\cos\omega t)$. Here, P_{laser} is the average energy per unit time added to the water by the laser. The intensity distribution of the beam is assumed to be Gaussian, to be circularly symmetric with characteristic radius a, and to be exponential with an attenuation coefficient μ in the z direction. The heating function q consistent with the

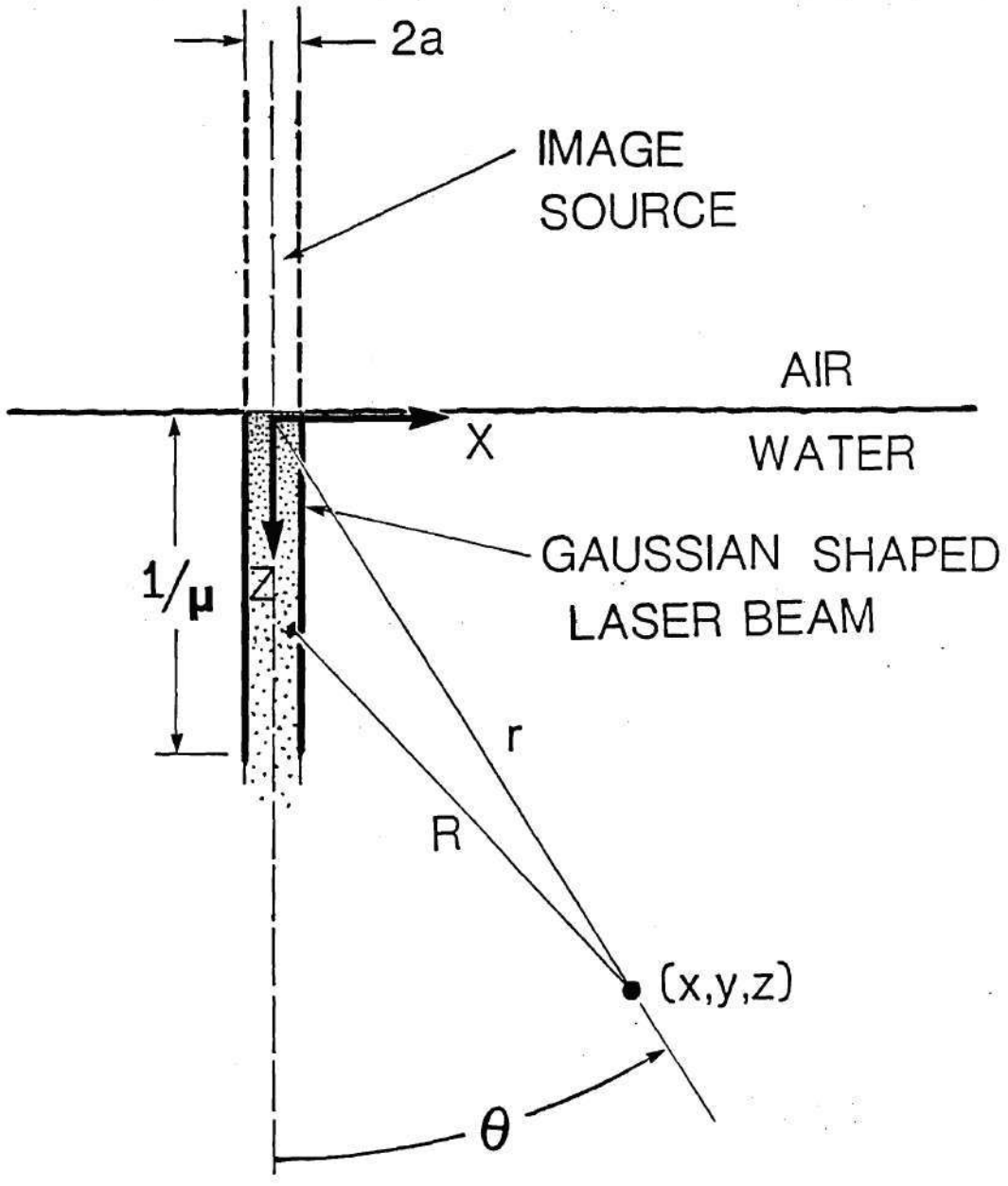

FIGURE 2.2 Geometry for the stationary modulated laser beam configuration.

above description can be written as

$$q(x,t) = \frac{\mu P_{laser}}{\pi a^2} (1+\cos\omega t)\, e^{-\mu|z|}\, e^{-(x^2+y^2)/a^2} \qquad (2.6\text{-}2)$$

Since the source function q oscillates sinusoidally with time, and since only the oscillatory portion of this function is responsible for the steady-state generation of sound, we can accordingly limit our derivation to the constant frequency case. Using the expressions $p = \mathrm{Re}\{ pe^{-i\omega t} \}$ and $q = q_o + \mathrm{Re}\{ qe^{-i\omega t} \}$ (where q_o is the non-oscillating portion of q, and where p and q stand for the complex amplitudes of p and q, respectively), and using the prescription $\partial/\partial t \rightarrow -i\omega$, we find that Eq. (2.6-1) becomes

$$p = -\frac{i\omega\beta}{4\pi c_p} \iiint q \frac{e^{ikR}}{R} \mathrm{sign}(z_o)\, dV_o \qquad (2.6\text{-}3)$$

To simplify the integration, we consider the situation in which the beam characteristic radius a is much smaller compared with the penetration depth $1/\mu$ and with the acoustic wavelength λ of the resulting disturbance (i.e., $\mu a << 1$ and $ka << 1$). This consideration enables us to regard every component in the integrand, except the gaussian factor, as being slowly varying functions in both the integration variables x and y. Then we may approximate the integrations over x and y consistent with this thin beam limiting case as

$$p = -\frac{i\omega\beta\mu P_{laser}}{4\pi c_p} \int_{-\infty}^{\infty} \mathrm{sign}(z_o) \frac{e^{ikR}}{R}\, dz_o \qquad (2.6\text{-}4)$$

To calculate the radiated acoustic power from the source, we need to estimate the complex pressure amplitude distributed on the surface of an imaginary hemisphere having radius $r = |x|$ that satisfies the farfield limiting conditions, $kr >> 1$ and $\mu r >> 1$. In this farfield case, the factor R [here $R^2 = x^2+y^2+(z-z_o)^2$] is replaced by r in the denominator and by $r - z_o\cos\theta$ in the exponential factor of the integrand. Here the angle $\theta = \cos^{-1}(z/r)$ is the polar coordinate in a spherical

system measured with respect to the z axis. [In subsequent sections of the thesis, angles are measured from the horizontal.] The above yields a farfield expression for p as

$$p = -\frac{\omega\beta\mu P_{laser}}{4\pi c_p} \frac{2k\cos\theta}{\mu^2 + k^2\cos^2\theta} \frac{e^{ikr}}{r} \tag{2.6-5}$$

The time-averaged radial component intensity $I_{r,av}$ at the above-considered hemispherical surface is asymptotically equal to $|p|^2/2\rho c$. Consequently, the time-averaged acoustic power P_{ac} radiated from the source is given by

$$P_{ac} = 2\pi \int_0^{\pi/2} \frac{|p|^2}{2\rho c} r^2 \sin\theta \, d\theta$$

$$= \frac{1}{4\pi} \frac{c}{\rho} \left(\frac{\beta}{c_p}\right)^2 P_{laser}^2 \, k^2 F(\mu/k) \tag{2.6-6}$$

where

$$F(\sigma) = \sigma \int_0^{\tan^{-1}(1/\sigma)} \sin^2\xi \, d\xi$$

$$= (\sigma/2)\left[\tan^{-1}(1/\sigma) - \frac{\sigma}{1+\sigma^2}\right] \tag{2.6-7}$$

Dividing P_{ac} by P_{laser}, we obtain the expression for the transduction efficiency as

$$\eta_{SMLB} = \frac{1}{4\pi} \frac{c}{\rho} \left(\frac{\beta}{c_p}\right)^2 P_{laser} \, k^2 F(\mu/k) \tag{2.6-8}$$

Next, we would like to search for the maximum value of η_{SMLB} in Eq. (2.6-8). The first derivative of $F(\sigma)$ with respect to σ is taken and subsequently set equal to zero, i.e.

$$F'(\sigma) = \tfrac{1}{2}\tan^{-1}(1/\sigma) - \frac{\sigma}{1+\sigma^2} - \frac{\sigma(1-\sigma^2)}{2(1+\sigma^2)^2} = 0 \tag{2.6-9}$$

Since the parameter σ has to be a positive quantity, we look for roots of Eq. (2.6-9)

only in the range $\sigma > 0$. The equation is solved with an elementary numerical scheme and the solution is found to be $\sigma = 0.548$ (accurate up to three significant figures). Furthermore, the second derivative $F''(\sigma)$ is less than zero when evaluated at $\sigma = 0.548$. Therefore, we conclude that the maximum value of F is equal to F(0.548) = 0.178.

The above result implies, for a given value of k, that the efficiency η_{SMLB} attains a maximum when the value of μ is 0.548 times k. Furthermore, because the function $G(k) = k^2 F(\mu/k)$ increases monotonically with increasing k for fixed μ/k, one may assert that the maximum η_{SMLB} increases monotonically with increasing k, and therefore increases with increasing modulation frequency ω. By setting $F(\sigma) = 0.178$ in Eq. (2.6-8), we obtain an expression for the maximum achievable efficiency at a given value of k for the thin beam limiting case as

$$\eta_{SMLB.max} = 0.0142 \frac{c}{\rho} \left(\frac{\beta}{c_p}\right)^2 k^2 \; P_{laser} \tag{2.6-10}$$

This result is used in Sec. 5.5 for comparison with the transduction efficiency obtained when the laser-induced heating configuration moves over the surface.

In the paper by Bozhkov and Bunkin (1975), a general transient SMLB problem, with the inclusion of the effect of viscosity and thermal conduction, was analyzed. A lengthy expression of the pressure perturbation was obtained using the Laplace transformation technique. A similar expression for η,

$$\eta_{SMLB} = \frac{1}{4\pi} \frac{c}{\rho} \left(\frac{\beta}{c_p}\right)^2 \; P_{laser} \; \frac{\mu k}{a^2(\mu^2 + k^2)} \tag{2.6-11}$$

is obtained for the wide laser beam case ($ka >> 1$) with μ/k arbitrary. The maximum efficiency under such circumstances is achieved when $\mu = k$ in Eq. (2.6-11), i.e.

$$\eta_{SMLB} = \frac{1}{4\pi} \frac{c}{\rho} \left(\frac{\beta}{c_p}\right)^2 \; \frac{P_{laser}}{a^2} \tag{2.6-12}$$

Since ka is assumed large, $1/a^2$ is considered to be much less than k^2 in this

derivation. Consequently, the efficiency predicted by Eq. (2.6-12) is much less than that of (2.6-10). One concludes that thin laser beams are more efficient sound radiators than wide beams.

CHAPTER III

SIMPLIFIED ANALYTICAL MODELS TO EXPLORE CONSEQUENCES OF THE PUMPING PRINCIPLE

In the preceding chapter, the concept that judicious placement of heat within the water can increase the optical-acoustic energy transduction efficiency η was introduced. When efficiency of energy transduction is important, and for laser-induced-sound devices which use the thermal effect as the primary mechanism, the design should, if possible, include a conscientious application of the pumping principle. In the present chapter, a heating configuration is described which would be representative of one which exploits the acoustic pumping principle.

3.1 General Features of Analytical Models for Laser-Generated Sound

3.1.1 Introduction

The details of designing an optical system (possibly including diffraction gratings and rotating mirrors) capable of generating the heating configuration studied in the present chapter is not discussed in this thesis. Although it is anticipated that the actual development of such a system would be a challenging problem in state-of-the-art optical design, it is here assumed that it is feasible to build a laser system which will add heat to the surface of a liquid in any desired pattern and that this pattern can be moved over the surface with an arbitrary velocity versus time profile.

3.1.2 Parameters Describing the Laser-Induced Heating Configuration

There are several points that one should consider concerning the configuration of the heat deposition in the design of a future opto-acoustic system. First, the heating pattern on the surface should be able to continuously track

whatever wave crest(s) is/are generated at the initial stage of laser illumination, so that higher amplitude sound waves result at the end of the pumping process. Second, to create signals that are useful for transmitting information, one should be able to control the shape of the pulsed signal. This would be achieved, for example, if one could generate either AM or FM signals with desired amplitude or frequency patterns. It is not necessary to modulate the intensity of the laser beam as was done in various previous studies (e.g. Bozhkov, Bunkin, and Kolomenskii 1977; Bozhkov and Kolomenskii 1978; Berthelot and Busch-Vishniac 1985), because the energy of the laser beam can be fully used and yet achieve a time varying and spatially varying energy deposition at each point simply by varying the placement and the spreading of the laser beam on the surface with time. The generation of oscillations within the acoustic signal could be achieved with a spatial heating configuration where the laser intensity distribution on the surface has a portion which oscillates. Last, the direction of the generated sound beam should be steerable and the beamwidth should also be controllable.

A tentative design of such a sound generation system that could yield a heating configuration with the desired properties is sketched in Fig. 3.1. An intricate optical (laser) system located inside the airborne vehicle, not necessarily a helicopter, launches a broadened and split bundle of laser beams onto the surface of the water. Within the water near the surface, this beam forms a series of parallel light-slabs with constant spacing between every two successive slabs. The widths of these slabs (not shown in the figure) are of the same magnitude and depend on the extent that the beam is broadened. The slabs penetrate through the water at an exponentially decaying rate such that at a distance $1/\mu$ the intensity has decreased by a factor of $1/e$. This distance is called the penetration depth of the light-slabs. Also, depending on the incident angle of the laser beam, the light-slabs, after refraction at the air-water interface, make a slant angle θ_S with the vertical (the variation in slant angle among all the slabs becomes negligible when the distance between the optical

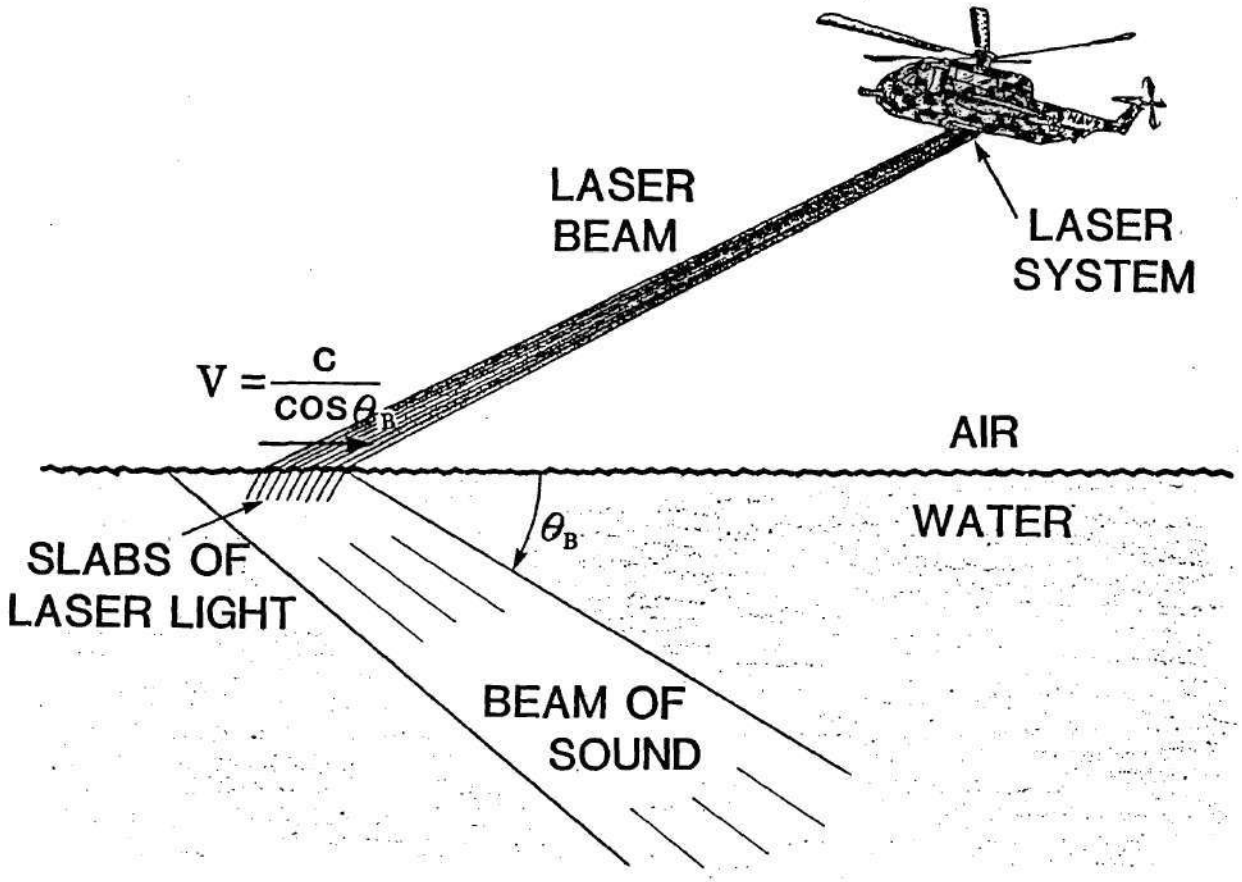

FIGURE 3.1 Concepts associated with the creation of an underwater acoustic beam using an airborne laser.

system and the spot of laser impingement is large compared with the surface track length). If one desires a beam of sound that makes an angle of θ_B with the horizontal, then the speed V with which the light-slabs are moved should be equal to $c/\cos\theta_B$. In Chapter VI, we consider V as not being constant, such that θ_B will vary in the far field from point to point. Doing such enables one to accurately control the angular width of the resulting sound beam. However, for the present simplified discussion, we consider that θ_B is constant and V is independent of time. The angle θ_S ideally should be chosen to be equal to θ_B, although for typical choices of laser parameters and properties of water the farfield sound is not extremely sensitive to these two angles being the same. We carry through the analysis in this chapter with θ_S not equal to θ_B.

If one lets the total number of slabs be n, the configuration in the water simulates a heating pattern of n cycles of ripple moving rectilinearly along the water surface at speed V. These n cycles of heating pattern thermally excite an acoustic wave propagating obliquely downward into the water. The angle θ_B measured from the horizontal, at which the wave propagates, can be readily controlled by adjusting the speed V of the heating configuration on the surface. Furthermore, if all light-slabs are equally spaced, the dominant acoustic wavelength of the generated signal λ_B is equal to the horizontal distance between every two adjacent light-slabs times the angular factor $\cos\theta_B$, and the dominant frequency f_B is then given by c/λ_B. The bandwidth of this signal is of the order of $2f_B/c$. If the characteristic dimensions of the heating configuration, including its travelling distance, are large compared to λ_B, what one has shortly after the termination of the pumping process is a collimated beam. The generated acoustic energy is confined within this rectangular beam up to some distance, and then spreads away as the beam gradually turns into a directional spherical wave.

3.1.3 Discussion of Idealizations and Physical Constraints

In previous works which discussed laser-induced sound, the amplitude of the generated acoustic signal was predicted to be directly proportional to the laser power P. For the classes of laser-induced heating configurations studied here, we would like to learn how the various parameters associated with the laser and the geometry affect the resulting acoustic signal. The parameter μ can affect the transduction efficiency η as well as the resulting signal amplitude because, for a deeper penetration of the light-slabs, a longer radiation period of heat is provided to the previously created oblique propagating waves. For a similar reason, the angular factor θ_B affects the above results simply because any created waves propagating with a larger oblique angle θ_B receive less benefit from the pumping mechanism as the waves leave the surface region at a faster rate.

If one wishes to decrease the frequency bandwidth of the acoustic signal, a natural way is to increase the number of light-slabs. On the other hand, the resulting pressure amplitude of the acoustic disturbance is affected by the choice of the total area covered by the heating configuration on the surface. Since the laser power is finite, the energy added per unit time per unit surface area diminishes as the total depositional area increases. The amount of power deposited into each light-slab decreases as the number of the light-slabs increases. Furthermore, if the laser emits light in finite pulses, the energy depositing process has to cease after a certain period of time because the total pulse energy is limited. The possibility of generating detectable farfield acoustic signals will inevitably be improved if future technology produces lasers with (i) higher laser power output, (ii) longer laser pulse duration, and (iii) higher laser pulse energy.

In this present chapter, we limit ourselves to the ideal ocean. The effect of the water wave on the surface should be of minor influence if the light penetration depth is much longer than the rms water wave height and if the fluctuating water slope angles (in radians) are substantially less than μ/k_B. This is further discussed in Sec.

6.7.

Since the laser light-slabs undergo refraction when passing through the interface dividing the air and water, a theoretical upper limit exists for the slant angle θ_S. The upper limit θ_{Smax}, equal to the critical incident angle θ_c of light at the water surface, is

$$\theta_c = \sin^{-1}(n_a/n_w) \simeq 50° \tag{3.1-1}$$

where $n_a = 1.0$ and $n_w = 1.33$ are the absolute refractive indexes of air and water, respectively (AIP Handbook 1972, p. 6-105). The presence of this limit may make it infeasible to improve the transduction efficiency when the desired beaming angle θ_B is greater than 50°. One expects interest to be primarily in much smaller values of θ_B. For example, if one desires to couple sound into any underwater sound channel, the largest departure angle (we may call it θ_{Bmax}) for sources located at the surface is small. This largest departure angle can be estimated with the Snell's law. For instance, using the formula (Tappert 1977)

$$\theta_{Bmax} = \cos^{-1}(c_{min}/c_{max}) \simeq (2\Delta c/c_o)^{1/2} \tag{3.1-2}$$

where c_{min} is the sound speed near the surface of the water, c_{max} is the maximum sound speed at the extent of the depths of interest, $\Delta c = c_{max} - c_{min}$, and c_o is the average sound speed. Representative values are $c_o = 1500$ m/s and $\Delta c = 40$ m/s, which would give $\theta_{Bmax} = 13°$.

3.1.4 List of Principal Assumptions used in Analytical Models

In examining the consequences of generating sound with a moving heating configuration such as sketched in Fig. 3.1, one can make a number of assumptions to simplify the initial analysis. These assumptions are as follows:

(i) The air-water interface is perfectly flat.

(ii) The slabs are of finite thicknesses and are distributed near the water surface in a manner such that they closely simulate a sinusoidal distribution.

(iii) The electromagnetic energy intensity dies out exponentially with propagation distance in the water.

(iv) The water surface is considered with regard to underwater sound propagation as a pressure release surface.

(v) All properties of the water are constants, independent of spatial coordinates and time.

(vi) The range of the temperatures considered is such that the corresponding values for the thermal expansion coefficient β are reasonably remote from being zero.

(vii) Because the speed of sound is constant in the water, the generated sound beam propagates in a straight line (i.e., no ray bending phenomenon).

3.2 Steady-State Two-Dimensional Sinusoidal Heat Deposition Model

As a preliminary step in understanding sound generation for circumstances when a heating configuration moves over the surface, we present a mathematical derivation of the solution for the pressure perturbation p excited as a result of a simplified two-dimensional model (Fig. 3.2). From this model, one can learn things about the generated sound, such as the direction of propagation, peak pressure amplitude, efficiency, and so forth. The coordinates in the figure are such that x and y point horizontally at the surface toward the right and out of the paper, respectively, and z points vertically downward measuring depth below the water surface. We assume that the heat deposition is independent of the y coordinate; consequently, the generated sound field is also independent of y. On the surface, the heating configuration resembles a continuous sinusoidal heat intensity variation in the x-direction. Presumably the configuration is the result of the impingement of a large number of laser light-slabs described previously, so the intensity of the laser heat dies

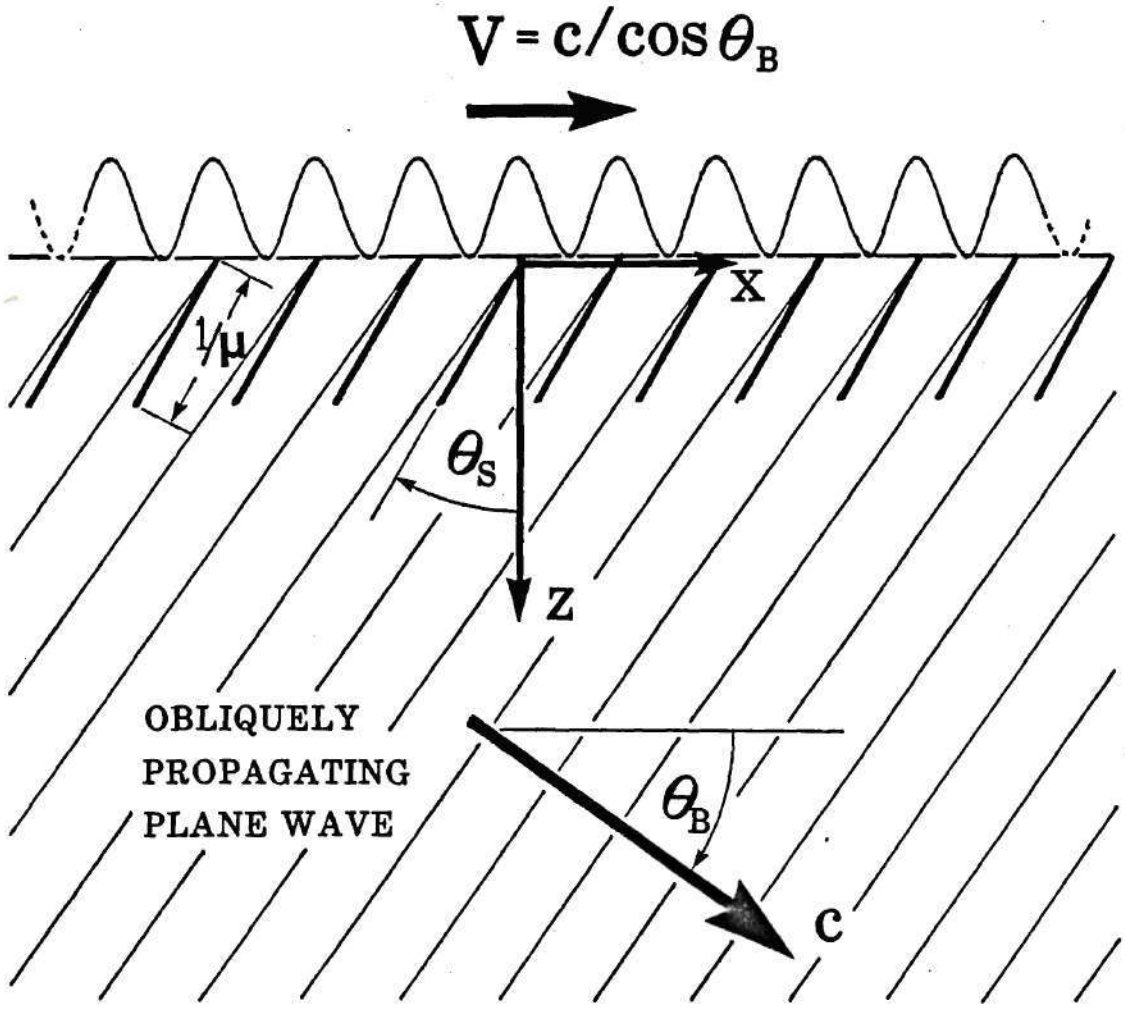

FIGURE 3.2 Geometry for the two-dimensional steady-state heat deposition model. A sinusoidally modulated heating configuration moves over the water surface at speed V and generates an acoustic plane wave propagating at an angle θ_B with the horizontal.

out exponentially as $e^{-\mu s}$ with propagation distance s through the water. Furthermore, the slab-like sinusoidal pattern has a slant angle of θ_S from the vertical as shown in the figure. The pattern travels with a phase speed $V = c/\cos\theta_B$ in the $+x$ direction. The model's prediction has some resemblance to reality if the width of the light-slabs is of the order of a acoustic wavelength or greater, if the pressure wavefronts are measured close to a vertical plane which contains the laser track over the surface. and if the total number of light-slabs n is large compared to unity. This two-dimensional model should be helpful in understanding a three-dimensional transient situation, and has the advantage that the analysis for the former is considerably simpler.

The acoustic pressure p in the positive-z semi-infinite space (i.e. in the water) is governed by the inhomogeneous wave equation

$$\nabla^2 p - \frac{1}{c^2}\frac{\partial^2 p}{\partial t^2} = -\frac{\beta}{c_p}\frac{\partial q}{\partial t} \tag{3.2-1}$$

where the definitions for c. β, and c_p are previously given in Sec. 2.1; the latter quantities are properties of water. The function q representing the rate of heat added per unit volume appropriate to the above description for the heating configuration can be taken as

$$q = K\, e^{-\mu_e z}\, \{1 + \sin(\omega_B t + k_x[x + z\tan\theta_S])\} \tag{3.2-2}$$

where ω_B is the angular frequency of the generated acoustic disturbance and $k_x = \omega_B\cos\theta_B/c$ is the wavenumber of the ripples in the heating configuration on the surface. The symbol μ_e $(=\mu/\cos\theta_S)$ denotes the effective absorption coefficient of light intensity in the z-direction for the case of oblique impingement of the laser light-slabs. Also, the quantity K is the product of μ_e and the average power deposited per unit area of water surface, i.e.,

$$K = \mu_e \int_0^\infty (q)_{av}\, dz \tag{3.2-3}$$

With conscious incorporation of the trace velocity matching principle (Pierce 1981), we conclude that it is possible to represent the solution p in terms of a complex amplitude function F(z) such that

$$p = \frac{\omega_B \beta K}{c_p} \, \mathrm{Re}\{ F(z) \, e^{-i\omega_B t} \, e^{ik_x x} \} \tag{3.2-4}$$

Doing such, one determines that F(z) needs to satisfy an ordinary differential equation (the reduced wave equation)

$$\frac{d^2F}{dz^2} + (k_x \tan\theta_B)^2 F = - e^{(-\mu_c + ik_x \tan\theta_S)z} \tag{3.2-5}$$

with the boundary condition that F be zero at $z=0$.

To solve Eq. (3.2-5), we use a Green's function technique and use the method of images to account for the pressure release boundary condition at $z=0$. The radiation condition at large z is also used. Here, the appropriate freefield Green's function is found to be

$$g(z \,|\, z_o) = \frac{1}{2ik_x \tan\theta_B} \, e^{ik_x \tan\theta_B \, |z - z_o|} \tag{3.2-6}$$

and the solution F expressed in terms of the Green's function integral is identified as

$$F(z) = - \int_{-\infty}^{\infty} \mathrm{sign}(z_o) \, e^{(-\mu_c + ik_x \tan\theta_S)|z_o|} \, g(z \,|\, z_o) \, dz_o \tag{3.2-7}$$

which can then be evaluated in a closed form:

$$F(z) = \frac{e^{ik_x z \tan\theta_B} - e^{(-\mu_c + ik_x \tan\theta_S)z}}{(-\mu_c + ik_x \tan\theta_S)^2 + k_x^2 \tan^2\theta_B} \tag{3.2-8}$$

A more detailed discussion of applying the freefield Green's function along with the heat source reconstruction using a mirror-image source to solve the problem of this type is covered in Sec. 4.2.4. Substituting Eq. (3.2-8) into (3.2-4), we obtain the pressure field as a result of the steady-state sinusoidal heat addition at the surface of

the water.

3.2.1 Controllable Parameters

The results of the previous section can be used in analyses relating to the design of the heating configuration. With this purpose, it is helpful to list those parameters that one can control for the overall system.

One parameter that can be controlled is the speed V with which the heating configuration moves across the surface in the x-direction. In order to beam a sound wave obliquely into the water at a desired angle θ_B with respect to the horizontal, the trace velocity matching principle leads to the prediction that the speed V should be equal to $c/\cos\theta_B$. Without loss of generality, the possible values of θ_B in the present analysis are confined to ones within the first quadrant.

Another controllable parameter is the slant angle θ_S with which the laser light-slabs make with the vertical. Ideally, this angle should be equal to the angle θ_B so that the pumping principle is more fully exploited. However, in many cases the actual sound output is relatively insensitive to the difference of the angles, $\theta_B - \theta_S$. This is discussed further below in Sec. 3.2.3. To achieve a given θ_S, one specifies the incident angle of the laser beam before entering the water using Snell's law (AIP Handbook, p. 6-95):

$$\theta_{incident} = \sin^{-1}[(n_w/n_a)\sin\theta_S] = \sin^{-1}[1.33\ \sin\theta_S] \qquad (3.2\text{-}9)$$

The next controllable parameter to be considered is k_x, representing the wave number in Eq. (3.2-2) of the ripples in the heating configuration on the surface Since k_x is related to the wavenumber of the generated pulse disturbance as $k_x = k_B\cos\theta_B$, the product of k_x and the speed V determines the resulting pulse frequency ω_B. An associated controllable parameter is n, the number of cycles within the acoustic pulse (or the number of light-slabs that are generated). The choice of n determines the extent to which the acoustic pulse is narrow band. The order of magnitude of the

band-width is given by two times the frequency of the pulse divided by n.

In regard to the laser system itself, one has some latitude in the choices of the power output P of the laser, the total pulse duration 2T if the laser is pulsed, and the optical frequency of the light which the laser generates. The latter determines the absorption coefficient μ for light intensity propagation in water. Related to the former two parameters, P and 2T, is the total energy of the pulsed laser E which is computed as P times 2T. The operating parameters of all commercially available lasers are summarized annually in an special issue of Laser Focus (see Laser Focus/Electro-Optics Buyers'Guide 1986).

Additional parameters of interest are those which describe the horizontal dimensions of the moving heating configuration on the surface, $2L_x$ and $2L_y$. The former measures the span of the configuration in the x-direction. This measurement can also be represented by $2\pi n/k_x$. The latter measures the width of the configuration in the y-direction, which is the width of the generated light-slabs.

3.2.2 Application of the simplified model for Fresnel Region radiation

In the radiation of sound and electromagnetic waves by objects of bounded extent, the term Fresnel region is often applied to the radiation which can be discerned at distances that are somewhat larger than a wavelength from the source but are not yet so far away that spherical spreading is prevalent. In the present simplified analysis, the spatial extent of the source is idealized as being very large, because we use the two-dimensional model for q given by Eq. (3.2-2). Consequently, the radiation we predict at distances $1/\mu$ below the water surface or further can be considered as that within the Fresnel region. We use the term here because the same result shows up when one analyzes sources of finite extent in what is identified as the Fresnel region.

Consider that we have a traveling heat deposition pattern that has a width $2L_y$ in the y direction and a duration of n cycles or a span of $n\lambda_B/\cos\theta_B$ (or of $2L_x$) the x

direction, where $\lambda_B = 2\pi c/\omega_B$ is the wavelength of the generated sound. The pattern moves a net distance 2VT on the water surface in the x direction from "turn-on" to "turn-off" of the laser. Furthermore, we assume that the lengths $2L_y$, $2L_w$ ($=2VT\sin\theta_B$), and $2L_x$ are all large (five or more times) compared to λ_B, and that the span $2L_x$ is somewhat less than the heating pattern travel distance 2VT. Given such conditions, geometrical acoustics applies in good approximation for the dominant portion of the acoustic disturbance that exists shortly after the laser is "turned-off." What is generated can be roughly described as a collimated rectangular beam of sound of transverse dimensions $2L_y$ and $2L_w$, propagating obliquely downward into the water at an angle θ_B with respect to the horizontal. Propagating within this beam is a tone-burst of sound having angular frequency ω_B and a duration of n cycles. The result described by Eqs. (3.2-4) and (3.2-8) for the pressure should apply in this generated principle sound beam within the Fresnel region.

3.2.3 Effects of $\theta_S \neq \theta_B$ and μ/k_B on Pressure Amplitude

In generating underwater sound based on the design discussed above, uncertainties are to be expected in the values of θ_S and θ_B. It is desired, therefore, to find out what changes would result in the amplitude of the signal if θ_S deviates from the value of θ_B. Also, when the penetration depth becomes shorter, it is unclear whether $\theta_S = \theta_B$ would still be the most favorable situation, for it is conceivable that the pumping effect would gradually become insignificant. To answer these questions, we investigate the simplified model shown in Fig. 3.2 with θ_S not equal to θ_B in the function q [see Eq. (3.2-2)]. We assume the condition $e^{-\mu_c z} << 1$ for the region that we are interested in. The substitution of the approximate expression for (3.2-8) appropriate to the above condition into Eq. (3.2.4) yields

$$|p| \simeq \frac{(\omega_B \beta K/c_p)}{|\,\mu_c^2 + k_x^2(\tan^2\theta_B - \tan^2\theta_S) - i2\mu_c k_x \tan\theta_S\,|}$$

$$= \frac{c\beta P k_B}{4\pi c_p n L_y} D_p(\sigma, \theta_B, \theta_S) \qquad (3.2\text{-}10)$$

where

$$D_p = \frac{\cos\theta_S \cos\theta_B}{\{ [\sigma + \sigma^{-1}\sin(\theta_B - \theta_S)\sin(\theta_B + \theta_S)]^2 + (2\sin\theta_S\cos\theta_B)^2 \}^{1/2}} \qquad (3.2\text{-}11)$$

Here the indicated mathematical steps make use of the relationship between the parameter K and the laser power P

$$P = 4KL_xL_y/\mu_e \qquad (3.2\text{-}12)$$

and use the abbreviation σ for μ/k_B.

The plot of the directionally dependent multiplicative function D_p versus the slant angle θ_S for four values of σ (0.01, 0.1, 1.0, and 10.0) is presented in Fig. 3.3. Here the oblique beam angle θ_B is taken to be 20 degrees. Note that, as μ/k_B tends to zero, D_p sharply peaks when $\theta_S = \theta_B$. For this extremely low μ/k_B case, a slight deviation of θ_S from θ_B causes the value of D_p to drop considerably. On the other hand, for any μ/k_B greater than unity, the D_p curves appear to be rather insensitive to changes in θ_S. Furthermore, it can be shown from the plot in Fig. 3.3 [or from Eq. (3.2-11)] that, as σ goes beyond a particular value (depending on θ_B) of the order of one, D_p always peaks at $\theta_S=0$ regardless of the value of θ_B. The asymptotic expression for this peak value of D_p for $\sigma >> 1$ is given by $\cos\theta_B/\sigma$. Therefore, if the amplitude of the generated sound is not to be inordinately small, lasers that generate radiation with very short penetration depths in water may not be appropriate for the present design. On the other hand, the figure indicates that to acquire the maximum possible amplitude in the $\sigma >> 1$ (short penetration) cases, the value of D_p is nearly independent of θ_S, although D_p is a maximum when the slant angle of the light-slabs is such that all slabs are in the vertical position. Since the actual pressure amplitude [Eq. (3.2-10)] depends on the laser parameters as P times D_p, for the large σ cases,

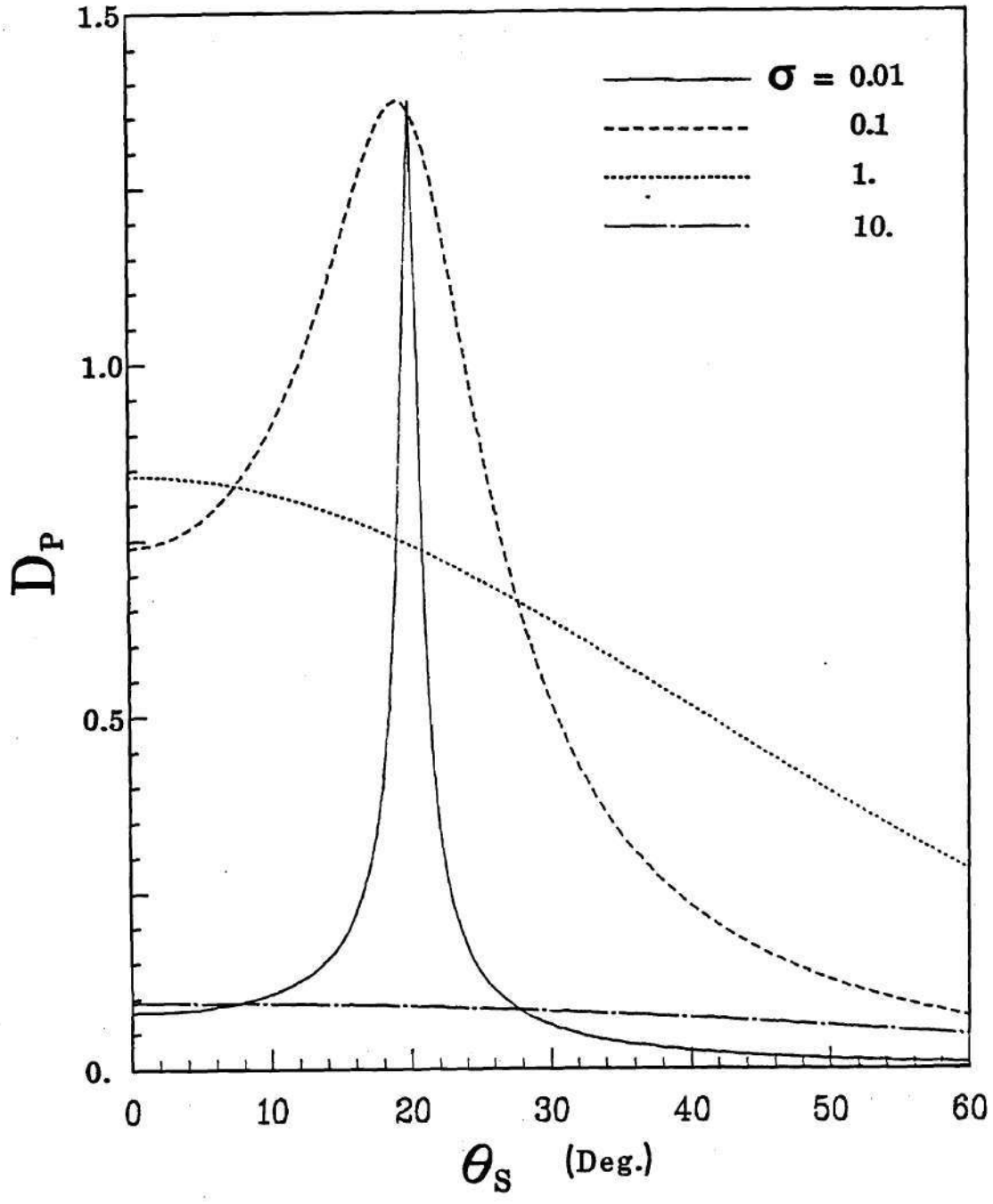

FIGURE 3.3 Plot of directivity function D_p defined by Eq. (3.1-11) versus slant angle θ_S for various values of the ratio of laser beam absorption coefficient μ to acoustic wave number k_B. The acoustic beam's propagation angle θ_B is 20°.

the parameter P/σ (or P/μ when k_B is fixed) is important in judging whether a particular type of laser is suitable. Figure 3.4 shows some of the commercially available lasers (Laser Focus Buyers' Guide 1986) that have relatively higher values of P/μ (frequency considered is 10 kHz) and appropriate for use in the the general design considered here of laser-induced sound systems for the moderate to large μ/k_B case.

For small σ (corresponding to $1/\mu$ of the order of a wavelength or greater), and given that θ_S is close to θ_B, Eq. (3.2-11) reduces to

$$D_p \simeq \frac{\sigma \cot\theta_B}{2[(\theta_B-\theta_S)^2 + \sigma^2]^{1/2}} \tag{3.2-13}$$

which indicates that D_p drops by a factor of $\sqrt{2}$ or more from its peak value (with $\theta_S=\theta_B$) when $|\theta_S-\theta_B| > \sigma$. thus the optical design should try to maintain the deviation $|\theta_S-\theta_B|$ to be of the order of μ/k_B or less. If μ and k_B are of the same order of magnitude so that σ is of the order of one, then $\theta_S-\theta_B$ could be comparable to a radian (57.3°).

A plot of that value of θ_S which maximizes D_p versus θ_B for five values of σ (.01, .1, .25, .5, and .75) is presented in Fig. 3.5. The curves are obtained by setting the derivative $dD_p/d\theta_S$ equal to zero and subsequently solving for its root within the range $0°\le\theta_S\le90°$. The plot gives a general idea how one should pick the optimal slant angle for the laser light-slabs when the phase velocity and the parameter σ are prescribed.

For smaller values of μ/k_B, there are larger penalties in the amplitude if one does not maintain $\theta_S=\theta_B$. The directionally dependent multiplicative function, D_p, in Eq. (3.2-11) under the condition $\theta_S=\theta_B$ reduces to $\cos^2\theta_B/[\sigma^2+\sin^2 2\theta_B]^{1/2}$. Figure 3.6 shows the plot of this function versus the oblique angle, θ_B, for four relatively small values of σ (0.01, 0.05, 0.1, and 0.5). The figure shows only the portion of the curves for θ_B ranging from 0° to 20°, since beyond such a range (i.e. for $\theta_B>20°$), these curves die out as $1/(2\tan\theta_B)$. For the small-value range of θ_B, D_p for each given

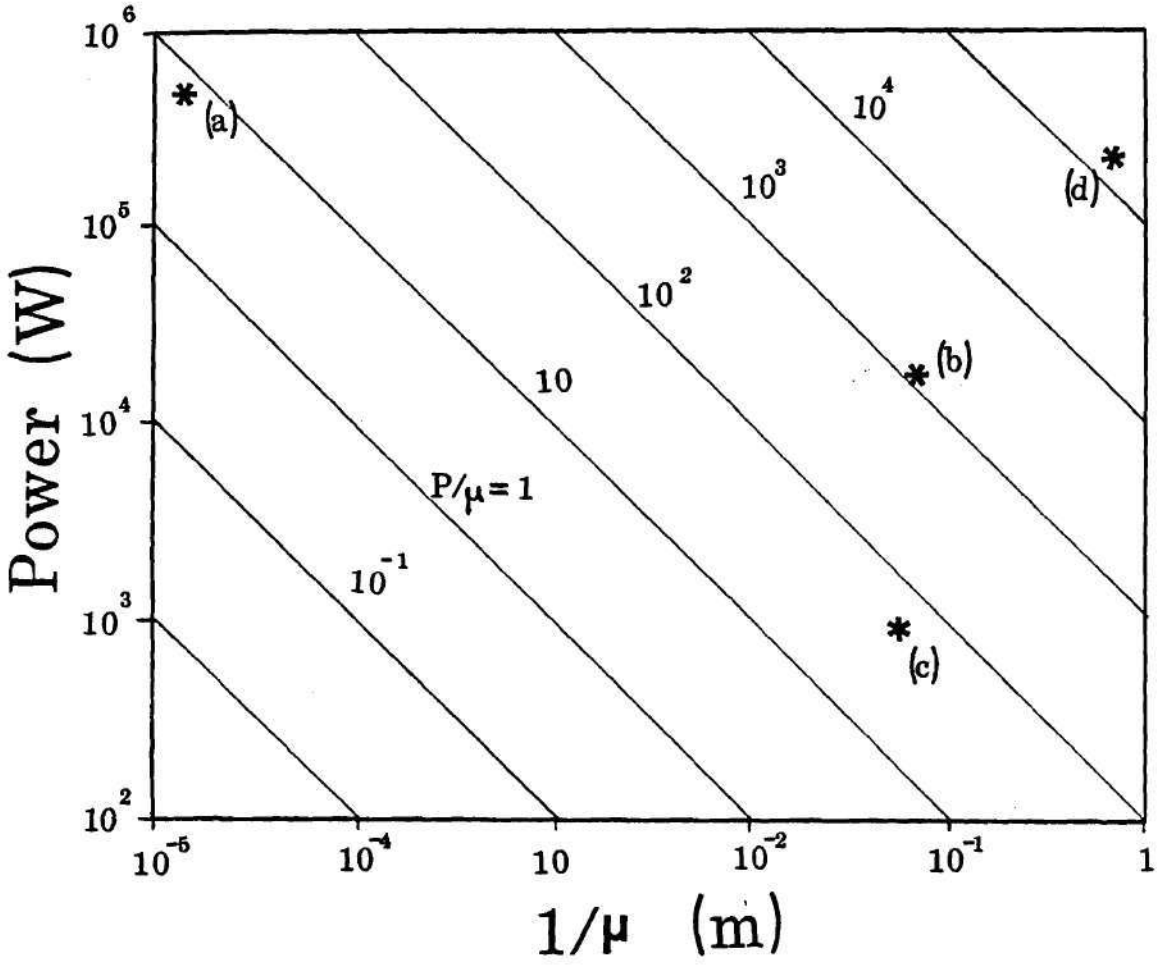

FIGURE 3.4 Laser power P and absorption coefficient μ with graphical comparison of the resulting P/μ for several commercially available lasers. (a)CO_2, 500kW, $\mu=800cm^{-1}$ (b)Nd:Glass, E=40J, T=2ms, P≃20kW, $\mu=13.7m^{-1}$ (c)Nd:YAG, P=900W, $\mu=0.17cm^{-2}$ (d)Ruby, E=400J, T=2ms, P≃200kW, $\mu=1.5m^{-1}$. For large μ/k_B, the generated acoustic pressure varies with P and μ as P/μ, so lasers that correspond to points that lie further to the upper right generate higher amplitude sound.

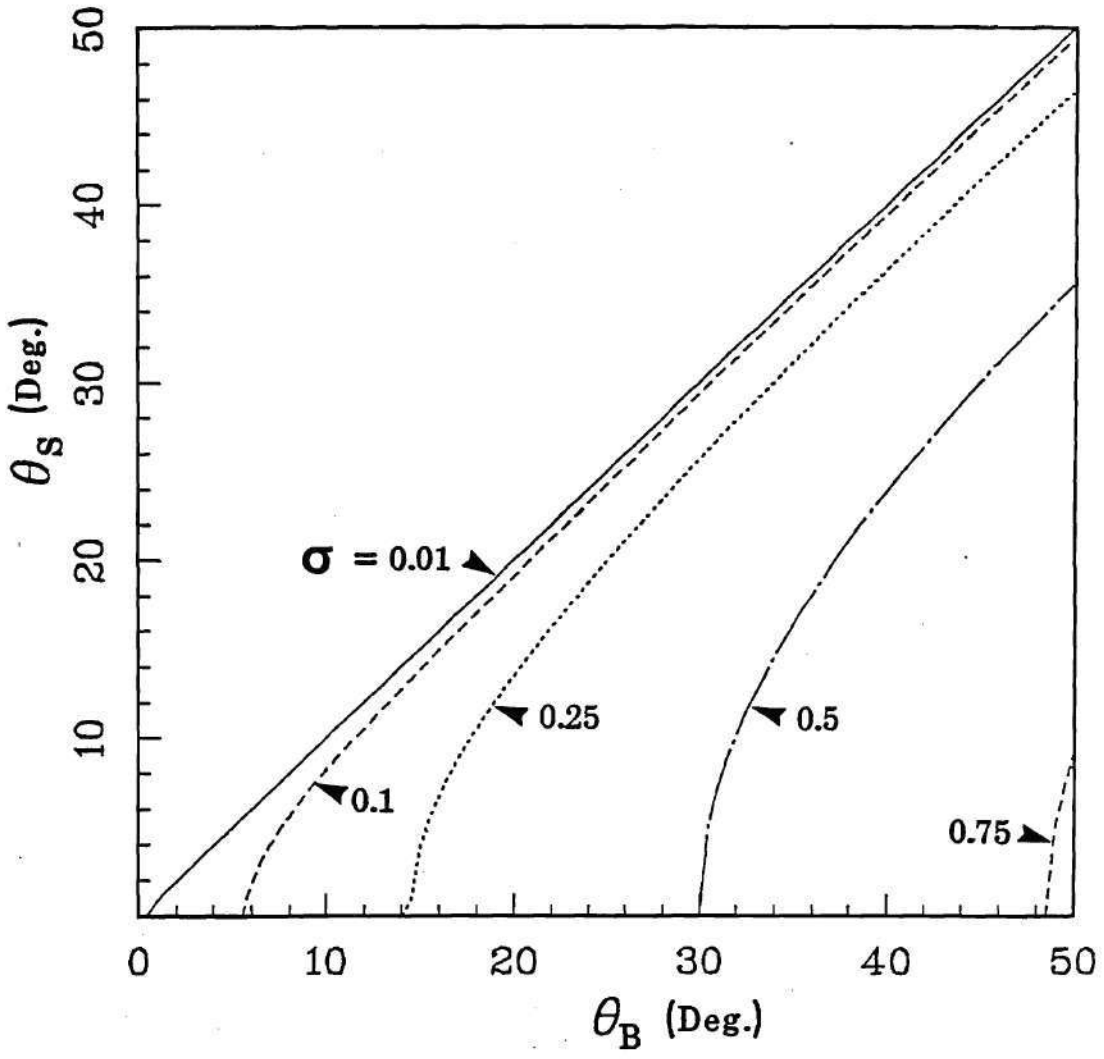

FIGURE 3.5 Plot of value of slant angle θ_S which maximizes function D_p in Eq. (3.2-11) versus the propagation direction θ_B for various values of $\sigma = \mu/k_B$.

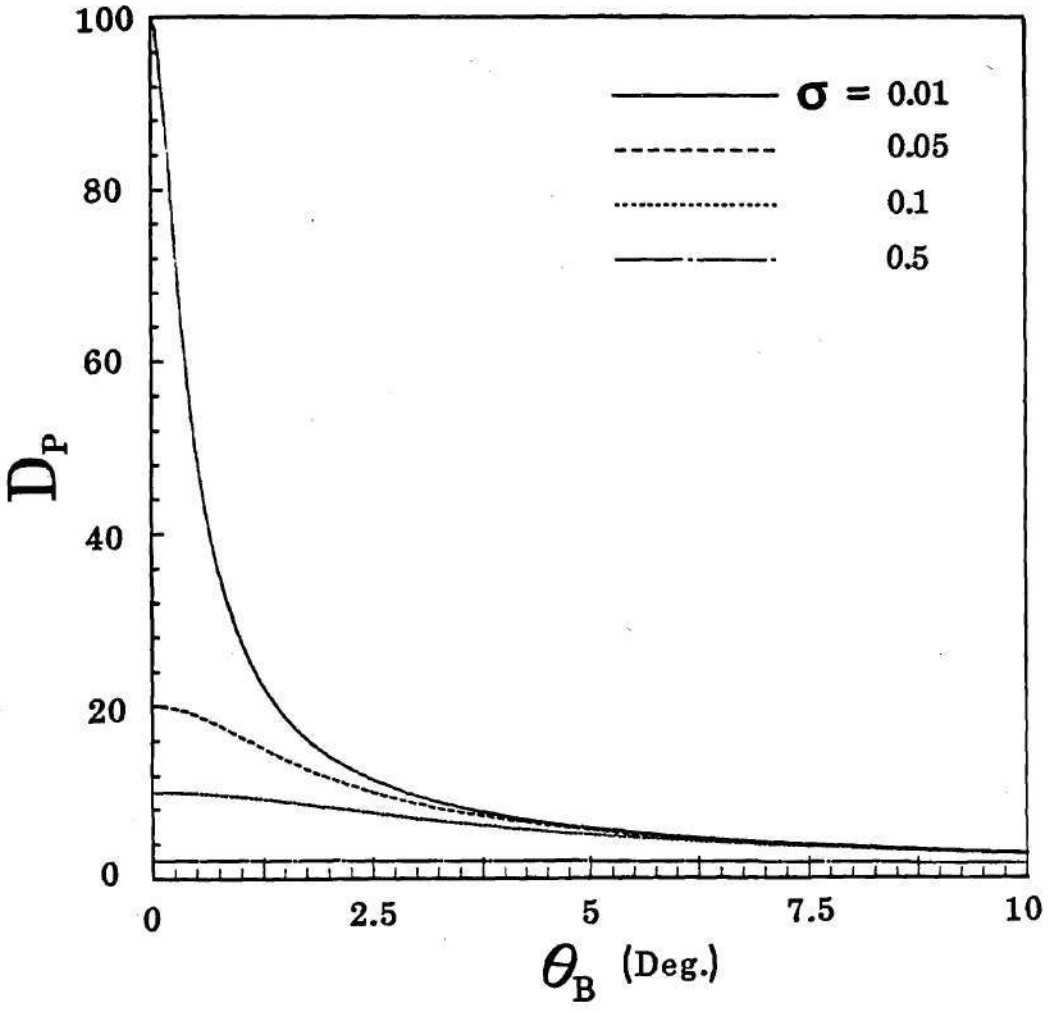

FIGURE 3.6 Plot of function D_p of Eq. (3.2-11) versus beaming angle θ_B for the case $\theta_S = \theta_B$ and for various values of $\sigma = \mu/k_B$.

σ increases monotonically with decreasing θ_B. A peak value for D_p is reached when θ_B is equal to zero. Furthermore, one can deduce that this peak value for D_p grows indefinitely as the value of σ approaches zero.

From the plot given in Fig. 3.6, it would seem that stronger pressure signals result for beaming the sound in the horizontal direction. On the other hand, the simplified model used in this chapter starts with the assumptions that the length of the heating configuration, L_x, and the duration time of the radiation, T, are arbitrarily long to guarantee Eq. (3.2-10) to be true. The fact that D_p is range independent somewhat suggests that the model may breakdown as $\theta_B \rightarrow 0$. A model appropriate for the latter case is discussed in Chapter VI.

3.2.4 Transduction Efficiency Analysis

The derivation of an expression for the transduction efficiency η is based on the consideration of the total acoustic energy generated from the given amount of input optical energy at the water. The energy, not the power, is considered because the actual problem involved in the present design is transient in nature. To proceed with the study, first we need to define a control volume (CV) that accommodates the following discussion. The chosen control volume is a rectangular box (see Fig. 3.7) which contains essentially the entire space that has been occupied by the deposited optical energy during the course of the heat addition. The acoustic energy generated shortly after the "turn-off" of the heat source leaves the control volume from the bottom right face of the box.

We take advantage of the present constant frequency model and write the approximate expression for the complex amplitude p for the excited pressure perturbation as

$$p \simeq \frac{(\omega_B \beta K / c_p)}{\mu_e^2 + k_x^2(\tan^2\theta_B - \tan^2\theta_S) - i2\mu_e k_x \tan\theta_S} e^{ik_x(x + z\tan\theta_B)} \quad (3.2\text{-}14)$$

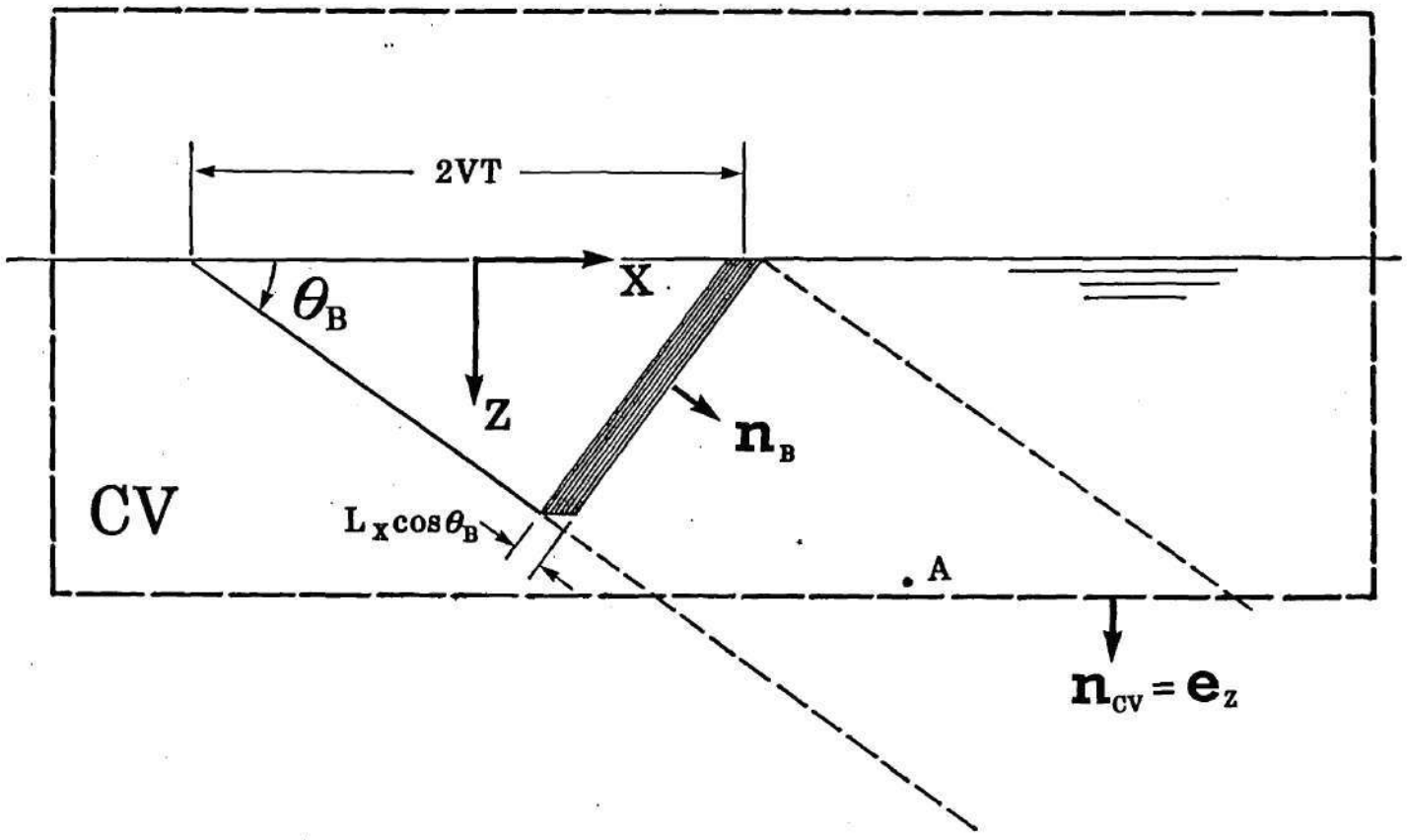

FIGURE 3.7 Control volume (CV) encasing energy deposition region. The beam propagating in direction $\mathbf{n}_B$ exits at angle θ_B.

Such an expression would be appropriate for defining the field characteristics at, for instance, the vicinity of Point A shown in Fig. 3.7. The intensity, **I**, in the acoustic field is p**v**, or $(p^2/\rho c)\mathbf{n}_B$ ($\mathbf{n}_B$ is the unit vector pointing in the direction of the sound beam) because the disturbance is a plane traveling wave. Furthermore, since we are considering constant frequency cases, the time averaged intensity vector, $\mathbf{I}_{av}$ is identified as $\frac{1}{2}\mathrm{Re}(p\mathbf{v}^*)$, or $(|p|^2/2\rho c)\mathbf{n}_B$. With p as given above in Eq. (3.2-14), one accordingly has

$$\mathbf{I}_{av} = \frac{1}{2\rho c} \frac{(\omega_B \beta K/c_p)^2 \, \mathbf{n}_B}{[\mu_e^2 + k_x^2(\tan^2\theta_B - \tan^2\theta_S)]^2 + (2\mu_e k_x \tan\theta_S)^2} \tag{3.2-15}$$

The time averaged energy radiated per unit time by the sound source per unit area of the CV's surface is

$$I_{z,av} = \mathbf{I}_{av} \cdot \mathbf{n}_{CV} \tag{3.2-16}$$

evaluated at the portion (bottom right) of the CV's boundary, through which the sound beam takes its exit. Here, $\mathbf{n}_{CV} = \mathbf{e}_z$ is the unit normal vector for the bottom right surface of the CV. The total acoustic energy E_{ac} radiated from the source can be roughly estimated by taking the product of $I_{z,av}$ with the surface area of the above mentioned bottom right portion of the CV's boundary, and then with a meaningful time duration. The area and the duration are identified as $(2VT)(2L_y)$ and $2L_x\cos\theta_B/c$, respectively. Then, the relation $V = c/\cos\theta_B$ leads one to the expression

$$E_{ac} = 8L_xL_yT\,|\mathbf{I}_{av}|\sin\theta_B \tag{3.2-17}$$

The factor of $\sin\theta_B$ in Eq. (3.2-17) results from the dot product of the unit vectors $\mathbf{n}_B$ and $\mathbf{e}_z$. Using Eq. (3.2-12) in (3.2-15), subsituting the resulting expression in Eq. (3.2-17), manipulating the terms, and finally dividing the E_{ac} by the total optical energy input from the light-slabs, (2T)P, one obtains the transduction efficiency as

$$\eta = \frac{1}{8\pi}\left(\frac{c}{\rho}\right)\left(\frac{\beta}{c_p}\right)^2 \frac{Pk_B}{nL_y} D_\eta(\sigma, \theta_S, \theta_B) \tag{3.2-18}$$

where

$$D_\eta = \frac{\sin\theta_B\cos\theta_B \cos^2\theta_S}{[\sigma + \sigma^{-1}\sin(\theta_B-\theta_S)\sin(\theta_B+\theta_S)]^2 + (2\sin\theta_S\cos\theta_B)^2} \tag{3.2-19}$$

is the directionally dependent multiplicative function for the efficiency expression and where σ once again denotes the ratio μ/k_B.

The function D_η for the transduction efficiency relates to the previous expression, D_p, for the pressure amplitude [see Eq. (3.2-12)] in a simple way as $D_\eta = D_p^2\sin\theta_B\cos\theta_B$. If one considers D_η as a function of θ_S, the factor $\sin\theta_B\cos\theta_B$ appearing in the expression can be regarded as a scaling constant for any given θ_B. Therefore, it is anticipated that the curves for the plot of D_η versus θ_S will behave very similar to that shown in Fig. 3.3. That is, the peak value of D_η for any given σ will emerge at the same value of θ_S for which the D-curve peaks, provided that θ_B is the same in both plots. Other features for D_η include that (i) as $\sigma \to 0$, the peak-D_η value approaches the value $1/(4\tan\theta_B)$ (the peak occurs at $\theta_S = \theta_B$), and (ii) for $\sigma >> \sin 2\theta_B$, the peak-D_η value can be asymptotically represented by $\sin\theta_B\cos\theta_B/\sigma^2$ (the peak occurs at $\theta_S = 0$).

Consider the case where $\theta_S = \theta_B$ for the present design. Clearly the function D_η has a zero value at $\theta_B = 0°$ and $\theta_B = 90°$; therefore, it is conceivable that, for any given σ value, D_η possesses a local maximum some place within the range of $0° < \theta_B < 90°$. This maximum is located by taking the derivative of D_η and subsequently setting the derivative equal to zero. Doing such we locate the angle θ_B which maximizes the value of D_η at any given σ by making θ_B satisfy the equation

$$f(\theta_B) = \sin^2 2\theta_B - \sigma^2(1-4\sin^2\theta_B) = 0 \tag{3.2-20}$$

Curves of D_η versus θ_B for four values of σ (0.01, 0.05, 0.1, and 0.5) are presented in Fig 3.8, and the value of θ_B at which D_η attains its peak value is plotted versus σ on

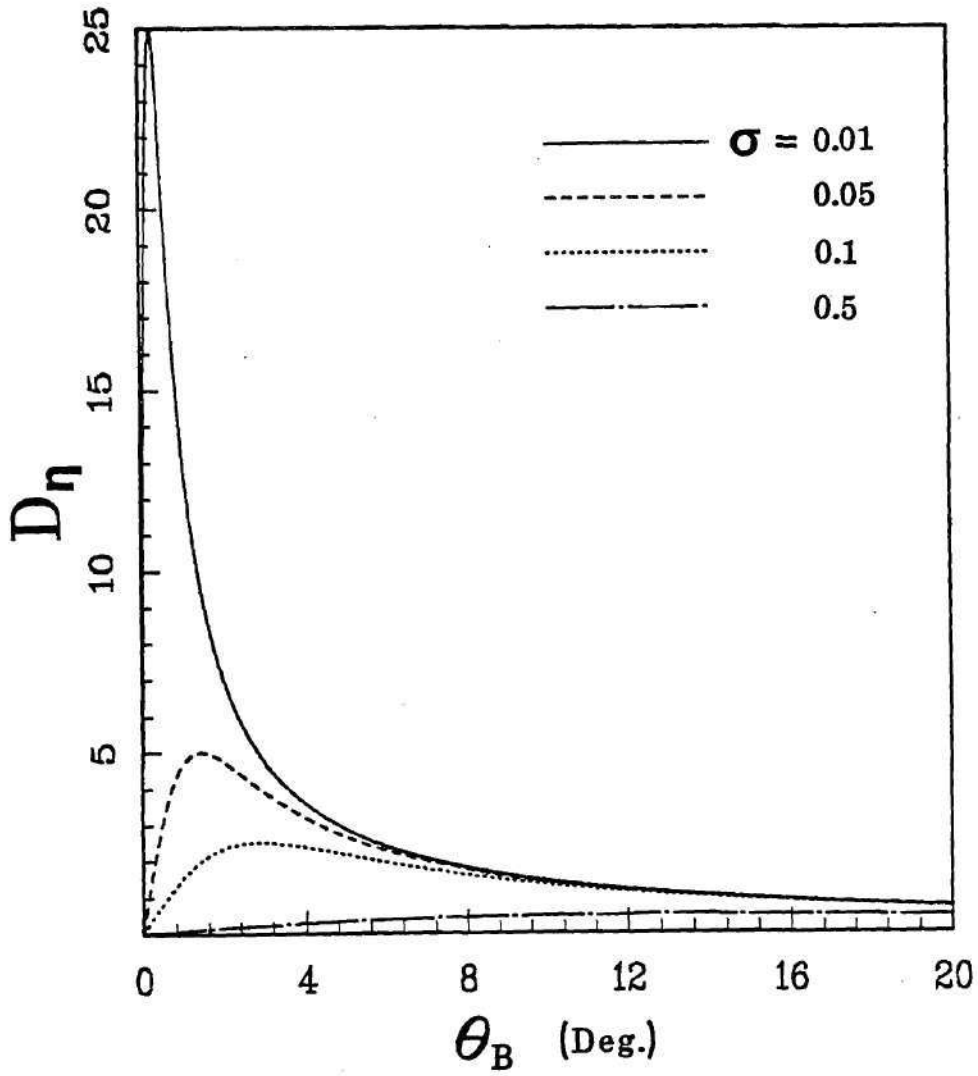

FIGURE 3.8 Plot of function D_η of Eq. (3.2-19) versus beaming angle θ_B for various values of σ for the case $\theta_S = \theta_B$. The function D_η gives the dependence of the transduction efficiency on beam propagation direction θ_B and absorption coefficient $\mu = k_B\sigma$. For small σ its peak occurs when θ_B in radians equals $\sigma/2$, the value at the peak being approximately $1/4\sigma$.

semi-logarithmic paper in Fig. 3.9.

One may note, when $\sigma << 1$ and near that θ_B at which D_η attains its peak, D_η,approximates to

$$D_\eta = \theta_B/(\sigma^2 + 4\theta_B^2) \qquad (3.2\text{-}21)$$

The peak value, obtained when $\theta_B = \sigma/2$, is equal to $1/(4\sigma)$ in this limit.

3.3 Relation of System Parameters to Farfield Sound Generation

Having in mind those parameters that should be controllable, we are now ready to investigate the performance of our proposed novel optical system in generating long range detectable signals based on the simplified model posed in Fig. 3.2. The heuristic discussion presented in the following shows that such a model could be used to estimate quantities such as the magnitude of an acoustic signal generated for a given set of controlled parameters, as well as the laser parameters (such as laser pulse energy, pulse duration, etc.) required for the generation of a specific acoustic signal. However, it is also important to understand that the discussion predicts results which are valid only for the circumstances in which we have a reasonably large energy depositional area such that within the distance marked by the source and receiver, the created disturbance propagates more or less without spreading. In other words, these cases correspond to ones which place the receiving location within the so-called Fresnel region of the sound radiation. Some simple heuristic considerations allow a quick extrapolation to estimate what would be obtained under more realistic situations. The detailed mathematical analysis for a more refined model is given in the next chapter.

Since it has been shown in the previous section that the sound field is relatively insensitive to the deviation of θ_S from θ_B, we consider only the special case where $\theta_S = \theta_B$ in the following discussion. Substituting Eq. (3.2-8) into (3.2-4), setting θ_S equal to θ_B, and assuming the depth z to be moderately greater than the

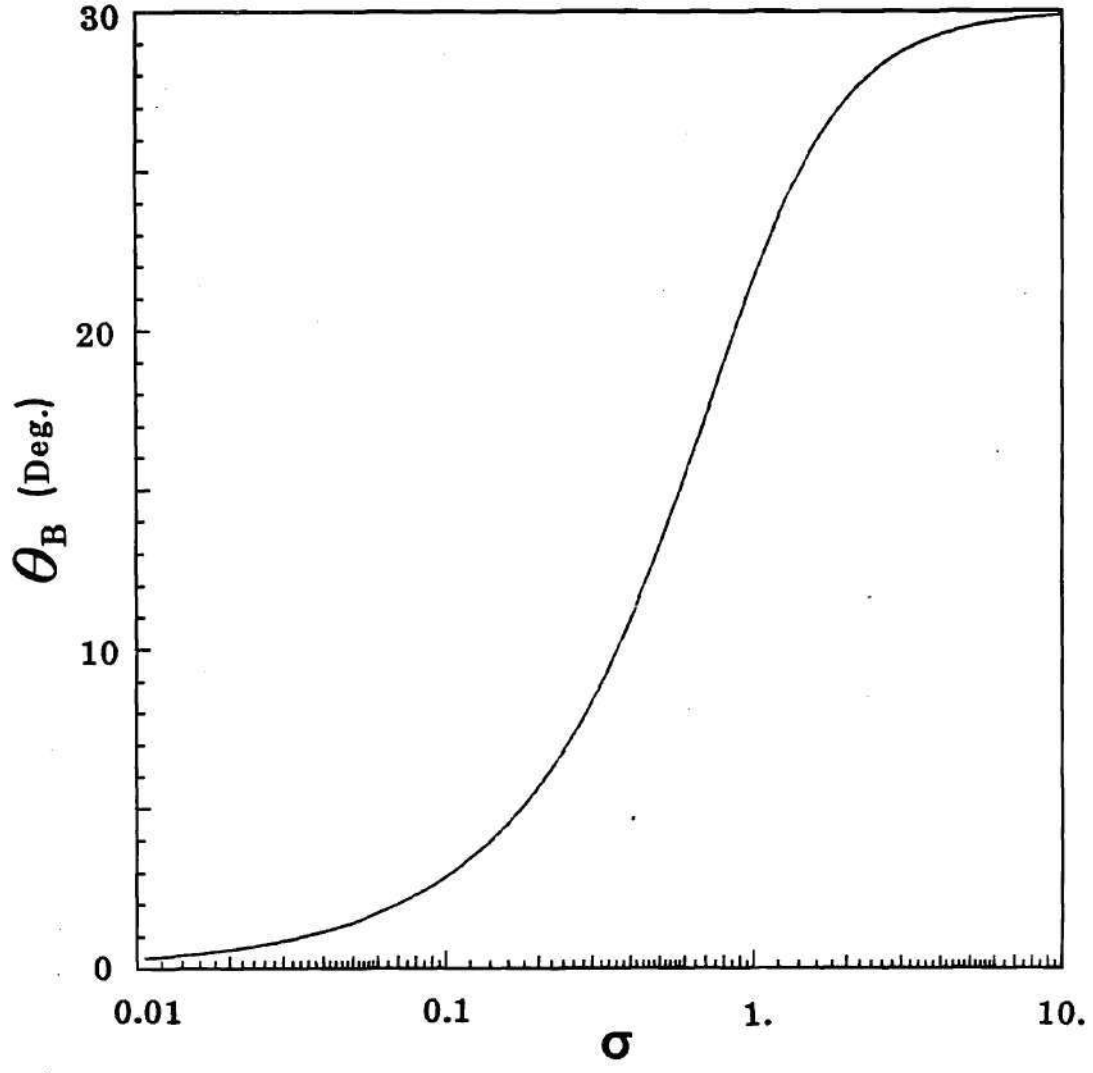

FIGURE 3.9 Plot of angle θ_B, for which D_η attains its peak value, versus σ. For small σ, the derived angle in radians is approximately $\sigma/2$.

effective penetration depth $1/\mu_e$ (so that the condition $e^{-\mu_e Z} << 1$ applies), one obtains an approximate expression for the acoustic pressure amplitude

$$|p| \simeq \frac{\omega_B \beta K / c_p}{[\mu_e^4 + 4\mu_e^2 k_x^2 \tan^2\theta_B]^{1/2}} \tag{3.3-1}$$

With all the conditions described earlier, one may argue that the peak pressure amplitude in the generated collimated tone-burst sound wave at a distance not far from the laser-irradiated region would be relatively unaffected by spreading loss (although still affected by seawater absorption) and should therefore be of the order of the product of Eq. (3.3-1) and an exponential attenuation factor. Thus we have, after minor rearrangements of Eq. (3.3-1),

$$|p|_r \simeq \frac{(c\beta K/\mu c_p)\cos^2\theta_B}{[\sin^2 2\theta_B + (\mu/k_B)^2]^{1/2}}\ e^{-\alpha r} \tag{3.3-2}$$

where r is the distance (range) of propagation from the laser-irradiated region and α is the attenuation coefficient (nepers per meter) for sound of angular frequency ω_B in seawater.

The identification of the factor K is such that

$$P = 4KL_xL_y\cos\theta_B/\mu \tag{3.3-3}$$

is the average energy deposited per unit time, or the power deposited, into the water by the laser during the time interval the laser is "on." This time interval is identified as

$$2T = 2L_w/(c\tan\theta_B) \tag{3.3-4}$$

The product of these two quantities is the total energy deposited into the water, so

$$E = 8KL_xL_yL_w\cos\theta_B/(\mu c\tan\theta_B) \tag{3.3-5}$$

Diffraction effects will eventually convert this collimated beam of sound into a directional spherical wave, for which the pressure amplitude decreases with propagation distance r as $(1/r)e^{-\alpha r}$. However, the distance at which this occurs could be quite large if L_y and L_w are chosen to be large. A comparison with results derived by Freedman (1960) for sound radiated by a rigidly baffled rectangular piston suggests that the peak amplitude continues to be of the same magnitude as that predicted by (3.3-2) up to a range of

$$r = (2/3)k_B L_y L_w \tag{3.3-6}$$

for L_y and L_w being roughly of the same magnitude. Equation (3.3-6) suggests that, if one seeks to "beam" sound out to a specified range r and if r is to be within the Fresnel region, one should design the laser heat deposition pattern such that

$$L_y = L_w = (1.5r/k_B)^{1/2} \tag{3.3-7}$$

3.3.1 Ambient Noise Considerations

Based on the criterion for L_x and L_w that we have developed in Eq. (3.3-7) for beaming sound to a distant receiver located in the Fresnel region whose field characteristics can be roughly represented by Eq. (3.3-2), we can now proceed to estimate the required laser parameters. The signal frequency $f_B = \omega_B/2\pi$ and the required amplitude $|p|_r$ at range r in direction θ_B must be prescribed in advance. The criterion on prescribing such a value for $|p|_r$ should be such that it guarantees the signal be "easily detectable" when received by an ordinary transducer. While such a criterion may not be unambiguous, we attempt to develop one that is based upon the consideration of the ambient noise in the ocean.

The procedure is that, if it is known in advance that what will be received is a narrow band signal of bandwidth Δf and center frequency f_B, one can proceed by estimating the relevant portion of the ocean noise and subsequently requiring the

amplitude of the signal to be a certain number of times higher than that of the noise. For a representative estimate of the former, we use data that appears in texts by Tolstoy and Clay (1966) and Clay and Medwin (1977) for circumstances when the wind speed is 4.5 m/s, the original data being taken from papers by Mellen (1952) and Ezrow (1962). The data is approximately fitted over the range of 10 kHz to 100 kHz by

$$p_f^2(f) = 1.2(10)^{-6}\,(10{,}000/f)^{1.6} \qquad Pa^2/Hz \tag{3.3-8}$$

where the frequency f is measured in hertz. If such noise were filtered through a narrow band filter of bandwidth Δf centered at f_B, the result would be roughly a sinusoidal signal whose pressure amplitude can be estimated as

$$|p|_{noise} = [2\,\Delta f\, p_f^2(f_B)]^{1/2} \tag{3.3-9}$$

where the factor of two inside the brackets converts the corresponding rms value to the peak amplitude value.

Now suppose that the narrow band signal one seeks to detect contains a duration of n cycles (oscillating at the frequency f_B), then a reasonable choice for the filter bandwidth that may be used when detecting it would be

$$\Delta f = 2f_B/n \tag{3.3-10}$$

(The factor of two can be replaced by a slightly larger number if more conservative estimates are desired.). Therefore, the amplitude of the noise signal one would have to contend with is

$$|p|_{noise} = 0.022\, n^{-1/2}\,(10{,}000/f_B)^{0.4} \tag{3.3-11}$$

3.3.2 Required Laser Parameters

Suppose now that one wishes to have an acoustic signal of pressure amplitude

$|p|_r$ at a given range r. We can estimate the required laser parameters from Eqs. (3.3-2) through (3.3-7) along with the identity $L_x = \pi n/k_x$. Doing so yields the required laser power, pulse duration, and pulse energy as

$$P_{required} = \frac{4\pi n c_p Y(\mu, \theta_B)\tan\theta_B}{c\beta k_B^{3/2}} (1.5r)^{1/2} |p|_r e^{\alpha r} \tag{3.3-12a}$$

$$2T_{required} = \frac{(1.5r/k_B)^{1/2}}{c \tan\theta_B} \tag{3.3-12b}$$

$$E_{required} = \frac{4\pi n c_p Y(\mu, \theta_B)}{c^2\beta k_B^2} 1.5r |p|_r e^{\alpha r} \tag{3.3-12c}$$

where

$$Y(\mu, \theta_B) = [1 + (\mu/k_B \sin 2\theta_B)^2]^{1/2} \tag{3.3-13}$$

An estimate of the three required laser parameters, P, 2T, and E, for an easily detectable signal at range r in direction θ_B ensues from Eqs. (3.3-11) and (3.3-12) when one assumes that $|p|_r$ be a fixed multiple of $|p|_{noise}$. Figures 3.10 and 3.11 exemplify the result of such an estimate for the case where the required signal amplitude is taken as five times the noise amplitude. This requirement would enforce that $|p|_r$ exceeds background by $10\log_{10}(5^2) = 14$ dB, which should be a generous allowance. In these two figures, the curves plotted are for $\theta_B = 20°$ and n = 10 cycles. The water temperature is taken as 10°C and the salinity as 35 parts per thousand, for which corresponding sea-water thermodynamic parameters (Pierce 1981, pp. 33-34) are c = 1526 m/s, c_p = 3993 J/kg°K, and $\beta = 2.44(10)^{-4}$ °K^{-1}. The acoustic absorption coefficient α is computed from semi-empirical formulas (Fisher and Simmons 1977) and ranges from $7(10)^{-5}$ nepers/m at 10 kHz to $4(10)^{-3}$ nepers/m at 100 kHz. The value of the optical attenuation coefficient is taken as 13.7 m^{-1} and corresponds to the value appropriate for a 1.06-micron-wavelength Nd:Glass laser (see Sec. 1.3).

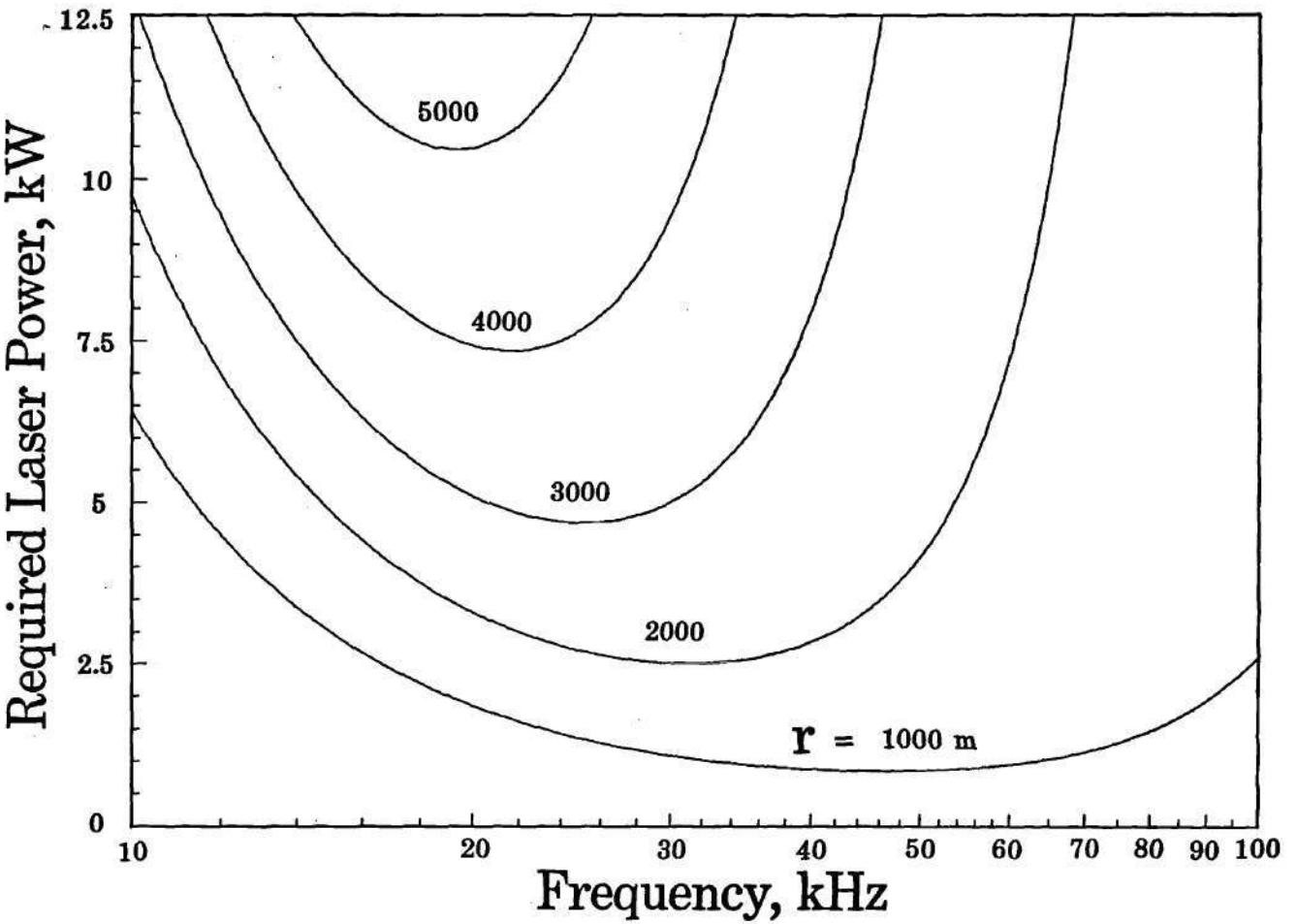

FIGURE 3.10 Estimates of required laser power to generate easily detectable acoustic pulses of specified frequency at given propagation range r. Calculations are based on results inferred from the 2-D steady-state model, and with various other assumptions described in the text.

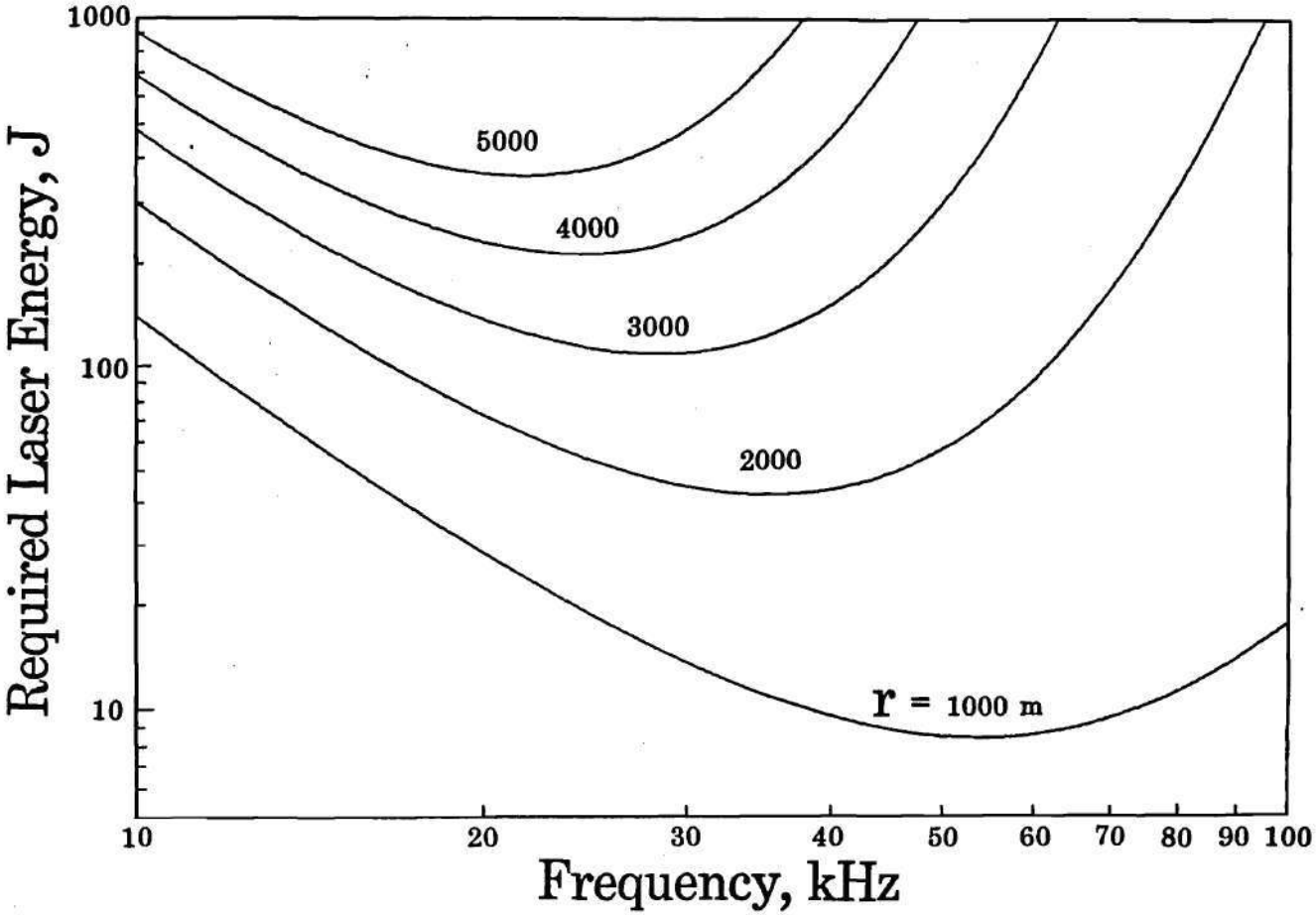

FIGURE 3.11 Estimates of required laser pulsed energy to generate easily detectable acoustic pulses of specified frequency at given propagation range r. Calculations are based on the 2-D steady-state model.

One may note from Fig. 3.10 that, for any given r, there is a frequency for which the required laser power is a minimum. The physical significance of the presence of such an optimum frequency is due to two factors. On the high frequency side, the factor $e^{\alpha r}$ in Eq. (3.3-12a) is dominantly responsible for the rapid increase in the requirement of higher laser power, as the factor $\alpha(f)$ in the exponent grows with frequency approximately as f^{2}. On the low frequency side, this acoustic absorption effect is somewhat masked by the frequency factors contained elsewhere in the expression for $P_{required}$ in Eq. (3.3-12a). One natural result of reducing the frequency is that the parameter $\sigma = \mu/k_B$ increases.

The curves plotted in Fig. 3.11 for the required energy versus frequency manifest similar features to that of Fig. 3.3, except that the frequencies at which the minima occur are lower. The shift is imposed by the presence of the factor k_B^{-2}, rather than $k_B^{-3/2}$, in Eq. (3.3-12c).

CHAPTER IV

DEVELOPMENT OF A TRANSIENT THREE-DIMENSIONAL ANALYTICAL MODEL OF SOUND BEAM GENERATION

The previous chapter presented a simplified two-dimensional model for analyzing the acoustic field when laser-induced heat is added to water in such a manner as to exploit the pumping principle and to generate narrow beam width pulses of nearly constant frequency. This model predicts the optoacoustic transduction efficiency η of the sound generation process and the acoustic field within the generated sound beam. These predictions enable one to estimate the required laser parameters based on the criterion that the signal created be easily detectable at the specified propagation distance and at a prescribed signal frequency. The analysis in the previous chapter does not incorporate the ubiquitous effect of the spreading loss, especially when the propagation distance is beyond the range of "near field." The estimation assumes sufficiently high frequencies and large energy depositional areas such that the distant points to which one desires to beam the sound always stay within the Fresnel region.

Recall that the parameter L_x is directly related to the controlled parameters n and k_x as $\pi n/k_x$. From one of the considerations discussed in Sec. 3.1. we deduce that choosing values for n (number of ripples in the heating configuration) which are large enough to achieve narrow band signals always guarantees the condition $k_xL_x>>1$. Application of Freedman's criterion [Eqs. (3.4-6) and (3.4-7)] also suggests that in order to beam the sound to a Fresnel-region receiver we should choose $k_xL_y>>1$ and $k_xL_w>>1$. While energy depositions which provide sufficiently large L_y and L_w (when compared with the acoustic wavelength) may be able to efficiently beam sound to the receiving location with negligible reduction in the signal amplitude (this is what is meant by the Fresnel-region concept of generating

sound), we should not restrict ourselves to only this case. When the magnitudes of both L_y and L_w gradually decrease, the sound field at the same receiving location will be characteristic of a farfield location, where the pressure amplitude within the beam decreases as 1/r with the propagation distance r. Concurrently, the nearfield pressure amplitude increases with gradual decrease in the heat deposition area with the total deposited energy E kept fixed, because the energy per unit time per light-slab increases at the same rate as L_y and L_w decrease. Specifically, we refer to the case for which the listener is located roughly in the farfield region as the farfield concept of generating sound.

From the above argument, it is difficult to judge from common sense which of the two conceptual energy deposition strategies, Fresnel region or farfield region concepts, is preferable for generating easily detectable long-range signals at a given point. A mathematical analysis for a refined model to resolve this question is developed in this chapter. The model also furnishes additional insight into the nature of the generated signal and its dependence on the energy deposition scheme.

The case of short pulse duration T (i.e. $k_x cT << 1$) is not of interest for two reasons. First, the sound waves resulting from this type of heat radiation are less likely to have characteristics sufficient to distinguish them from the background noise.This contradicts our previously stated design consideration which lead to the requirement $k_x L_x >> 1$. Second, the small T case does not allow sufficient time for the energy transduction process to exploit the pumping principle. Therefore, in the upcoming analysis, we keep the assumption $k_x cT >> 1$.

Since an optical system that substantially broaden the laser beam in the y direction may be difficult to achieve in the immediate future, the present chapter also discusses the case of $k_x L_y << 1$ in addition to the large L_y case. Furthermore, as θ_B gets smaller for fixed T the condition $k_x L_w >> 1$ no longer holds because $L_w = cT\tan\theta_B$ goes to zero as θ_B goes to zero. The framework for developing a model that applies for the small θ_B case is developed here, but the presentation of the

model for such cases is postponed to Chapter VI.

4.1 Idealized Three-Dimensional Model of Heat Deposition

Most principal features of the generated sound field can be quantitatively examined with the aid of the idealized model sketched in Fig. 4.1. A spatially periodic and amplitude modulated pattern of light with spatial period $2\pi/k_x$ moves over the water in the x-direction with a speed V, which is taken to be greater than the sound speed c. An angle θ_B whose cosine is c/V is subsequently identified as the angle which the generated beam of sound makes with the horizontal direction. The trace velocity matching principle leads to the conclusion that this sound beam has a wavelength $\lambda_B=(2\pi/k_x)\cos\theta_B$ and an angular frequency $\omega_B=2\pi c/\lambda_B$.

Determination of the acoustic disturbance in the water requires solutions of the inhomogeneous wave equation that governs the generation of sound when thermal energy is added to the water. This equation has been given earlier in Eq. (3.2-1). The laser energy q deposited in the water by the laser beam per unit time per unit volume is taken as varying with the spatial coordinates and time t as

$$q = F_P(k_xN)\, E_M(N,y)\, E_T(t)\, e^{-\mu_e z} \tag{4.1-1}$$

The funciton F_p is periodic and can, for simplicity, be taken as

$$F_P(k_xN) = K(1 + \cos k_xN) \tag{4.1-2}$$

such that it oscillates back and forth between 0 and 2K. The constant K characterizes the strength of the heat source and can be related to the total energy E deposited in the water with the requirement that the total integral of q over volume and time must be E. Because the laser power is finite, the volume in the water over which this pattern extends at any instant is limited; this is taken into account with an envelope factor, $E_M(N,y)$, enclosing the periodic pattern (the subscript M on E_M is mnemonic

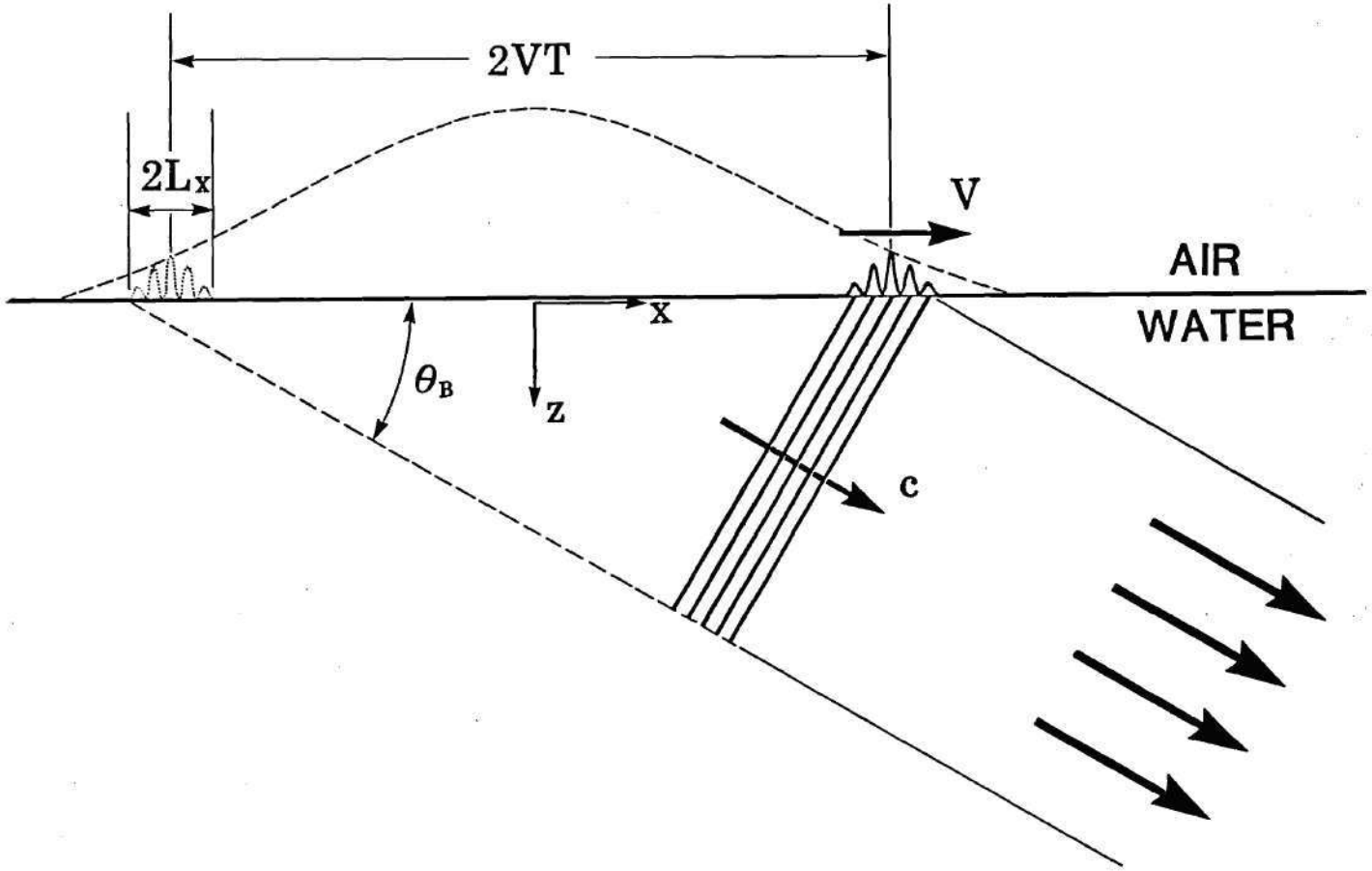

FIGURE 4.1 Principal features of analytical model (with Gaussian envelope functions), indicating considered spatial and temporal configuration of heat deposition near water surface and resulting sound beam.

for "moving"), where N abbreviates the combination

$$N = x + z \tan\theta_S - \int_0^t V(\tau)d\tau \qquad (4.1\text{-}3)$$

The combination $x + z \tan\theta_S$ in N describes the instantaneous heat intensity distribution created as a result of depositing laser energy in the form of light-slabs into the water. θ_S is the slant angle for the slabs. With the additional term, $-\int_0^t V(\tau)d\tau$, added to such a combination, the heating pattern q is then set to move with speed V in the x-direction. Since V is the chief parameter for controlling the direction of the generated acoustic signal, it is not necessarily a fixed quantity for the design. In general, the speed V can be some known function of time or of x, and the spread in V affects the angular width of the sound beam. Also, because the total energy in a laser pulse is limited, an additional envelope factor $E_T(t)$ is incorporated in q. Typical examples for such a factor (the pulse-shape) can be found in Fig. 1.1. Since the laser intensity dies out exponentially as $e^{-\mu s}$ with propagation distance s through the water, a decaying factor $e^{-\mu_e z}$ is installed in q using the previously defined attenuation coefficient μ_e $(=\mu/\cos\theta_S)$ to account for the effective absorption of laser intensity in the z-direction.

In the subsequent analysis we assume that the speed V is a fixed quantity focusing on developing the theory for single-direction sound beaming. In addition, the moving envelope $E_M(N,y)$ is taken as Gaussian shaped in both N and y. This double envelope, moving with the speed V, is described by the function

$$E_M(N,y) = e^{-N^2/L_x^2}\, e^{-y^2/L_y^2} \qquad (4.1\text{-}4)$$

where L_x and L_y characterize the dimensions of the envelope. For the suggested optical design using gratings and other beam broadening devices, the choice of Gaussian tapered heat-energy distribution in both the x- and y-directions is somewhat more realistic than one which assumes energy being sharply chopped off at

some points [for instance, a rectangular envelope, $\{H(x-L_x)-H(x+L_x)\}$]. Furthermore, the Gaussian choice eliminates sharp edges in the heating pattern which could be very helpful in many stages of the mathematical development. By incorporating a double envelope as given in Eq. (4.1-4) into the heating configuration, one can regard the configuration at the surface as having effective dimensions of $2L_x$ and $2L_y$ in the x- and y-directions, respectively.

For a similar reason, we assume the pulse shape (describing how the total power entering the water varies with t), $E_T(t)$, is Gaussian, which is expressly written

$$E_T(t) = e^{-t^2/T^2} \tag{4.1-5}$$

Here, the parameter T characterizes the duration time of the overall light irradiation. As before, we regard 2T as the effective duration of this laser pulse.

The analysis in Sec. 3.2 shows that, depending on the ratio μ/k_B. the generation of sound is either most efficient when $\theta_S = \theta_B$ or else relatively insensitive to θ_S. Here, to simplify the analysis we proceed with the assumption $\theta_S = \theta_B$. The changes in the results due to deviation of θ_S from θ_B are easily assessed with reference to Sec. 3.2.3. The above assumption enables one to rewrite Eq. (4.1-3) as

$$N = x + z\tan\theta_B - Vt \tag{4.1-6}$$

Accordingly we will have $\mu_c = \mu/\cos\theta_B$.

Based on the above assumptions, the constant K appearing in Eq. (4.1-2) can be readily evaluated as

$$K = \frac{\mu_c E}{\pi^{3/2} L_x L_y T} \tag{4.1-7}$$

To solve for the above described boundary value and initial value problem, the causality condition and the boundary condition that $p = 0$ at $z = 0$ are to be imposed on the solution p(x,y,z,t). The interpretation of the causality condition as a

mathematical statement is discussed in Sec. 4.2.3.

The inhomogeneous wave equation (3.2-1) with q taken in the form (4.1-1) has an exact solution as a three fold integral

$$p = \frac{\beta}{4\pi c_p} (\partial/\partial t) \iiint \frac{q(x_o,y_o,|z_0|,t-R/c)}{R} \operatorname{sign}(z_o)\, dx_o\, dy_o\, dz_o \qquad (4.1\text{-}8)$$

where

$$R = [(x-x_o)^2 + (y-y_o)^2 + (z-z_o)^2]^{1/2} \qquad (4.1\text{-}9)$$

A computer program to evaluate this integral written during the course of this thesis is discussed in the next chapter. However, the direct numerical evaluation of the integral for cases of interest is not appropriate for lucid interpretation of the overall characteristics of the generated sound field and of how these characteristics depend on the parameters that enter into Eqs. (4.1-2)-(4.1-4). Consequently, the remainder of the present chapter is devoted to determining an analytic approximate solution of the inhomogeneous wave equation.

4.2 Fourier Transform Solution of Inhomogeneous Wave Equation

Sustained contemplation of several references (Bath 1968, Bleistein and Handelsman 1975, and Bleistein 1984) suggests that a combination of Fourier transforms and Green's function techniques can provide the solution in a convenient integral form, which is equivalent to that of Eq. (4.1-8), but which is more conducive to analytical approximations. This solution can be subsequently simplified to obtain approximate solutions appropriate to relevant limiting cases.

4.2.1 Fourier Integral Representation

As of a first step, the solution for p(x,y,z,t) is expressed as a triple inverse Fourier transform of a function of "frequency domain variables" ω, α_x, and α_y, along with the depth coordinate z,

$$p(x,y,z,t) = \int_{-\infty}^{\infty} \int_{-\infty}^{\infty} \int_{-\infty}^{\infty} \psi(\alpha_x,\alpha_y,z,\omega)\, e^{-i\omega t}\, e^{i\alpha_x x}\, e^{i\alpha_y y}\, d\omega\ d\alpha_x\, d\alpha_y \qquad (4.2\text{-}1)$$

The function ψ appearing in the integrand is required to satisfy an ordinary differential equation in z, i.e.,

$$\frac{d^2\psi}{dz^2} + l^2\psi = \frac{i\omega\beta}{c_p} Q \qquad (4.2\text{-}2)$$

where l abbreviates a combination of the three frequency domain variables such that,

$$l^2 = (\omega/c)^2 - \alpha_x^2 - \alpha_y^2 \qquad (4.2\text{-}3)$$

The symbol Q on the right hand side of Eq. (4.2-2) is identified as the triple Fourier transform of the laser heating function q given in Eq. (4.1-1).

4.2.2. Fourier Transform of the Heating Function

To demonstrate how an explicit expression for Q is obtained, the transformation is first defined as an integral of some other intermediate transformation,

$$Q = (1/8\pi^3) \int_{-\infty}^{\infty} I(\alpha_x,\alpha_y,z,t)\, e^{i\omega t}\, dt \qquad (4.2\text{-}4a)$$

$$I = \int_{-\infty}^{\infty} \int_{-\infty}^{\infty} q(x,y,z.t)\, e^{-i\alpha_x x}\, e^{-i\alpha_y y}\, dx\, dy \qquad (4.2\text{-}4b)$$

An inspection of the two terms contained on the right hand side of Eq. (4.1-2) indicates that the second term pertains to an oscillatory excitation of angular frequency ω_B ($=k_x V$) while the first pertains to a null frequency exciter. It is also known from the wave equation (3.2-1) that the source term, as well as the amplitude of the signal generated, depends directly upon the time derivative of q. For all practical purposes (i.e. for the cases in which the charateristic length of the laser pulse, T, is much larger than $1/\omega_B$), we deduce that the effect on the resulting sound excitation due to the second term is far more important than that due to the first.

Hence, we will neglect the first term (which was originally installed to guarantee that the heating pattern q be non-negative) of F_p in (4.1-2) in the following analysis. Furthermore, to comfort the subsequent derivation, it is convenient to reexpress the function F_p, after simplification, as a sum of its complex representations. Thus, with the first term deleted from Eq. (4.1-2), we have

$$F_p(k_xN) = \tfrac{1}{2}K\, e^{ik_xN} + \tfrac{1}{2}K\, e^{-ik_xN} \tag{4.2-5}$$

From here on to the very end of the derivation, we are going to focus on how to obtain the "plus" pressure component, $p^{(+)}$, resulting from the excitation of $q^{(+)}$, which is the "plus" component of the laser heat source and can be obtained from Eq. (4.1-3) by replacing F_p by the first term given in Eq. (4.2-5). The principle for obtaining the "minus" pressure component, $p^{(-)}$, as a result of using $\frac{1}{2}Ke^{-ik_xN}$ for F_p in q is quite similar; the procedure will be briefly discussed afterwards. By virtue of the superposition principle [a basic property of the linear wave equation (3.2-1)], the ultimate solution for p is then represented by the sum of $p^{(+)}$ and $p^{(-)}$.

Substituting Eqs. (4.1-1) and (4.2-5) into Eq. (4.2-4b) for the i-th component only, one obtains

$$I = E_T(t) \int_{-\infty}^{\infty} \int_{-\infty}^{\infty} \tfrac{1}{2}K\, e^{ik_xN}\, E_M(N,y)\, e^{-i\alpha_x x}\, e^{-i\alpha_y y}\, dx\, dy \tag{4.2-6}$$

From Eq. (4.1-4), we note that the integrand is homogeneous in x and y, and from Eq. (4.1-6), that the parameter N varies at a rate identical to that of the parameter x when other variables (z and t) are held constant. The double integration can then be replaced by a product of two single integrations. The y integral is readily done, i.e.,

$$\int_{-\infty}^{\infty} e^{-y^2/L_y^2}\, e^{-i\alpha_y y}\, dy = \pi^{1/2} L_y\, e^{-\frac{1}{4}L_y^2\alpha_y^2} \tag{4.2-7}$$

while the integration over x is converted into one over N (the limits of integration remain the same). The result is given by

$$\int_{-\infty}^{\infty} \tfrac{1}{2}K\, e^{ik_xN}\, e^{-N^2/L_x^2}\, e^{-i\alpha_x x}\, dx$$

$$= \tfrac{1}{2}K\, e^{i\alpha_x z\tan\theta_B} e^{-i\alpha_x Vt} \int_{-\infty}^{\infty} e^{-N^2/L_x^2}\, e^{i(k_x-\alpha_x)N}\, dN$$

$$= \tfrac{1}{2}\pi^{1/2}K\, L_x\, e^{i\alpha_x z\tan\theta_B}\, e^{-i\alpha_x Vt}\, e^{-\frac{1}{4}L_x^2(\alpha_x-k_x)^2} \qquad (4.2\text{-}8)$$

Using Eqs. (4.2-6), (4.2-7), and (4.2-8) in (4.2-4a), and carrying out the t integration in a manner similar to what has been done in Eq. (4.2-8), we arrive at the Fourier transform of q as

$$Q = G(\alpha_x,\alpha_y,\omega)\, e^{(-\mu_c + i\alpha_x\tan\theta_B)z} \qquad (4.2\text{-}9a)$$

$$G = \frac{KL_xL_yT}{16\pi^{3/2}}\, e^{-\frac{1}{4}T^2(\omega-\alpha_xV)^2}\, e^{-\frac{1}{4}L_x^2(\alpha_x-k_x)^2}\, e^{-\frac{1}{4}L_y^2\alpha_y^2} \qquad (4.2\text{-}9b)$$

With this expression for Q substituted back into Eq. (4.2-2), we are about ready to solve for the ordinary equation for ψ.

4.2.3 Interpretation of the Causality Condition

Recall that ψ must conform to causality. To study the properties that l should possess to satisfy this causality condition, the following integral suggested by Pierce and Posey (1971) can be used for illustration.

$$I_0 = \int_{-\infty+i\epsilon}^{\infty+i\epsilon} \psi\, e^{-i\omega t}\, d\omega \qquad (4.2\text{-}10)$$

Notice that Eq. (4.2-10) is actually a sub-integral extracted from Eq. (4.2-1). Here, the device "$i\epsilon$" (ϵ being positive) is used in the limits to avoid the integration contour crossing over any branch points or poles lying on the real axis in the ω-plane, so the new path becomes the line defined by $\mathrm{Im}(\omega)=\epsilon$ (see Fig. 4.2). The prerequisite here is that one can choose an ϵ sufficiently large to enable the new integration path to pass above all poles and branch lines of the integrand, so the

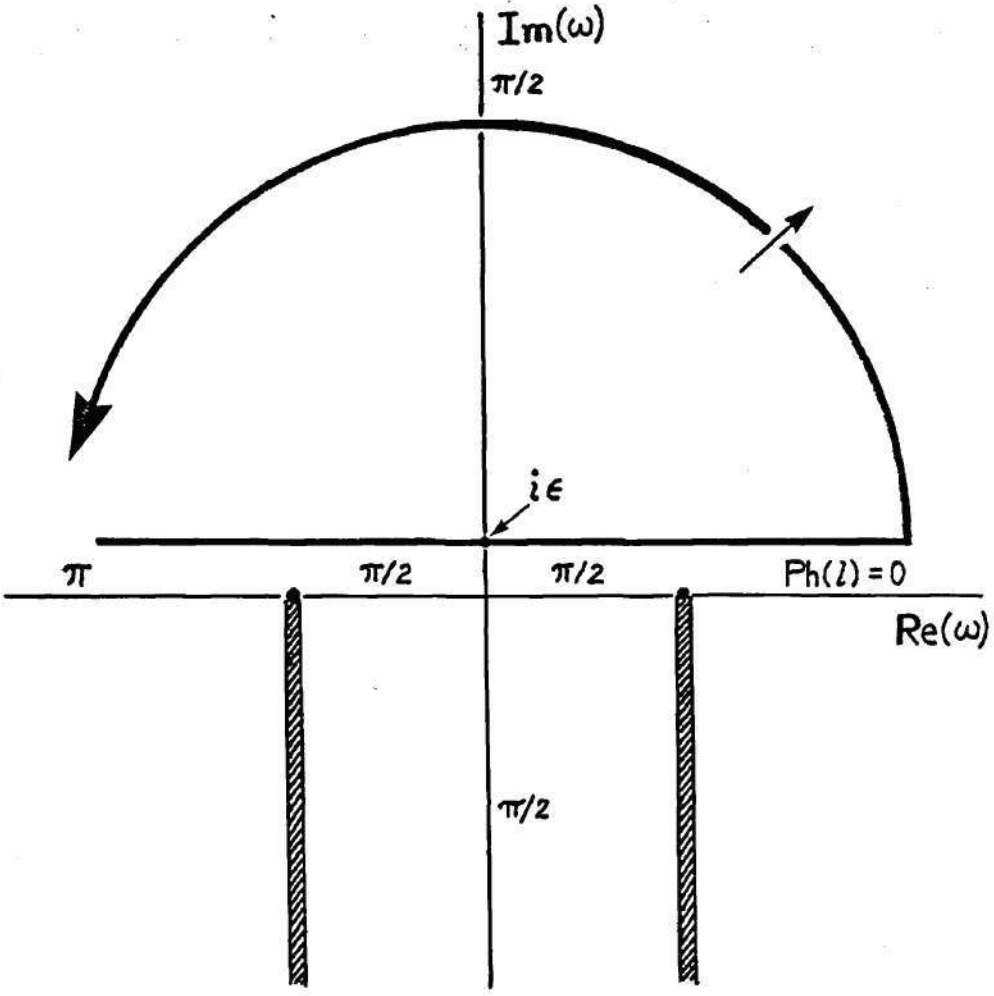

FIGURE 4.2 Sketch of complex ω-plane showing selected contour for interpretation of the causality condition and determination of the phase Ph(l) of quantity $l=[(\omega/c)^2-\alpha_x^2-\alpha_y^2]^{1/2}$ for fixed real α_x and α_y.

integral I_0 over ω vanishes identically at times $t < t_0$, where t_0 corresponds to the time at which the source is initially turned on. Undoubtly, the function ψ must possesses the properties which are in agreement to what has just been mentioned. It follows that for all $z > 0$, the complex function $\psi e^{-i\omega t_0}$ should be analytic everywhere in the portion of the upper half ω-plane which is above the line $\mathrm{Im}(\omega) = \epsilon$ and the magnitude $|\psi e^{-i\omega t_0}|$ should vanish as $\mathrm{Im}(\omega)$ tends to infinity when $t < t_0$. This requirement specifically suggests that ψ should have no singularities including poles or branch lines in the region for which $\mathrm{Im}(\omega) > \epsilon$. The fact that the above indeed guarantees causality can be verified from Eq. (4.2-1), since p(x,y,z,t) will then vanish for all $t < t_0$.

In conventional acoustic theories, the causality condition is interpreted as requiring that p behave as an outgoing wave in regions remote from the source (radiation condition). Thus, the conditions we mentioned earlier for p in Sec. 4.1 are translated into ones that are suitable for ψ, i.e.

$$\psi|_{z=0} = 0 \tag{4.2-11a}$$

$$\psi|_{z\to\infty} \to (\text{something})\, e^{ilz} \tag{4.2-11b}$$

where the "something" represents some function of variables other than z.

Insofar as to be consistent with the previous descriptions concerning properties of ψ required to conform with causality, we are able to determine the proper choices for the phase of l. One may first consider the cases when both α_x and α_y are real. From the condition given in Eq. (4.2-11b), l should have no branch lines above the line $\mathrm{Im}(\omega) = \epsilon$ in the complex ω-plane. Furthermore, the phase of l has to approach either $+\mathrm{Ph}(\omega)$ or $-\mathrm{Ph}(\omega)$ [see Eq. (4.2-3)] as $|\omega|$ approaches infinity for $\mathrm{Im}(\omega) > 0$. To ascertain which of these two possibilities is applicable, one again relies on the causality condition. By letting $z\to\infty$ and $\omega\to i\infty$, one can deduce that $\mathrm{Ph}(l) = +\mathrm{Ph}(\omega)$. Next from the requirement of analytic continuity (Carrier, Krook, and

Pearson 1966), we deduce that $\mathrm{Ph}(l) = \mathrm{Ph}(\omega)$ everywhere as $|\omega| \to \infty$ except at the very bottom of the ω-plane between the two branch lines (see Fig. 4.2). Specifically, we identify that, along the real axis of the ω-plane, the specification for the phase of l in the case for which both α_x and α_y are real is given by

$$\mathrm{Ph}(l) = \mathrm{Ph}(\omega) \quad |(\alpha_x^2 + \alpha_y^2)^{\frac{1}{2}}| < |\omega|$$

$$= \pi/2 \qquad |(\alpha_x^2 + \alpha_y^2)^{\frac{1}{2}}| > |\omega| \tag{4.2-12}$$

The specification can be extended to include complex values of α_x and/or α_y by placing branch lines in the complex α_x- or α_y-planes and requiring that the phase of l be continuous everywhere except at these branch lines. However, it will be found that the information provided by (4.2-12) is actually by far more useful than that for complex α_x and α_y in regard to the subsequent derivation.

4.2.4 Green's Function Technique

The solution to ψ is to be found with the Green's function technique (Pierce 1981, pp. 469-471). One first expresses the solution as a superposition of contributions received from weighted point sources located at all values of $z=z_o$. Each of these contributions is represented by the product of the monopole-amplitude function, $Q_g|_{z=z_o}$, per unit length of z and a Green's function, $g(z|z_o)$, which satisfies both an ordinary differential equation

$$\left(\frac{d^2}{dz^2} + l^2\right) g(z|z_o) = \delta(z-z_o) \tag{4.2-13}$$

for all z, and the radiation condition as $|z| \to \infty$. The $\delta(\ )$ in Eq. (4.2-13) is the Dirac Delta function. The weighting function $Q_g(z)$ is constructed directly from the product of the factor $i\omega\beta/c_p$ and Q in accordance to the mirror image method (note that Q is defined only for the positive half-space). The pressure release condition at the water surface ($z=0$) requires that $Q_g(z)$ for $z < 0$ equals the negative image of

$(i\omega\beta/c_p)Q$ for $z > 0$. Thus,

$$Q_g = (i\omega\beta/c_p)\, G(\alpha_x,\alpha_y,\omega)\, \mathrm{sign}(z)\, e^{(-\mu_e + i\alpha_x \tan\theta_B)|z|} \tag{4.2-14}$$

where the function sign( ) is equal to $+1$ or -1 depending on the sign of its argument and is a natural outcome of the mirror image reconstruction. The resulting solution for ψ found by combining Eqs. (4.2-2), (4.2-13), and (4.2-14), along with the proper solution for the Green's function, is

$$\psi(\alpha_x,\alpha_y,z,\omega) = (i\omega\beta/c_p)\, G \int_{-\infty}^{\infty} \mathrm{sign}(z_o)\, e^{(-\mu_e + i\alpha_x \tan\theta_B)|z_o|}\, g(z\,|\,z_o)\, dz_o \tag{4.2-15a}$$

$$g(z\,|\,z_o) = \frac{1}{2il}\, e^{il\,|z-z_o|} \tag{4.2-15b}$$

Based on the preceding discussion in Sec. 4.2.3, we are able to evaluate the integral in Eq. (4.2-15a) in a closed form, i.e.,

$$\psi(\alpha_x,\alpha_y,z,\omega) = \psi_1 + \psi_2 \tag{4.2-16a}$$

$$\psi_1(\alpha_x,\alpha_y,z,\omega) = -(i\omega\beta/c_p)\, G\, \frac{e^{ilz}}{(-\mu_e + i\alpha_x \tan\theta_B)^2 + l^2} \tag{4.2-16b}$$

$$\psi_2(\alpha_x,\alpha_y,z,\omega) = (i\omega\beta/c_p)\, G\, \frac{e^{(-\mu_e + i\alpha_x \tan\theta_B)z}}{(-\mu_e + i\alpha_x \tan\theta_B)^2 + l^2} \tag{4.2-16c}$$

Eqations. (4.2-16), show that ψ_1 and ψ_2 cancel each other when $z=0$. This is in accord with the requirement that the Fourier integral expression [Eq. (4.2-1)] for p satisfy the pressure release boundary condition at the surface. The main concern here is for the circumstances for which $e^{-\mu_e z} << 1$ and the observation point is reasonably remote from the water surface such that the depth z is moderately greater than the effective absorption length of the laser beam. Therefore, we neglect the component ψ_2 in the derivation given below for the inverse Fourier transform. Furthermore, it is

demonstrated in a subsequent section (Sec. 5.2) that the asymptotic expression for p, derived based on the replacement of ψ by ψ_1, tends to zero as the receiving depth moves toward the surface (z=0) at moderate distance r away from the source. Regardless of feature of the result, one may roughly quantify the parameters for which the moderate depth approximation is valid along the axis of the sound beam. For instance, if the range r of interest is greater than 10 meters and if μ is equal to 13.7 m^{-1}, then the beaming angle θ_B can be taken as low as $\tan^{-1}[-(13.7x10)\ln(0.1)]$ degrees (or $\simeq 1°$) such that the approximation is still valid. Note also that within the region of interest for which the moderate depth approximation is applicable, the transduction process of laser light to sound (through heat) is more or less completed.

4.3 Approximate Aymptotic Solutions for the High Frequency Limit

In the preceding chapter, we mentioned that the aim of the present design is to generate an acoustic signal which is of high directivity and narrow band so as to increase the signal to noise ratio. This goal can be achieved if the initially created acoustic pulse possesses all the "high frequency" characteristics. What we really mean when referring to the term "high frequency" is that the wave period is small compared with the duration of the created pulse. An alternate interpretation of this condition is that one of the characteristic lengths L_x of the sound source is much greater than the wavelength λ_B of the generated acoustic signal. Furthermore, we will asssume that the other two lengths characterizing the dimension of the source, L_y and cT, and the distance r between the receiver and the "source," are large when compared with λ_B. However, we will see later that the theory for small L_y can be obtained in a very similar manner to the large L_y case, given that r is sufficiently remote from the "source." The conditions that will always be retained for the analyses are the "high frequency" limiting condition (i.e. $\lambda_B << L_x$) and the long-irradiation-duration condition. The conditions for the present study are summarized as:

$$k_x L_x, \quad k_x L_y, \quad k_x r, \quad k_x cT >> 1 \tag{4.3-1}$$

Here $k_x = k_B \cos\theta_B$ is assumed to be always positive without loss of generality (θ_B is within the range of $[0, \pi/2]$). To derive an asymptotic expression for $p^{(+)}$ consistent with the limiting cases (4.3-1), we substitute the result for ψ [Eq. (4.2-16b)] into (4.2-1) and subsequently rewrite the Fourier integral representation for the pressure in a convenient form:

$$p^{(+)} \simeq \frac{-i\beta K L_x L_y T}{16 c_p \pi^{3/2}} \int_{-\infty}^{\infty} \int_{-\infty}^{\infty} \int_{-\infty}^{\infty} F\, e^{\Phi}\, d\omega\ d\alpha_x\, d\alpha_y \tag{4.3-2a}$$

$$\Phi = i\alpha_x x + i\alpha_y y + ilz - i\omega t$$

$$- \tfrac{1}{4} T^2(\omega - \alpha_x V)^2 - \tfrac{1}{4} L_x^2(\alpha_x - k_x)^2 - \tfrac{1}{4} L_y^2 \alpha_y^2 \tag{4.3-2b}$$

$$F = \frac{\omega}{(-\mu_e + i\alpha_x \tan\theta_B)^2 + l^2} \tag{4.3-2c}$$

4.3.1 Nondimensionalization

Since the characteristic time is $1/k_x c$ and the characteristic length is $1/k_x$, we shall develop our theory in a system of units such that distances are measured in units of $1/k_x$ and time is measured in units of $1/k_x c$. Thus, a set of nondimensionalized variables (with superscript-asterisk) are defined as follows

$$x = x^*/k_x; \quad y = y^*/k_x; \quad z = z^*/k_x; \quad r = r^*/k_x;$$

$$L_x = L_x^*/k_x; \quad L_y = L_y^*/k_x; \quad \mu_e = k_x \mu_e^*;$$

$$\alpha_x = k_x \alpha_x^*; \quad \alpha_y = k_x \alpha_y^*; \quad l = k_x l^*;$$

$$t = t^*/k_x c; \quad T = T^*/k_x c; \quad \omega = k_x c \omega^* \tag{4.3-3}$$

$$l^{*2} = \omega^{*2} - \alpha_x^{*2} - \alpha_y^{*2} \tag{4.3-4}$$

The nondimensionalized version of Eqs. (4.3-2) then becomes

$$p^{(+)*} = \frac{-iL_x^* L_y^* T^*}{16\pi^{3/2}} \int_{-\infty}^{\infty} \int_{-\infty}^{\infty} \int_{-\infty}^{\infty} F^* e^{\Phi^*} d\omega^* d\alpha_x^* d\alpha_y^* \tag{4.3-5a}$$

$$\Phi^* = i\alpha_x^* x^* + i\alpha_y^* y^* + il^* z^* - i\omega^* t^*$$

$$- \tfrac{1}{4}T^{*2}(\omega^* - \alpha_x^* M)^2 - \tfrac{1}{4}L_x^{*2}(\alpha_x^* - 1)^2 - \tfrac{1}{4}L_y^{*2}\alpha_y^{*2} \tag{4.3-5b}$$

$$F^* = \frac{\omega^*}{(-\mu_e^* + i\alpha_x^* \gamma)^2 + l^{*2}} \tag{4.3-5c}$$

where

$$M = V/c = \sec\theta_B \tag{4.3-6a}$$

$$\gamma = \tan\theta_B \tag{4.3-6b}$$

Here, the pressure component $p^{(+)}$ is nondimensionalized with respect to the source constant K, frequency parameter k_x, and properties of water such that

$$p^{(+)*} = p^{(+)} c_p k_x / \beta c K \tag{4.3-7}$$

To carry on the derivation at this point, we shall first omit the superfluous asterisks in Eqs. (4.3-5) and carefully distinguish the new meaning of each of the unasterisked variables from the old ones. The high frequency limiting condition mentioned earlier, along with the large depositional area, long range, and long irradiation conditions are translated into

$$L_x,\ L_y,\ r,\ T >> 1 \tag{4.3-8}$$

4.3.2 Saddle Point Approximations

The leading behavior of $p^{(+)}$ consistent with the limiting conditions stated in Eq. (4.3-8) can be best studied in the context of the saddle point method (DeBruijn

1981; Bender and Orszag 1978). The method is based on the premise that there exist, in the complex ω-α_x-α_y space, some points at which the exponential term e^{Φ} [given by Eqs. (4.3-5a) and (4.3-5b)] sharply peaks as the parameters such as appeared in (4.3-8) approach infinity. If such a behavior for e^{Φ} indeed exists, then the analysis will be proceeded by deforming the original contour of integration on the "landscape" of e^{Φ} to one that goes along the path of ssteepest descents as the contour progresses away from each of the saddle points. After performing the contour deformation, one can reasonably approximate the integral (4.3-5a), whose integration domain spans the entire real-space of ω, α_x, and α_y, with the integration of the approximate versions of the original integrand function over ω, α_x, α_y in the small neighborhoods of the saddle points along the corresponding path of steepest descents.

To perform the saddle point analysis for the present problem, we rewrite the exponent Φ in terms of our latest notion for the symbols (nondimensionalized but without the asterisk indicator):

$$\Phi = i\alpha_x x + i\alpha_y y + ilz - i\omega t$$

$$- \tfrac{1}{4}T^2(\omega-\alpha_x V)^2 - \tfrac{1}{4}L_x^2(\alpha_x-1)^2 - \tfrac{1}{4}L_y^2\alpha_y^2 \qquad (4.3\text{-}9)$$

Here, Φ is defined as a funciton of three independent variables ω, α_x, and α_y. Also, $l=[\omega^2-\alpha_x^2-\alpha_y^2]^{1/2}e^{PH(l)}$ and the information regarding PH(l), the phase of l, can be found in Sec. 4.2.3.

For the upcoming discussion, the partial derivatives of l with respect to ω, α_x, or α_y, up to the second order, are obtained from Eq. (4.3-4). These results are summarized as follows:

$$l_{\omega} = \omega/l; \quad l_{\alpha_x} = -\alpha_x/l; \quad l_{\alpha_y} = -\alpha_y/l \qquad (4.3\text{-}10a)$$

$$l_{\omega\omega} = -(\alpha_x^2+\alpha_y^2)l^{-3}; \quad l_{\alpha_x\alpha_x} = (\alpha_y^2-\omega^2)l^{-3}; \quad l_{\alpha_y\alpha_y} = (\alpha_x^2-\omega^2)l^{-3};$$

$$l_{\omega\alpha_x} = \omega\alpha_x l^{-3}; \quad l_{\alpha_x\alpha_y} = -\alpha_x\alpha_y l^{-3}; \quad l_{\alpha_y\omega} = \alpha_y\omega l^{-3} \tag{4.3-10b}$$

To pinpoint the saddle points, we first obtain the partial derivatives of Φ with respect to the three frequency domain variables [with incorporation of the identities given in Eq. (4.3-10a) for l_ω, l_{α_x}, and l_{α_y}]

$$\Phi_\omega = iz\omega/l - it - \tfrac{1}{2}T^2(\omega-\alpha_x M) \tag{4.3-11a}$$

$$\Phi_{\alpha_x} = ix - iz\alpha_x/l + \tfrac{1}{2}MT^2(\omega-\alpha_x) - \tfrac{1}{2}L_x^2(\alpha_x-1) \tag{4.3-11b}$$

$$\Phi_{\alpha_y} = iy - iz\alpha_y/l - \tfrac{1}{2}L_y^2\alpha_y \tag{4.3-11c}$$

Next, we need to set these derivatives to zero and solve for the resulting three simultaneous equations. Any root, $(\omega, \alpha_x, \alpha_y)$, which satifies the three equations simultaneously can be considered as one of saddle points of e^{Φ}. An inspection of Eqs. (4.3-11) indicates that these equations are nonlinear and therefore are in general difficult to be solved in closed form if no further simplifications are made. From general physical insight, however, the peak amplitude of the generated acoustic signal at any instance is anticipated to occur in the center of the sound beam when t=r (this corresponds to t=r/c in terms of original physical quantities) ; the center of the beam is defined as the intersection of the two constraints:

(i) $y = 0$

(ii) $x = z/\tan\theta_B = r\cos\theta_B$

Furthermore, we expect that the resulting sound beam generated consistent with assumption (4.3-8) and the situation in which the beaming angle θ_B is sufficiently large would be a relatively thin beam pointing in the direction θ_B. Therefore, it is conceivable that the sound field in the dominant region and time can be well predicted under the assumptions of t=r, y=0, and $x=z/\tan\theta_B$. With such a simplifications incorporated into Eqs. (4.3-11), we locate the single saddle point on the "landscape" of e^{Φ_B}; this point, indicated with the subscript "sp", is given by

$$(\omega, \alpha_x, \alpha_y)_{sp} = (M, 1, 0) \tag{4.3-12a}$$

$$l_{sp} = \gamma = (M^2 - 1)^{1/2} \tag{4.3-12b}$$

Next, the analysis proceeds by approximating the exponent Φ in Eq. (4.3-9) with Taylor series expansions to second order about the saddle point. At the same time, the slowly varying portion of the integrand in (4.3-5a) is approximated by its value at the saddle point. Thus, we have

$$F \sim F_{sp} \tag{4.3-13a}$$

$$\begin{aligned}\Phi \sim\ & \Phi_{sp} + \Delta\omega\,(\Phi_{\omega})_{sp} + \Delta\alpha_x(\Phi_{\alpha_x})_{sp} + \Delta\alpha_y(\Phi_{\alpha_y})_{sp} \\ & + \tfrac{1}{2}(\Delta\omega)^2(\Phi_{\omega\omega})_{sp} + \tfrac{1}{2}(\Delta\alpha_x)^2(\Phi_{\alpha_x\alpha_x})_{sp} + \tfrac{1}{2}(\Delta\alpha_y)^2(\Phi_{\alpha_y\alpha_y})_{sp} \\ & + \Delta\omega\Delta\alpha_x(\Phi_{\omega\alpha_x})_{sp} + \Delta\alpha_x\Delta\alpha_y(\Phi_{\alpha_x\alpha_y})_{sp} + \Delta\alpha_y\Delta\omega\,(\Phi_{\alpha_y\omega})_{sp}\end{aligned} \tag{4.3-13b}$$

where

$$\Delta\omega = \omega - M \tag{4.3-14a}$$

$$\Delta\alpha_x = \alpha_x - 1 \tag{4.3-14b}$$

$$\Delta\alpha_y = \alpha_y \tag{4.3-14c}$$

and where the subscript "sp" abbreviates "saddle point." The differentials in Eq. (4.3-5a) are transformed into the appropriate ones for the new integration variables defined in Eqs. (4.3-14), i.e.,

$$d\omega\ d\alpha_x\, d\alpha_y = d(\Delta\omega)\, d(\Delta\alpha_x)\, d(\Delta\alpha_y) \tag{4.3-15}$$

Evaluating the partial derivatives of l [see Eqs. (4.3-10)] at the saddle point, we find

$$l_{\omega} = M\gamma^{-1}; \quad l_{\alpha_x} = -\gamma^{-1}; \quad l_{\alpha_y} = 0 \tag{4.3-16a}$$

$$l_{\omega\omega} = -\gamma^{-3}; \quad l_{\alpha_x\alpha_x} = -M^2\gamma^{-3}; \quad l_{\alpha_y\alpha_y} = -\gamma^{-1};$$

$$l_{\alpha_x\omega} = M\gamma^{-3}; \quad l_{\alpha_x\alpha_y} = 0; \quad l_{\alpha_y\omega} = 0 \tag{4.3-16b}$$

With the symbols M and γ [see Eqs. (4.3-6)], we can explicitly express the term F_{sp} given in Eq. (4.3-12a) as

$$F_{sp} = \frac{M}{\mu_e^2 - i2\mu_e\gamma} \tag{4.3-17}$$

The coefficients of the expansions in Eq. (4.3-13b) (namely the functions Φ itself and its derivatives with respect to the "frequency space variables" evaluated at the saddle point) are obtained directly from Eqs. (4.3-9) using the chain rule and the information provided by Eqs. (4.3-16). For the purpose of easier referral in the subsequent derivation, the coefficients pertinent to Φ are renamed with symbols A_{ij} and are identified as

$$A_{00} = (\Phi)_{sp} = ix + i\gamma z - iMt \tag{4.3-18a}$$

$$A_{10} = (\Phi_{\omega})_{sp} = iM\gamma^{-1}z - it \tag{4.3-18b}$$

$$A_{20} = (\Phi_{\alpha_x})_{sp} = ix - i\gamma^{-1}z \tag{4.3-18c}$$

$$A_{30} = (\Phi_{\alpha_y})_{sp} = iy \tag{4.3-18d}$$

$$A_{11} = \tfrac{1}{2}(\Phi_{\omega\omega})_{sp} = -\tfrac{1}{2}i\gamma^{-3}z - \tfrac{1}{4}T^2 \tag{4.3-18e}$$

$$A_{22} = \tfrac{1}{2}(\Phi_{\alpha_x\alpha_x})_{sp} = -\tfrac{1}{2}iM^2\gamma^{-3}z - \tfrac{1}{4}M^2T^2 - \tfrac{1}{4}L_x^2 \tag{4.3-18f}$$

$$A_{33} = \tfrac{1}{2}(\Phi_{\alpha_y\alpha_y})_{sp} = -\tfrac{1}{2}i\gamma^{-1}z - \tfrac{1}{4}L_y^2 \tag{4.3-18g}$$

$$A_{12} = (\Phi_{\alpha_x\omega})_{sp} = iM\gamma^{-3}z + \tfrac{1}{2}MT^2 \tag{4.3-18h}$$

$$A_{23} = (\Phi_{\alpha_x\alpha_y})_{sp} = 0 \tag{4.3-18i}$$

$$A_{31} = (\Phi_{\alpha_y\omega})_{sp} = 0 \tag{4.3-18j}$$

The double subscripts adopted in defining the symbols A_{ij} are chosen such that the subscript "0" corresponds to the function of interest without derivatives and subscripts "1", "2", and "3" correspond to the functions' derivatives with respect to ω, α_x, and α_y, respectively.

4.3.3 Asymptotic Expression for Representative Term $p^{(+)}$ in Solution

To proceed with the asymptotic analysis for $p^{(+)}$, we insert the approximations given in Eqs. (4.3-12) into the triple Fourier integral (4.3-5a). In order to be consistent with the limiting cases considered in Eq. (4.3-8), the regions of integration over $\Delta\omega$, $\Delta\alpha_x$, and $\Delta\alpha_y$ are defined within a cube of dimensions 2ϵ(ϵ being a very small positive number) centered at the origin in the $\Delta\omega$-$\Delta\alpha_x$-$\Delta\alpha_y$ space. The integration limits corresponding to the cubical region are then extended from $[-\epsilon,\epsilon]$ to $[-\infty,\infty]$ since doing so will introduce only an exponentially small error to the approximation. Thus, the expression for the pressure component $p^{(+)}$ becomes

$$p^{(+)} \simeq \frac{-iL_xL_yTM}{16\pi^{3/2}(\mu_c^2 - i2\mu_c\gamma)}\, e^{A_{00}}\, I_1\, I_2 \tag{4.3-19}$$

where we use the abbreviations

$$I_1 = \int_{-\infty}^{\infty} e^{A_{30}\Delta\alpha_y} e^{A_{33}(\Delta\alpha_y)^2}\, d(\Delta\alpha_y) \tag{4.3-20a}$$

$$I_2 = \int_{-\infty}^{\infty}\int_{-\infty}^{\infty} e^{H(\Delta\omega,\Delta\alpha_x)}\, d(\Delta\omega)\, d(\Delta\alpha_x) \tag{4.3-20b}$$

$$H(\Delta\omega,\Delta\alpha_x) = A_{10}\Delta\omega + A_{20}\Delta\alpha_x$$

$$+ A_{11}(\Delta\omega)^2 + A_{22}(\Delta\alpha_x)^2 + A_{12}\Delta\omega\Delta\alpha_x \qquad (4.3\text{-}20c)$$

In Eq. (4.3-20a), the coefficients of the exponents (A_{30} and A_{33}) are complex in nature; nevertheless, the integral can be evaluated in a closed form by a proper choice of contour deformation. Since the integration is to be performed along the real axis from $-\infty$ to ∞ in the α_y-plane, the requirement that the real part of the coefficient A_{33} be negative is a necessary condition for the existence of this integral. Fortunately, this condition is guaranteed by the expression given in Eq. (4.3-18g). The result of the integration is

$$I_1 = \pi^{1/2}\,(-A_{33})^{-1/2}\,e^{-A_{30}^2/4A_{33}} \qquad (4.3\text{-}21)$$

For the double integral I_2 in Eq. (4.3-20b), both the $\Delta\omega$ and $\Delta\alpha_x$ integrations are performed along the real axes in the $\Delta\omega$- and $\Delta\alpha_x$-planes respectively. Similarly, the requirements on the coefficient A_{ij} in guaranteeing the existence of this integral are that $\mathrm{Re}(A_{11})<0$ and $\mathrm{Re}(A_{22})<0$, which are assured by Eqs. (4.3-18e) and (4.3-18f). Since there are no poles and branch cuts in the plane of $\Delta\omega$ and $\Delta\alpha_x$, the double integrations in I_2 are performed one by one (in arbitrary order) in the same way as that done for I_1. The result, expressed in terms of A_{ij}, is symmetric in $\Delta\omega$ and $\Delta\alpha_x$ and is identified as

$$I_2 = 2\pi\,e^{\Psi}\,[4A_{11}A_{22} - A_{12}^2]^{-1/2} \qquad (4.3\text{-}22a)$$

$$\Psi = -\,[A_{10}^2A_{22} + A_{20}^2A_{11} - A_{10}A_{20}A_{12}]/[4A_{11}A_{22} - A_{12}^2] \qquad (4.3\text{-}22b)$$

Substituting Eqs. (4.3-21) and (4.3-22) into (4.3-19), we obtain the asymptotic expression for $p^{(+)}$ within the sound beam and at times close to the dominant arrival.

4.3.4 Asymptotic Solution in Terms of Nondimensionalized Parameters

Before entering into the study of what we can learn regarding the

characteristics of the sound beam generated from the result given by Eqs. (4.3-19) through (4.3-22), we would like to briefly discuss how the other pressure component, $p^{(-)}$, is obtained. The techniques used for deriving $p^{(-)}$ are identical to those used for $p^{(+)}$, except that somewhere along the line, the signs of few terms need to be changed: For the derivation of $p^{(-)}$, the appropriate modifications to Eqs. (4.2-6)-(4.3-2) are obtained by replacing "k_x" by "$-k_x$." The nondimensionalization is still done in the previous manner [for instance, $x=x^*/k_x$, but not $x=x^*/(-k_x)$]; then, we determine that the "–1" appearing in both (4.3-9) and (4.3-10c) will have to be replaced by "+1." Doing such, the saddle point at which e^{Φ} sharply peaks is identified as $(\omega, \alpha_x, \alpha_y)_{sp} = (-M, -1, 0)$. The expansions carried out in Eqs. (4.3-12) become those about the new saddle point [i.e., the minus signs in Eqs. (4.3-13) are to be switched to plus signs]. The derivation will remain the same thereafter until one gets to Eqs. (4.3-16). From the phase consideration of l discussed in Sec. 4.2.3, we determine

$$l_{sp} = -\tan\theta_B = -\gamma \tag{4.3-23}$$

since for the range of θ_B considered, γ is positive. Therefore, all the signs for the terms on the right sides of the equalities in (4.3-16b) are to be altered. Next, Eq. (4.3-17) should read

$$F_{sp} = \frac{-M}{\mu_e^2 + i2\mu_e\gamma} \tag{4.3-24}$$

because now F_{sp} represents the expression (4.3-9c) evaluated at the new saddle point. For Eqs. (4.3-18) the first-derivative coefficients A_{10}, A_{20}, and A_{30} are left unchanged, while the second-derivative coefficients, as well as A_{00}, are replaced by their corresponding complex conjugates. At this point, we can conclude that, based on the previous expressions in Eqs. (4.3-19), (4.3-21), and (4.3-22), the solution $p^{(-)}$ is in fact the complex conjugate of that for $p^{(+)}$.

Since $p^{(+)}$ and $p^{(-)}$ are a complex conjugate pair, the final asymptotic expression for p, which is the sum of $p^{(+)}$ and $p^{(-)}$, under the presently considered "high frequency" limiting circumstance, is equal to twice the real part of $p^{(+)}$ [or $p^{(-)}$]. The result is summarized as follows:

$$p = 2\,\mathrm{Re}\,\{p^{(+)}\} \tag{4.3-25a}$$

$$p^{(+)} = \frac{-iL_y MT\gamma}{2(\mu_e^2 - i2\mu_e\gamma)\xi_1\xi_2}\, e^{\Phi_1} \tag{4.3-25b}$$

$$\Phi_1 = i(x+\gamma z-Mt) - (x+\gamma z-Mt)^2/L_x^2 - y^2/\xi_1^2 - (Mz-\gamma t)^2/\xi_2^2 \tag{4.3-25c}$$

where

$$\xi_1^2 = L_y^2 + i2\gamma^{-1}z \tag{4.3-26a}$$

$$\xi_2^2 = (\gamma T)^2 + i2\gamma^{-1}z \tag{4.3-26b}$$

4.3.5 Asymptotic Expression for Acoustic Pressure p

Note that all items presented in Eqs. (4.3-25) and (4.3-26) remain in their nondimensionalized form. To translate these expressions back to dimensional form, the supersript asterisks are re-installed to all the variables in these equations (except for M and γ), including the two new parameters, ξ_1 and ξ_2. Next, the identities in Eqs. (4.3-3) and (4.3-7), along with $\xi_1^* = k_x\xi_1$ and $\xi_2^* = k_x\xi_2$, are used in these equations to obtain:

$$p = 2\,\mathrm{Re}\,\{p^{(+)}\} \tag{4.3-27a}$$

$$p^{(+)} = \left(\frac{L_y L_w}{\xi_1\xi_2}\right) \frac{-i(c\beta K/2c_p\mu)\cos^2\theta_B}{[\mu/k_B - i\sin 2\theta_B]}\, e^{\Phi_1} \tag{4.3-27b}$$

$$\Phi_1 = ik_xN + N^2/L_x^2 - y^2/\xi_1^2 - (z/\cos\theta_B - ct\tan\theta_B)^2/\xi_2^2 \tag{4.3-27c}$$

where

$$\xi_1^2 = L_y^2 + i2z/k_B\sin\theta_B \tag{4.3-28a}$$

$$\xi_2^2 = L_w^2 + i2z/k_B\sin\theta_B \tag{4.3-28b}$$

Here, the parameters $L_w = VT\sin\theta_B$ and $N = x + z\tan\theta_B - Vt$ are used and are consistent with their previous definitions [see Sec. 3.4.1 and Eq. (4.1-6)].

4.4 Acoustic Disturbance when Laser Track Widths are Very Narrow

At this point, we will make a pause on the discussion of the $k_xL_y >> 1$ case and reconsider the Fourier integral in Eqs. (4.3-2) for a different set of limiting conditions:

$$k_xL_x,\quad k_xr,\quad k_xcT >> 1\ ;\qquad k_xL_y << 1 \tag{4.4-1}$$

An asymptotic expression for $p^{(+)}$ can be obtained using the previously introduced saddle point method. For the ease of manipulation, we again use nondimensionlized variables. The results described in Sec. 4.3.1 are fully applicable here except that Eq. (4.3-8) must be rewritten as

$$L_x,\quad r,\quad T >> 1\ ;\qquad L_y << 1 \tag{4.4-2}$$

To perform the saddle point analysis, we first group the terms in Φ of Eq. (4.3-9) into two convenient categories such that the terms containing large parameters will be put together separately from the others. Hence, we have

$$\Phi = \Phi_A + \Phi_B \tag{4.4-3a}$$

$$\Phi_A = i\alpha_x x + i\alpha_y y + ilz - i\omega t - \tfrac{1}{4}T^2(\omega-\alpha_x M)^2 - \tfrac{1}{4}L_x^2(\alpha_x-1)^2 \tag{4.4-3b}$$

$$\Phi_B = -\tfrac{1}{4}L_y^2\alpha_y^2 \tag{4.4-3c}$$

Since it is more likely for Φ_A to be dominantly responsible for the sharp peak on the "landscape" of e^{Φ} (described in Sec. 4.3.2), we are going to exclusively look for the saddle points of e^{Φ_A} as the conditions in (4.4-2) are met. To pinpoint the saddle points, we obtain the partial derivatives of Φ_A with respect to the variables ω, α_x, and α_y similar to the ones presented in Eqs. (4.3-11). In fact, the three first-order derivatives we will get here for Φ_A are almost identical to Eqs. (4.3-11) only dropping the term $\frac{1}{2}L_y^2\alpha_y$ in Eq. (4.3-11c). The next step will be to solve for the sets of ω, α_x, and α_y for which these first derivatives vanish simultaneously. Again we encounter the previous difficulty that the equations to be solved are nonlinear and somewhat cumbersome. Analogous simplifications to those done previously of these nonlinear equations are essential for locating any existing saddle point. The dominant region for the acoustic field is expected to be in the vicinity of the surface of a cone whose axis coincides with the x-axis and whose apex angle is equal to θ_B (see Fig. 4.3). Since a spherical coordinate system as presented in Fig. 4.3 is likely to be more convenient for the present discussion, we will write the constraint equation for the dominant region in terms of such a coordinate system. These contraints are (i) $t = r$ and (ii) $x = r\cos\theta_B$. Thus we locate the single saddle point on the "landscape" of e^{Φ} :

$$(\omega, \alpha_x, \alpha_y)_{sp} = (M, 1, \gamma\sin\phi) \tag{4.4-4}$$

Consequently, we have $l_{sp} = \gamma\cos\phi$ from Eq. (4.3-4). The symbols M and γ retain their previous definitions [Eqs. (4.3-6)]. Next, we proceed with steps similar to those given in Eqs. (4.3-13); the F in (4.3-13a) is replaced by Fe^{Φ_B} and all Φ's in (4.3-13b) are replaced by Φ_A. Furthermore, the slowly varying portion of the integral in Eq. (4.3-9) can be explicitly expressed as

$$(Fe^{\Phi_B})_{sp} = \frac{M}{\mu_e^2 - i2\mu_e\gamma - \gamma^2\sin^2\phi}\; e^{-\frac{1}{4}(L_y\gamma\sin\phi)^2} \tag{4.4-5}$$

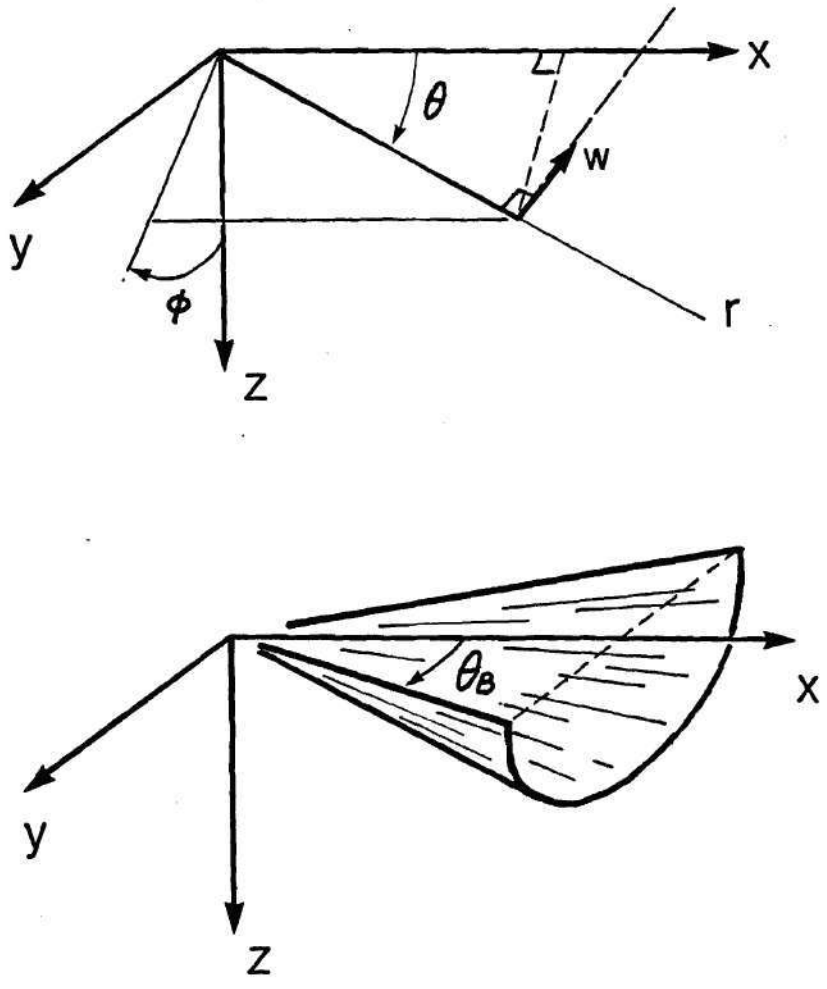

FIGURE 4.3 Geometry for cases when laser track width L_y is very narrow. (a) Cylindrical coordinate system. (b) Resulting sound field concentrated near surface of Mach cone.

The coefficients analogous to those written in Eqs. (4.3-18) for the present small L_y case are identified as follows:

$$A_{00} = (\Phi)_{sp} = iM(r-t) - \tfrac{1}{4}L_y^2\gamma^2\sin^2\phi \tag{4.4-6a}$$

$$A_{10} = (\Phi_{\omega})_{sp} = iMzl_{sp}^{-1} - it \tag{4.4-6b}$$

$$A_{20} = (\Phi_{\alpha_x})_{sp} = ix - izl_{sp}^{-1} \tag{4.4-6c}$$

$$A_{30} = (\Phi_{\alpha_y})_{sp} = 0 \tag{4.4-6d}$$

$$A_{11} = \tfrac{1}{2}(\Phi_{\omega\omega})_{sp} = -i\tfrac{1}{2}(1+\gamma^2\sin^2\phi)zl_{sp}^{-3} - \tfrac{1}{4}T^2 \tag{4.4-6e}$$

$$A_{22} = \tfrac{1}{2}(\Phi_{\alpha_x\alpha_x})_{sp} = i\tfrac{1}{2}(\gamma^2\sin^2\phi - M^2)zl_{sp}^{-3} - \tfrac{1}{4}M^2T^2 - \tfrac{1}{4}L_x^2 \tag{4.4-6f}$$

$$A_{33} = \tfrac{1}{2}(\Phi_{\alpha_y\alpha_y})_{sp} = -i\tfrac{1}{2}\gamma^2zl_{sp}^{-3} \tag{4.4-6g}$$

$$A_{12} = (\Phi_{\alpha_x\omega})_{sp} = iMzl_{sp}^{-3} + \tfrac{1}{2}MT^2 \tag{4.4-6h}$$

$$A_{23} = (\Phi_{\alpha_x\alpha_y})_{sp} = -izl_{sp}^{-3}\gamma\sin\phi \tag{4.4-6i}$$

$$A_{31} = (\Phi_{\alpha_y\omega})_{sp} = iMzl_{sp}^{-3}\gamma\sin\phi \tag{4.4-6j}$$

Up to this stage, our derivation for the asymptotic expression for the pressure component $p^{(+)}$ can be summarized as

$$p^{(+)} \simeq \frac{-iL_xL_yTM}{16\pi^{3/2}(\mu_e^2 - i2\mu_e\gamma - \gamma^2\sin^2\phi)}\, e^{A_{00}}\, e^{-\frac{1}{4}(L_y\gamma\sin\phi)^2}\, I_3 \tag{4.4-7}$$

where

$$I_3 = \int_{-\infty}^{\infty}\int_{-\infty}^{\infty}\int_{-\infty}^{\infty} e^{H(\Delta\omega,\Delta\alpha_x,\Delta\alpha_y)}\, d(\Delta\omega)\, d(\Delta\alpha_x)\, d(\Delta\alpha_y) \tag{4.4-8a}$$

$$H(\Delta\omega,\Delta\alpha_x,\Delta\alpha_y) = A_{10}\Delta\omega + A_{20}\Delta\alpha_x + A_{30}\Delta\alpha_y + A_{11}(\Delta\omega)^2 + A_{22}(\Delta\alpha_x)^2$$

$$+ A_{33}(\Delta\alpha_y)^2 + A_{12}\Delta\omega\Delta\alpha_x + A_{23}\Delta\alpha_x\Delta\alpha_y + A_{31}\Delta\omega\Delta\alpha_y \qquad (4.4\text{-}8b)$$

For the triple integral I_3 in Eq. (4.4-8a), the $\Delta\omega$, $\Delta\alpha_x$, and $\Delta\alpha_y$ integrations are performed along the real axes in the $\Delta\omega$-, $\Delta\alpha_x$-, and $\Delta\alpha_y$-planes, respectively. Since there are no poles and branch cuts in any of these three complex planes, the three integrations in I_3 can be performed one by one (in arbitrary order). The steps for actually performing these integrations are straight forward but tedious and therefore are not shown here. The result of the integration is identified to be

$$I_3 = 2\pi^{3/2} D^{-1/2} e^{\Psi} \qquad (4.4\text{-}9)$$

where we have used the abbreviations:

$$D = -4A_{11}A_{22}A_{33} + A_{12}^2A_{33} + A_{23}^2A_{11} + A_{31}^2A_{22} - A_{12}A_{23}A_{31} \qquad (4.4\text{-}10a)$$

$$\Psi = (4D)^{-1}[4A_{11}A_{22}A_{30}^2 + 4A_{22}A_{33}A_{10}^2 + 4A_{11}A_{33}A_{20}^2$$

$$- A_{10}^2A_{23}^2 - A_{20}^2A_{31}^2 - A_{30}^2A_{12}^2 + 2A_{10}A_{20}(A_{23}A_{31}-2A_{12}A_{33})$$

$$+ 2A_{10}A_{20}(A_{12}A_{31}-2A_{23}A_{11}) + 2A_{10}A_{20}(A_{12}A_{23}-2A_{13}A_{22})] \qquad (4.4\text{-}10b)$$

Replacing the coefficients A_{ij} in Eqs. (4.4-10) by those given in Eqs. (4.4-6) and dropping all terms containing A_{30} reduce the expressions for D and Ψ to

$$D = (1/8)iz l_{sp}^{-3} L_x^2 [(\gamma T)^2 + i2z l_{sp}^{-1}] \qquad (4.4\text{-}11a)$$

$$\Psi = (MA_{10}+A_{20})^2/L_x^2 + \gamma^2A_{10}^2/\xi^2$$

$$= -(r-t)^2/(L_x\cos\theta_B)^2 - \gamma^2(Mz l_{sp}^{-1} - t)^2/\xi^2 \qquad (4.4\text{-}11b)$$

where

$$\xi^2 = (\gamma T)^2 + i2zl_{sp}^{-1} \tag{4.4-12}$$

Substituting Eqs. (4.4-11) and (4.4-12) into (4.4-9) and subsequently using this result in Eq. (4.4-7), we obtain the asymptotic expression for $p^{(+)}$ in the limits of large L_x, r, T, and small L_y for the acoustic disturbance near the dominant time and region described before. The counterpart of $p^{(+)}$, $p^{(-)}$, can be determined using the approach of Sec. 4.3.4 for the large L_y case; $p^{(-)}$ is again the complex conjugate of $p^{(+)}$ obtained above.

Finally, we use the identities stated in Eqs. (4.3-3) and (4.3-4) to translate the expressions in Eqs. (4.4-11) and (4.4-12) back to the dimensional form. The overall asymptotic solution for the acoustic pressure, expressed in terms of actual physical variables, is summarized as follows:

$$p = 2\,\mathrm{Re}\,\{p^{(+)}\} \tag{4.4-13a}$$

$$p^{(+)} = \frac{L_w}{\xi} \frac{-(c\beta K L_y/2c_p\mu)\cos^2\theta_B\cos\phi}{(2r/k_B)^{1/2}\,[\sigma - i\sin 2\theta_B - (4\sigma)^{-1}\sin^2 2\theta_B\sin\phi]}\; e^{\Phi_2} \tag{4.4-13b}$$

$$\Phi_2 = i\pi/4 + ik_B(r - ct) - \tfrac{1}{4}k_B^2 L_y^2\sin^2\theta_B\sin^2\phi$$

$$- (r - ct)^2/(L_x\cos\theta_B)^2 - (Mz/\cos\phi - ct\,\tan\theta_B)^2/\xi^2 \tag{4.4-13c}$$

where

$$\xi^2 = L_w^2 + i2z/k_B\sin\theta_B\cos\phi \tag{4.4-14}$$

CHAPTER V

IMPLICATIONS AND NUMERICAL VERIFICATION OF THE TRANSIENT ANALYTICAL MODEL

The solution for the pressure perturbation resulting from the idealized heating model Eq. (4.1-1) appropriate to the moderate-depth approximation ($e^{-\mu_e z} << 1$) is pursued in Chap. IV. There the assumptions are that the length of the heating configuration in the x direction L_x is sufficiently large to include a great number of heating ripples (laser light-slabs) and that the net distance VT traveled by the configuration and the propagation distance r are large compared with the dominant acoustic wavelength λ_B of the generated signal. Regarding the length of L_y the theory is developed for both the limiting conditions $k_x L_y >> 1$ and $k_x L_y << 1$.

In this chapter, the features of the sound beam resulting from the proposed method of sequentially and temporally depositing laser energy at the water surface are investigated via an extensive study of the present theory for the idealized model of heat deposition. The investigation begins with a brief note on the theoretical limitations of the mathematical analysis. Following that is a scrutiny of the characteristics of the Gaussian beams resulting from the idealized model. The peak pressure amplitude appearing in the center of the beam as a function of propagation distance and beaming angle is then studied, from which some quantitative estimates are provided. And the optoacoustic transduction efficiency is rechecked with the refined heating model.

To check the approximations made in the analytical prediction of the resulting sound beam for various cases, a general code for evaluating the threefold integral in Eq. (2.6-1) numerically for the heating function $\partial q/\partial t$ was developed. A complete program listing for one particular example is provided in Appendix A. This code is used liberally to spot check the analytical result and to explore the

limitations of analytical approximations.

5.1 Theoretical Limitations of the Analytical Model

In our saddle point approximations, it was assumed that the variation of F in Eq. (4.3-2c) is negligible over the region of integration, i.e. the space enclosed by the little cube of dimensions 2ϵ mentioned in Sec. 4.3.3. This assumption would be acceptable if the zeroth order term of the expansion of F about the saddle point is large compared with the first order terms (and all other higher order terms) over the region in which the magnitude of the second order quantities in the exponent Φ are small. The point concerning exactly how large the zeroth order term should be relative to the higher order terms to guarantee the validity of the approximation depends on how large each of the large parameters contained in the exponents is. Here, we would like to develop criteria which roughly delimits the relative sizes of the parameters L_x, L_y, T, and r versus the magnitude of μ such that the result obtain so far for the idealized heating configuration would be applicable.

The asymptotic analysis leading to the solution described in Sec. 4.3.5 (for $k_xL_y>>1$) was carried out based on a single saddle point (M,1,0). However, this very location satisfies all equations in (4.3-11) exactly only if the listener is located right on the beam center. For those locations which are off the beam axis, this saddle point itself is an approximation. Therefore, it would be difficult to develop validity criteria for them in terms of the thought described in the previous paragraph. It is conceivable, however, such approximation for these off-axis locations would be acceptable if (i) the theory for on-axis locations is acceptable and (ii) these locations are "not too far away" from the beam axis. Since condition (ii) is too imprecise for analytical verification, in later sections we verify these results by direct numerical integration.

Similar to the large L_y case, the saddle point location (M, 1, $\gamma\sin\phi$) for $k_xL_y<<1$ is exact only for receiver locations right on the surface of the cone

sketched in Fig. 4.3. Off the cone surface, the analytical predictions have to be checked by numerical means.

In the analysis below, we only consider the case for $k_x L_y >> 1$. The analysis for the small L_y situation is analogous, so one can generalize from the large L_y study without much difficulty. The analysis is done in a nondimensionalized manner for simplicity sake; therefore, we consider the version of F given in Eq. (4.3-5c). Letting $F = \omega/D$, one can identify D as

$$D = (-\mu_e + i\alpha_x\gamma)^2 + l^2 \tag{5.1-1}$$

The various derivatives of F with respect to the three integration variables are listed in the following:

$$F_\omega = (1 - FD_\omega)/D \tag{5.1-2a}$$

$$F_{\alpha_x} = - FD_{\alpha_x}/D \tag{5.1-2b}$$

$$F_{\alpha_y} = - FD_{\alpha_y}/D \tag{5.1-2c}$$

$$F_{\alpha_y\alpha_y} = - (FD_{\alpha_y\alpha_y} + 2F_{\alpha_y} D_{\alpha_y}) /D \tag{5.1-2d}$$

where the derivatives for D are obtained from definition (5.1-1) as

$$D_\omega = 2\omega; \qquad D_{\alpha_x} = 2i\gamma (-\mu_e + i\alpha_x\gamma) - 2\alpha_x;$$

$$D_{\alpha_y} = - 2\alpha_y; \quad D_{\alpha_y\alpha_y} = - 2 \tag{5.1-3}$$

Considering the large L_y situation [condition (4.3-8)], at the saddle point, where$(\omega,\alpha_x,\alpha_y) = (M,1,0)$, we have

$$|D|_{sp} = |\mu_e^2 - 2i\mu_e\gamma| \tag{5.1-4}$$

$$|D_{\omega}|_{sp} = 2M; \quad |D_{\alpha_x}|_{sp} = |2i\mu_e\gamma + 2M^2|;$$

$$|D_{\alpha_y}|_{sp} = 0; \quad |D_{\alpha_y\alpha_y}|_{sp} = 2 \tag{5.1-5}$$

and hence from Eqs. (5.1-2), we have

$$|F_{\omega}/F|_{sp} = M^{-1} \mid 1 - FD_{\omega} \mid_{sp} = M^{-1} \mid \mu_e^2 - 2i\mu_e\gamma - 2M^2|/|D|_{sp} \tag{5.1-6a}$$

$$|F_{\alpha_x}/F|_{sp} = |D_{\alpha_x}/D|_{sp} = \mid 2i\mu_e\gamma + 2M^2|/|D|_{sp} \tag{5.1-6b}$$

$$|F_{\alpha_y}/F|_{sp} = |D_{\alpha_y}/D|_{sp} = 0 \tag{5.1-6c}$$

$$|F_{\alpha_y\alpha_y}/F|_{sp} = |D_{\alpha_y\alpha_y}/D|_{sp} = 2/|D|_{sp} \tag{5.1-6d}$$

where

$$|F|_{sp} = M/|D|_{sp} \tag{5.1-7}$$

Next, we study the deviation of the function F from F_{sp} along the path of steepest descents near the saddle point. To find the description for the steepest descents in each of the three complex planes while the other two Δ-variables are kept zero, we devise the following three positive real quantities ζ_1^2, ζ_2^2, and ζ_3^2 such that

$$\zeta_1^2 = \Delta\omega^2 \left[i\tfrac{1}{2}M^{-1}\gamma^{-2}s + \tfrac{1}{4}T^2\right] \tag{5.1-8a}$$

$$\zeta_2^2 = \Delta\alpha_x^2 \left[i\tfrac{1}{2}M\gamma^{-2}s + \tfrac{1}{4}M^2T^2 + \tfrac{1}{4}L_x^2\right] \tag{5.1-8b}$$

$$\zeta_3^2 = \Delta\alpha_y^2 \left[i\tfrac{1}{2}M^{-1}s + \tfrac{1}{4}L_y^2\right] \tag{5.1-8c}$$

Here, the combinations on the right side of the equations are constructed according to the second order coefficients A_{11}, A_{22}, and A_{33}, respectively, given in Eqs. (4.3-18). The validity criterion for the analysis is taken to be such that F deviates from F_{sp} by

no more than 20 percent in the vicinity of saddle point within the region:

$$|\zeta_1^2| < 3 \tag{5.1-9a}$$

$$|\zeta_2^2| < 3 \tag{5.1-9b}$$

$$|\zeta_3^2| < 3 \tag{5.1-9c}$$

The value 3 used on the right side of the three inequalities (5.1-9) is chosen based on the knowledge that contributions to the saddle point integral received from the portions of steepest descent beyond the point at which the second order factor drops to $1/e^3$ of its peak value are negligible. Since the value of F in the neighborhood of the saddle point can be expressed by its truncated Taylor series about that point, the difference between F and F_{sp} is approximately written as

$$F - F_{sp} \simeq \Delta\omega\,(F_\omega)_{sp} + \Delta\alpha_x\,(F_{\alpha_x})_{sp} + (\Delta\alpha_y)^2\,(\tfrac{1}{2}F_{\alpha_y\alpha_y})_{sp} \tag{5.1-10}$$

Using the above stated validity criterion, we can write

$$|\Delta\omega|\,|F_\omega/F|_{sp} < 0.2 \tag{5.1-11a}$$

$$|\Delta\alpha_x|\,|F_{\alpha_x}/F|_{sp} < 0.2 \tag{5.1-11b}$$

$$|\Delta\alpha_y|^2\,|\tfrac{1}{2}F_{\alpha_y\alpha_y}/F|_{sp} < 0.2 \tag{5.1-11c}$$

where the region of interest for $|\Delta\omega|$, $|\Delta\alpha_x|$, and $|\Delta\alpha_y|^2$ are defined by Eqs. (5.1-8) and (5.1-9). Using that information along with Eqs. (5.1-6) and subsequently rewriting everything in terms of actual physical parameters, we obtain the following three criteria (again, we use the symbol σ to denote the combination μ/k_B):

$$\frac{20(3^{1/2})\tan\theta_B}{[(k_BL_w)^4 + 4(k_Bs)^2]^{1/4}} < \frac{\sigma\,(\sigma^2 + \sin^2 2\theta_B)^{1/2}}{[(\sigma^2 - 2M^{-2})^2 + \sigma^2\sin^2 2\theta_B]^{1/2}} \tag{5.1-12a}$$

$$\frac{20(3^{1/2})\sin 2\theta_B}{[k_B^4(L_w^2+L_x^2\sin^2\theta_B)^2 + 4(k_Bs)^2]^{1/4}} < \frac{\sigma\,(\sigma^2+\sin^2 2\theta_B)^{1/2}}{(1+\sigma^2\gamma^2)^{1/2}} \qquad (5.1\text{-}12b)$$

$$\frac{60\cos^2\theta_B}{[(k_BL_y)^4 + 4(k_Bs)^2]^{1/2}} < \sigma\,(\sigma^2+\sin^2 2\theta_B)^{1/2} \qquad (5.1\text{-}12c)$$

In the limit $\sigma << 1$ and moderate values of θ_B ($\theta_B < \pi/4$), we have

$$\frac{20(3^{1/2})}{[(k_BL_w)^4 + 4(k_Bs)^2]^{1/4}} < \sigma \qquad (5.1\text{-}13a)$$

$$\frac{20(3^{1/2})}{[k_B^4(L_w^2+L_x^2\sin^2\theta_B)^2 + 4(k_Bs)^2]^{1/4}} < \sigma \qquad (5.1\text{-}13b)$$

$$\frac{30}{[(k_BL_y)^4 + 4(k_Bs)^2]^{1/2}} < \sigma\tan\theta_B \qquad (5.1\text{-}13c)$$

If both σ and θ_B are very small compared to unity, the criteria become

$$\frac{40(3^{1/2})\,\theta_B}{[(k_BL_w)^4 + 4(k_Bs)^2]^{1/4}} < \sigma\,(\sigma^2+4\theta_B^2)^{1/2} \qquad (5.1\text{-}14a)$$

$$\frac{40(3^{1/2})\,\theta_B}{[k_B^4(c^2T^2+L_x^2)^2\theta_B^4 + 4(k_Bs)^2]^{1/4}} < \sigma\,(\sigma^2+4\theta_B^2)^{1/2} \qquad (5.1\text{-}14b)$$

$$\frac{60}{[(k_BL_y)^4 + 4(k_Bs)^2]^{1/2}} < \sigma\,(\sigma^2+4\theta_B^2)^{1/2} \qquad (5.1\text{-}14c)$$

Recall that all the above criteria are only meaningful for verifying the solution for locations on the beam axis. In Eqs. (5.1-13) and (5.1-14), the small σ ($=\mu/k_B$) case is inspected. Since μ is the only non-varying quantity in the denominator of F in Eq. (4.3-2c), one naturally expects that complication would arise regarding the application of the saddle point approximation when σ gets very small. One can also observe that the condition (5.1-13a) [or (5.1-14a)] automatically guarantees condition (5.1-13a) [or (5.1-14b)] to be true regardless of the value of L_x. Although the present study does not suggest a definitive constraint on the value of L_x, an appropriate suggestion is that the length should be long enough to contain at least five cycles of

heating ripples.

In the far field, where the effects of $(k_B s)^{-1/2}$ is enough to overcome the smallness of σ, Eqs. (5.1-13) indicates that the values for T and L_y can be taken as arbitrarily small. In the near field where s is very small, however, T and L_y have to stand alone (with no help from the $k_B s$ term) and contend with the small σ. This is the situation where the validity conditions may become very stringent. For example, taking a blue-green laser at 10kHz acoustic frequency and at $\theta_B = 20°$ ($k_B = 41.2$ m^{-1} and $\sigma = 0.0024$), the nearfield ($k_B s \simeq 0$) conditions require that $L_y > 4.5$ meters and $T > 0.63$ seconds. Such requirements on pulse duration time T, as well as the corresponding travel distance VT, are clearly unrealistic, but one should bear in mind that the approximations were introduced for large range propagation. Our interests are primarily in the Fresnel region and farfield region where s is large. In cases where σ is relatively moderate, the theory certainly is able to cover a wider range in the near field for reasonable sizes of L_y and T.

For extremely small beaming angle, the conditions (5.1-14) impose no additional constraints, other than that L_y may need to be set longer.

5.2 Sound Beam Predictions

The preceding section indicates what sort of restrictions regarding the relative sizes of the controlled parameters involved in the saddle analysis are inherently placed on the theory derived in Chapter IV for the idealized model of a heating configuration. Here, we study the predicted pressure disturbances resulting from the model in the limits of both large and small $k_x L_y$. The results obtained at the ends of Secs. 4.3 and 4.4 are summarized below for convenience of referral and given a more lucid interpretation.

5.2.1 Sound Beam Prediction for $k_x L_y >> 1$

The pressure disturbance described by Eqs. (4.3-27) and (4.3-28) can be

expressed

$$p = 2\,\mathrm{Re}\,\{p^{(+)}\} \tag{5.2-1a}$$

$$p^{(+)} = (\mathrm{Const.})\,(\mathrm{PWF})\,(\mathrm{PE})\,(\mathrm{BE})\,(\mathrm{SF}) \tag{5.2-1b}$$

where the five factors are identified as being a multiplicative constant (Const.), a plane wave factor (PWF), a pulse envelope (PE), a beam envelope (BE), and a spreading factor (SF). The constant is given by

$$\mathrm{Const.} = \frac{Ek_B}{2\pi^{5/2} n L_y c T}\,\frac{\beta c^2}{c_p}\,\frac{-i\cos^2\theta_B}{[(\omega/k_B) - i\sin 2\theta_B]} \tag{5.2-2}$$

where $k_B = k_x/\cos\theta_B$ is the dominant wavenumber of the sound in the beam (which is propagating obliquely downward at an angle of θ_B with the horizontal).

The plane wave factor in Eq. (5.2-1) corresponds to a plane wave of angular frequency $\omega_B = ck_B$ propagating in the direction of the center line of the beam and is given by

$$\mathrm{PWF} = e^{i(k_B s - \omega_B t)} \tag{5.2-3}$$

where $s = x\cos\theta_B + z\sin\theta_B$ is the distance along the sound beam from the origin. This plane wave is amplitude modulated in time by a pulse envelope factor

$$\mathrm{PE} = e^{-(s-ct)^2/L_s^2} \tag{5.2-4}$$

where $L_s = L_x\cos\theta_B$ is the characteristic half-length of the pulse along the beam axis; L_s/c is the characteristic half-duration of the pulse. The beam is gaussian in both the y direction and the w direction, where $w = x\sin\theta_B - z\cos\theta_B$ is the transverse coordinate that is perpendicular to both the y direction and the axis of the beam. This Gaussian property causes the plane wave to be encased by a beam envelope factor given by

$$BE = e^{-w^2/\xi_w^2}\, e^{-y^2/\xi_y^2} \tag{5.2-5}$$

Here, in accordance with the well-known properties of Gaussian beams , the lengths ξ_w and ξ_y, whose squares appear in the denominators of the corresponding exponents, are actually complex numbers whose squares have an imaginary part that increases linearly with propagation distance; the appropriate expressions are

$$\xi_w^2 = L_w^2 + i(2s/k_B) \tag{5.2-6a}$$

$$\xi_y^2 = L_y^2 + i(2s/k_B) \tag{5.2-6b}$$

where L_w is the characteristic w-dimension half-width of the beam in the early stages of propagation. The emergence of a spreading factor in the solution, given by

$$SF = \frac{L_w L_y}{\xi_w \xi_y} \tag{5.2-7}$$

is a natural by-product of the requirement that the product, of the Gaussian beam envelope, the plane wave factor, and the spreading factor, should be a solution of the scalar Helmholtz equation.

Figure 5.1 exemplifies a computer-simulated pressure disturbance [based on the formula given in Eqs. (5.2-1)] as a function of the normalized time, $t^* = k_B ct$. The pressure is normalized with part of the constant stated in Eq. (5.2-2) as

$$p^* = \frac{\pi^{5/2} n L_y c T}{E k_B} \frac{c_p}{\beta c^2}\, p \tag{5.2-8}$$

In this particular example, the perturbation is measured at a point on the beam axis (where $w = y = 0$) at a beaming angle $\theta_B = 20°$. The numerical inputs for various parameters are: $n = 10$ cycles, $k_B L_y = k_B L_w = 247.0$, $k_B s = 41167.$, and $\mu/k_B = 0.333$, all of which correspond to the case of having $f_B = 10$ kHz, $\mu = 13.7$ m^{-1}, $s = 1000$ m, and $L_y = L_w = 6$ m (the choice of L_y and L_w, along with that of f_B, places the extent of the Fresnel region of radiation at about 1 km from the origin). The

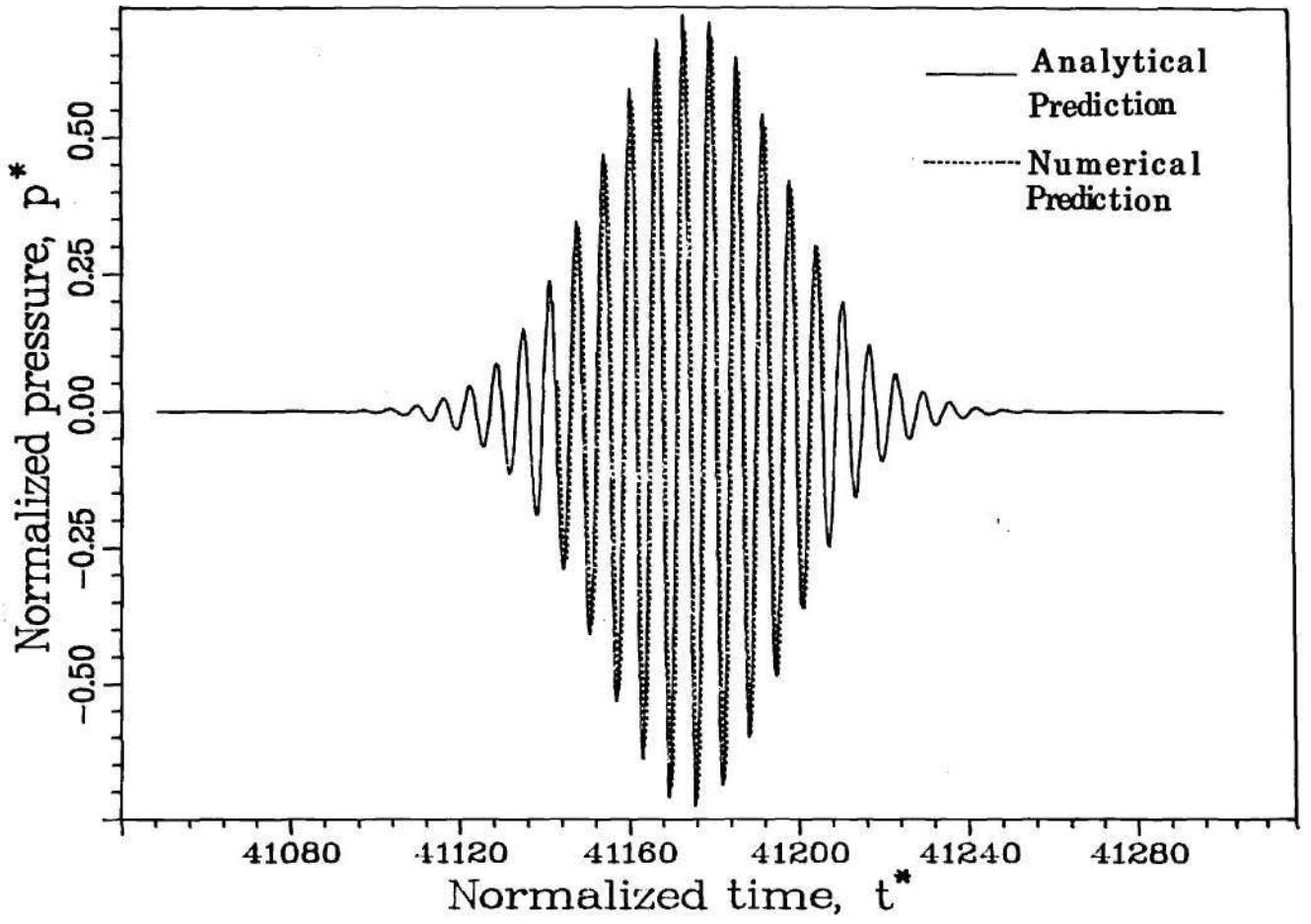

FIGURE 5.1 Computer simulation of acoustic pulse received on beam axis within Fresnel region. Pressure is normalized with respect to the factor appearing in Eq. (5.2-8) and time is normalized with respect to $1/\omega_B$. Numerical values of parameters defining the circumstances of the computation are as defined in the text.

observed pressure perturbation is roughly a narrow band, n-cycle, tone-burst of sound having a band center frequency f_B. Also plotted in this figure is the result predicted by the numerical integration scheme at conditions identical to that described above (dashed line). The numerical result shows good agreement with the analytical theory in predicting the acoustic pulse shape and the signal periodicity. However, a minor shift in time between the two predictions regarding the wave crests in the pulses is observed.

The sound beam defined by Eqs. (5.2-1) up to (5.2-7) is a solution that is valid for the near field in which $s << k_B L_y^2,\ k_B L_w^2$; for the far field in which $s >> k_B L_y^2,\ k_B L_w^2$; as well as for the transitional region from one to the other, in which $s \sim k_B L_y^2,\ k_B L_w^2$. (Numerical verification of this statement is given is Sec. 5.3.) One should also bear in mind that this solution results from the approximation in which the quantities $k_x L_x$, $k_x L_y$, and $k_x cT$ are assumed to be large compared to unity. Here we proceed by inspecting the behavior of the beam in the two extreme cases.

In the near field, the complex characteristic half-lengths, ξ_y and ξ_w, of the beam envelope can be expanded into power series for small values of $s/k_B L_y^2$ and $s/k_B L_w^2$. The factor SF is then accordingly approximated with the lowest order expansion and is identified as being equal to unity, while in the factor BE, the approximations for ξ_y^{-2} and ξ_w^{-2} are taken up to the first order. In doing so, the appropriate simplified version for $p^{(+)}$ becomes

$$p^{(+)}_{near} = \tfrac{1}{2} C_{near}\,(PE)\, e^{-y^2/L_y^2}\, e^{-w^2/L_w^2}\, e^{i\phi_{near}} \tag{5.2-9a}$$

$$C_{near} = \frac{E k_B}{\pi^{5/2} n L_y c T}\ \frac{\beta c^2}{c_p}\ D_{near}(\sigma, \theta_B) \tag{5.2-9b}$$

$$D_{near} = \frac{\cos^2\theta_B}{[(\mu/k_B)^2 + \sin^2 2\theta_B]^{1/2}} \tag{5.2-9c}$$

$$\phi_{near} = \tfrac{1}{2}\pi + \tan^{-1}\left(\frac{k_B \sin 2\theta_B}{\mu}\right) - (2s/k_B)\left(\frac{y^2}{L_y^4} + \frac{w^2}{L_w^4}\right) + k_B s - \omega_B t \tag{5.2-9d}$$

Note that the factor PE retains the original definition given in Eq. (5.2-4).

The amplitude of the nearfield pressure perturbation, $|p|_{near}$, can be obtained by substituting Eq. (5.2-9a) into (5.2-1a) and subsequently taking its absolute value. It can be seen that $|p|_{near}$ resembles a rectangular beam having dimensions $2L_y$ and $2L_w$ in the y and w directions, respectively. In the center of the beam ($y=w=0$), the peak pressure amplitude (where $s=ct$) is given by C_{near}, which is independent of the propagation distance s. This phenomenon is found typically in the nearfield of a vibrating piston in which the surface area has characteristic lengths much greater than the acoustic wavelength.

In regard to the farfield limiting case, the factors ξ_y and ξ_w are similarly expanded into power series except that now the small parameters are $k_B L_y^2/s$ and $k_B L_w^2/s$. Taking the zero order approximation yields $SF \simeq -ik_B L_y L_w/2s$, and the first order approximation for ξ_y^{-2} and ξ_w^{-2} in BE yields the farfield pressure expression as

$$p^{(+)}_{far} = \tfrac{1}{2} C_{far}\,(PE)\, e^{-y^2/(2s/k_B L_y)^2}\, e^{-w^2/(2s/k_B L_w)^2}\, e^{i\phi_{far}} \qquad (5.2\text{-}10a)$$

$$C_{far} = \frac{E k_B^2}{2\pi^{5/2} n s}\,\frac{\beta c^2}{c_p}\, D_{far}(\sigma,\theta_B) \qquad (5.2\text{-}10b)$$

$$D_{far} = \frac{\sin\theta_B \cos\theta_B}{[(\mu/k_B)^2 + \sin^2 2\theta_B]^{1/2}} \qquad (5.2\text{-}10c)$$

$$\phi_{far} = \tan^{-1}\left(\frac{k_B \sin 2\theta_B}{\mu}\right) + (k_B/2s)(y^2 + w^2) + k_B s - \omega_B t \qquad (5.2\text{-}10d)$$

Once again, the pulse envelope factor PE has the same definition as given by Eq. (5.2-4).

From Eqs. (5.2-10), the beam in the farfield is still found to be rectangular in shape; however, both effective edge dimensions of this rectangular cross section tend to increase linearly with the propagation distance s. Hence, the beam widths, θ_y and θ_w, in the two transverse directions, y and w, can be roughly identified as $(2/k_B L_y)$ and $(2/k_B L_w)$, respectively. In addition, the emergence of an s in the denominator of

C_{far} in Eq. (5.2-10b) demonstrates the eventual farfield spherical spreading behavior for the sound beam.

Also, one notices that, as the beam progresses from the near field to the far field, D_{near} evolves into D_{far} such that the factor $\cos\theta_B$ in the numerator of D_{near} is gradually replaced by $\sin\theta_B$. This feature is further discussed and verified numerically in Sec. 5.3.3.

Figure 5.2 gives numerical verification for the beam shape (or beamwidth) in the large L_y situation at locations fairly close to the outer extent of the Fresnel region. Here, the normalized pressure p^* [see Eq. (5.2-8)] is plotted against the distances, k_By and k_Bw, to the beam axis in the y and w directions, respectively. The numerical inputs for n, f_B, k_BL_y, k_BL_w, k_Bs, and μ/k_B for the present study are the same as those in Fig. 5.1; also θ_B is set equal to the same three different values (5°, 10°, and 20°) in both plots. The numerical results, given by the markers, show extremely good agreement with those predicted by the analytical theory. However, the theory does not adequately predict such results as the beam shape in the w direction when $\tan\theta_B < 3L_w/s$.

For a smaller beaming angle, given fixed k_BL_w, the characteristic pulse duration T must be longer. For example, for the parameters described above, one should have $T_{5°} = 2.02\ T_{10°} = 4.16\ T_{20°}$. It is also seen that, if the laser power is kept constant and if the pulse length can be made sufficiently long, one should be able to generate a higher amplitude signal at a shallower beaming angle. This is due to the difference in the degree of the capability to pump the laser energy into the created signal.

An inspection of Eqs. (5.2-1)-(5.2-7) has shown that the solution does not satisfy the pressure release boundary condition at the water surface (when $z=0$). The reason is that, back in the derivation in Sec. 4.2, a moderate depth approximation was assumed and a surfacial term ψ_2 was neglected in the Fourier transform of p, ψ. The importance of ψ_2 is obvious when the condition $e^{-\mu z} << 1$ is no longer satisfied.

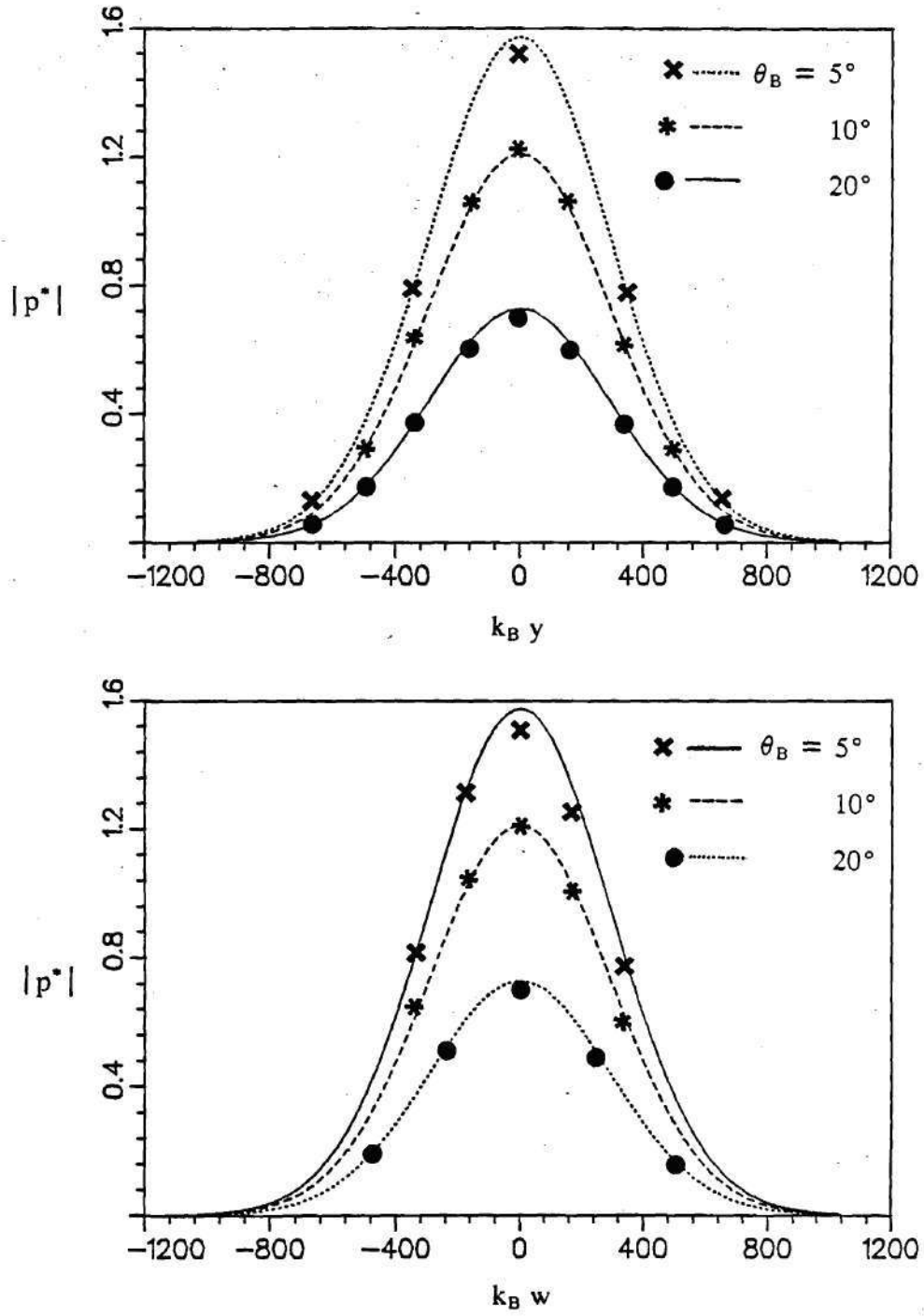

FIGURE 5.2 Beam shape in y and w directions at various beaming directions θ_B for cases $k_B L_y >> 1$.

In particular, the pressure perturbation resulting from ψ_2 is the essential element cancelling the disturbance resulting from ψ_1 (i.e. the moderate depth portion described in the present section) at z=0. The procedure for deriving the additional near-surface term due to ψ_2 is nearly identical to that done in Sec. 4.3 for ψ_1 under the same conditions as posed in Eq. (4.3-1), except that the mathematical complexity is less. Furthermore, the solution exhibited in this section as a result of the Fresnel-region approximation is a thin beam solution in the w direction (also in the y direction). At small distances from the beam axis, the intensity will be considerably smaller. For θ_B not too small compared to unity, say $\tan\theta_B \geq 3L_w/s$, the pressure amplitude drops to a negligible value at values of w that are less than that at which the w axis intersects the surface. Therefore, as long as the beaming angle is not extremely shallow, it is not necessary to retain the near-surface term in the solution. One should also not that the treatment discussed in Chapter IV was not intended for predicting the resulting disturbance for very shallow θ_B, anyway.

5.2.2 Sound Beam Prediction for $k_xL_y << 1$

The pressure disturbance described by Eqs. (4.4-13) and (4.4-14) is rearranged and, once again, presented using the form given in Eqs. (5.2-1) :

$$p = 2\,\mathrm{Re}\,\{p^{(+)}\} \tag{5.2-11a}$$

$$p^{(+)} = (\text{Const.})\ (\text{CWF})\ (\text{PE})\ (\text{BE})\ (\text{SF}) \tag{5.2-11b}$$

where the five factors are identified as being a multiplicative constant (Const.), a cylindrical wave factor (CWF), a pulse envelope (PE), a beam envelope (BE), and a spreading factor (SF). The constant is given by

$$\text{Const.} = \frac{Ek_B^{3/2}}{(8\pi^5)^{1/2}ncT}\ \frac{\beta c^2}{c_p}\ D(\theta_B,\phi,\sigma)\ e^{i\frac{1}{4}\pi} \tag{5.2-12a}$$

$$D = \frac{\cos^2\theta_B\cos\phi}{[\sigma - i\sin2\theta_B - (4\sigma)^{-1}\sin^2 2\theta_B\sin^2\phi]} \tag{5.2-12b}$$

The cylindrical wave factor in Eq. (5.2-11) corresponds to a cylindrical wave of angular frequency $\omega_B = ck_B$ propagating in the directions radially outward from the origin along the surface of the cone portrayed in Fig. 4.3 and is given by

$$CWF = r^{1/2} e^{i(k_B r - \omega_B t)} \tag{5.2-13}$$

where r is the spherical radial coordinate which measures distance along the sound "cone" from the origin. This cylindrical wave is amplitude modulated in time by a pulse envelope factor

$$PE = e^{-(r - ct)^2/L_s^2} \tag{5.2-14}$$

where $L_s = L_x \cos\theta_B$ represents the characteristic half-duration of the pulse when divided by the sound speed c. The beam is Gaussian in both transverse directions to the direction of propagation r. The two directions are the cone surface tangential direction (corresponding to the azimuthal coordinate ϕ) and the w direction, where w is the direction normal to the cone surface and is equal to $x \sin\theta_B - z \cos\theta_B$ when $\phi = 0$ (see Fig. 4.3). (This definition for w is slightly different from that introduced in the previous section.) This Gaussian property causes the cylindrical wave to be encased by a beam envelope factor given by

$$BE = e^{-w^2/\xi^2} e^{-\frac{1}{4}k_B^2 L_y^2 \sin^2\theta_B \sin^2\phi} \tag{5.2-15}$$

(The second factor here can be regarded as one, since we are assuming $k_B L_y << 1$.) Similar to the large L_y case, the length ξ, whose square appears in the denominator of the corresponding exponent, is a complex number whose square has an imaginary part that increases linearly with propagation distance; the appropriate expression is

$$\xi^2 = L_w^2 + i(2r/k_B) \tag{5.2-16}$$

where L_w is the characteristic w-dimension half-thickness of the conical-shell-like

beam in the early stages of propagation. Finally, the spreading effect in the w direction is taken care by the spreading factor in the solution, given by

$$SF = L_w/\xi \tag{5.2-17}$$

In Fig. 5.3, the beam shape for the small L_y case is plotted versus the azimuthal angle ϕ and the normalized w-direction parameter $k_B w$ when ϕ is taken as zero, for two values of θ_B (5° and 20°). The pressure is normalized according to Eq. (5.2-8) and all numerical inputs, except for $k_B L_y$, are taken to be the same as those used before in Fig. 5.2. The value of $k_B L_y$ is set equal to 2.47. Along with the analytical predictions in the plots are the spot-check marks obtained from the numerical code. It can be seen that the analytical theory (which assumed $k_B L_y << 1$) and the numerical predictions are in very good agreement even when $k_B L_y$ is not extremely small compared with unity.

5.2.3 Extended Validity of Wide-Laser-Track Result for Points on Beam Axis

In Secs. 5.2.1 and 5.2.2, the analytical results for the pressure disturbance for the two sets of conditions (i) $k_x L_y >> 1$ and $k_x cT >> 1$ and (ii) $k_x L_y << 1$ and $k_x cT >> 1$ were individually studied (we also refer to them as the large-L_y large-T case and the small-L_y large-T case, respectively). If one only desires predictions for the center of the beam, defined by the intersection of the two constraints $z = x \tan\theta_B$ and $y = 0$, the former case can be used to precisely describe the latter. This can be shown by letting the parameter L_y in the large-L_y large-T solution tend to zero and then comparing it with the small-L_y solution.

Another case studied is that of extremely short pulse duration time, i.e. $k_x cT << 1$, such that a spreading wave in the w direction results. This case is of less interest as the pulse will contain a wide band of frequencies and hence be less detectable unless the actual pulse shape is accurately known. However, the small-T result can be regarded as a building block, because all large-T processes are

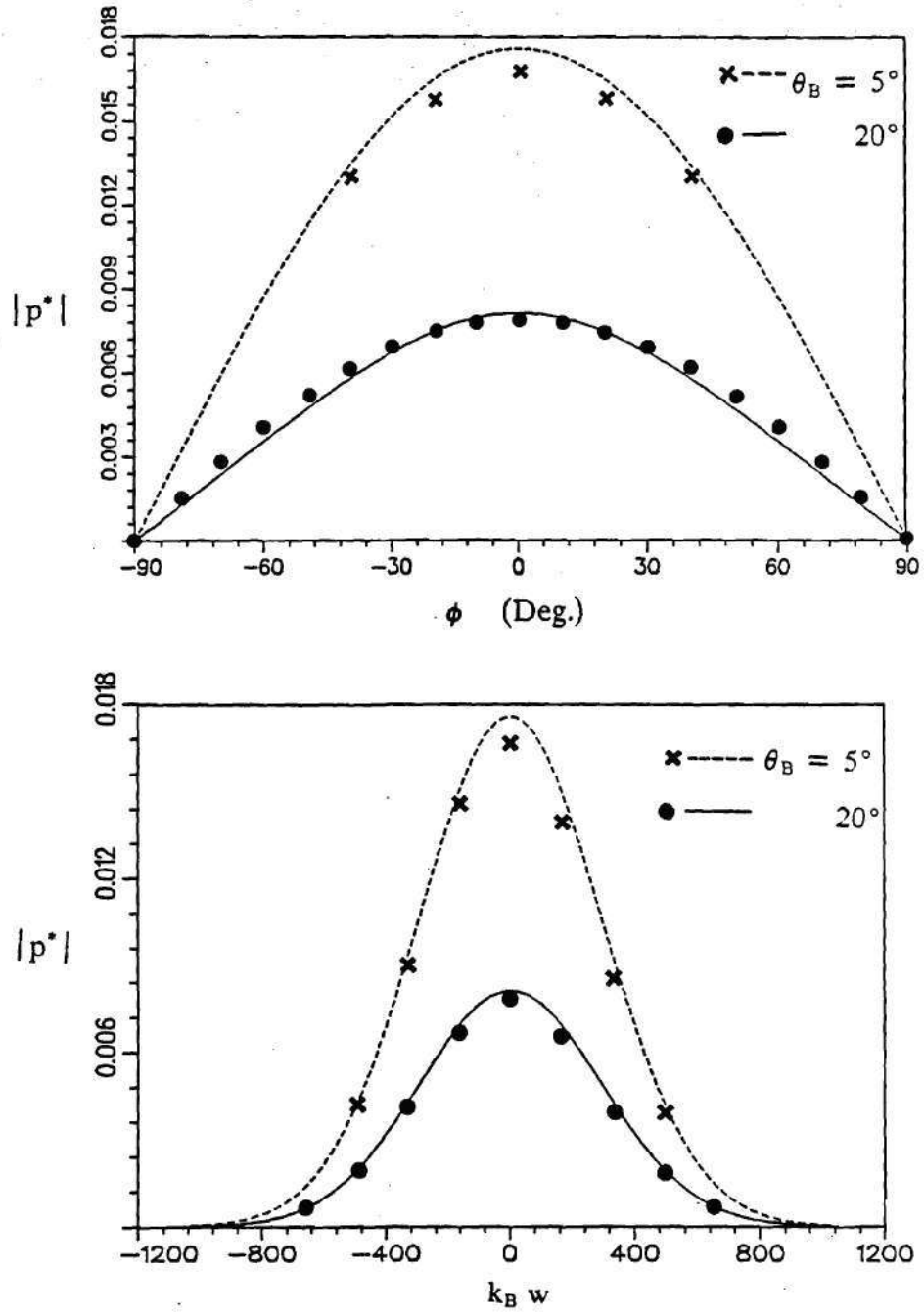

FIGURE 5.3 Beam shape in ϕ and w directions at various beaming directions θ_B for cases $k_B L_y << 1$.

superpositions of many small-T processes. An analysis similar to those discussed in Sec. 4.3 and 4.4 can be made for the small-T case, if, again, one is concerned with only the on-axis locations and if the propagation distance r is sufficiently large. Furthermore it turns out that such an on-axis behavior can be completely described by the large-L_y large-T solution. This fact is used in conjunction with the results of the large-T case in the next section to study how the pumping mechanism affects the resulting pressure amplitude at locations on the beam axis.

5.3 Properties of Acoustic Field along Center of Beam

The results described in Sec. 5.2 are here used to investigate the change in the pressure amplitude versus range relationship along the center of the beam (or the spreading wave), when the controlled parameters (discussed in Sec 3.2.1) are varied.

An observation from Eq. (5.2-9) concerning the application of the Fresnel-region concept is that the pulse duration time T in the denominator of C_{near} cancels the factor of T in the total energy E [$= \pi^{1/2}PT$ from Eq. (4.1-5)] in the numerator, and consequently leaves the expression for $|p|_{near}$ scaled by the peak laser power P but not the total energy E. This means one simply cannot increase the pressure amplitude indefinitely by prolonged dumping of laser energy into the water. Additional energy added to the water beyond a short period of time can only increase the width of the sound beam and the range to which it propagates before spherical spreading becomes important. In the farfield limit, however, $|p|$ is scaled by the total laser energy E [see Eq. (5.2-10b)]. In the following, the behavior of the beam-center pressure amplitude as it changes with variations in the controlled parameters is investigated in detail.

5.3.1 Peak Pressure Amplitude in the Center of the Sound Beam

The decrease of the beam-center pressure amplitude, $|p|_s$, with increasing propagation distance s is displayed in Fig. 5.4 and 5.5. The total laser energy E and

the beam angle θ_B are kept fixed. The value for θ_B is taken as 20 degrees. The pressure amplitudes per unit total energy input are normalized with respect to the multiplicative factor $\beta c^2/c_p$ and are plotted against the centerline distance s on a log-log paper. Values used in calculating these plots are are f_B = 10 kHz and μ = 13.7 m^{-1}.

In Fig. 5.4, the case of $L_y = L_w$ is considered. The first set of L_y and L_w is chosen equal to L_F, which is the length calculated according to Freedman's result [Eq. (3.3-7) with r replaced by s = 1000 meters]. The result is shown in the figure as the solid line. The other three curves are for $L_y = L_w = \tau L_F$ with τ = 0.01, 0.5, and 5. (represented by the dashed, dotted, and chain-dotted lines, respectively). In Fig. 5.5, L_w is kept fixed at a length equal to L_F, while L_y is set equal to τL_F for four τ values (0.01, 0.5, 1., and 5.). Again, these four curves are shown in the figure as the dashed, dotted, solid, and chain-dotted lines, respectively. Numerical verifications are performed selectively in the two figures and the accurateness of the theory's prediction with respect to the numerical result for the present study is confirmed.

The designs according to the solid curve corresponding to τ = 1 in Fig. 5.4 is of the most interest in this thesis. It takes advantage of all the features unique to the Fresnel region and effectively chooses the smallest possible values for L_y and L_w so that the maximum nearfield pressure amplitude is achieved. An example of a poor design with the Fresnel-region concept is the curve corresponding to τ = 5. For this case, the radiation surface area, L_y times L_w, is too large so that for a fixed energy input E, the power per unit length of the slab is significantly reduced. The curves with τ = 0.5 and 0.01 are examples for the farfield concept sound generation (the curve for τ=0.01 is not the best example since the resulting formation of sound tends to be of broad-band). It can be seen from the plot that because the radiation surface areas are chosen to be rather small, the disturbances arriving at the desired beaming distance, s = 1000 meters, already have 1/r spreading (indicated by "S"). In particular, the τ = 0.01 case shows no Fresnel-region behavior in the figure for the

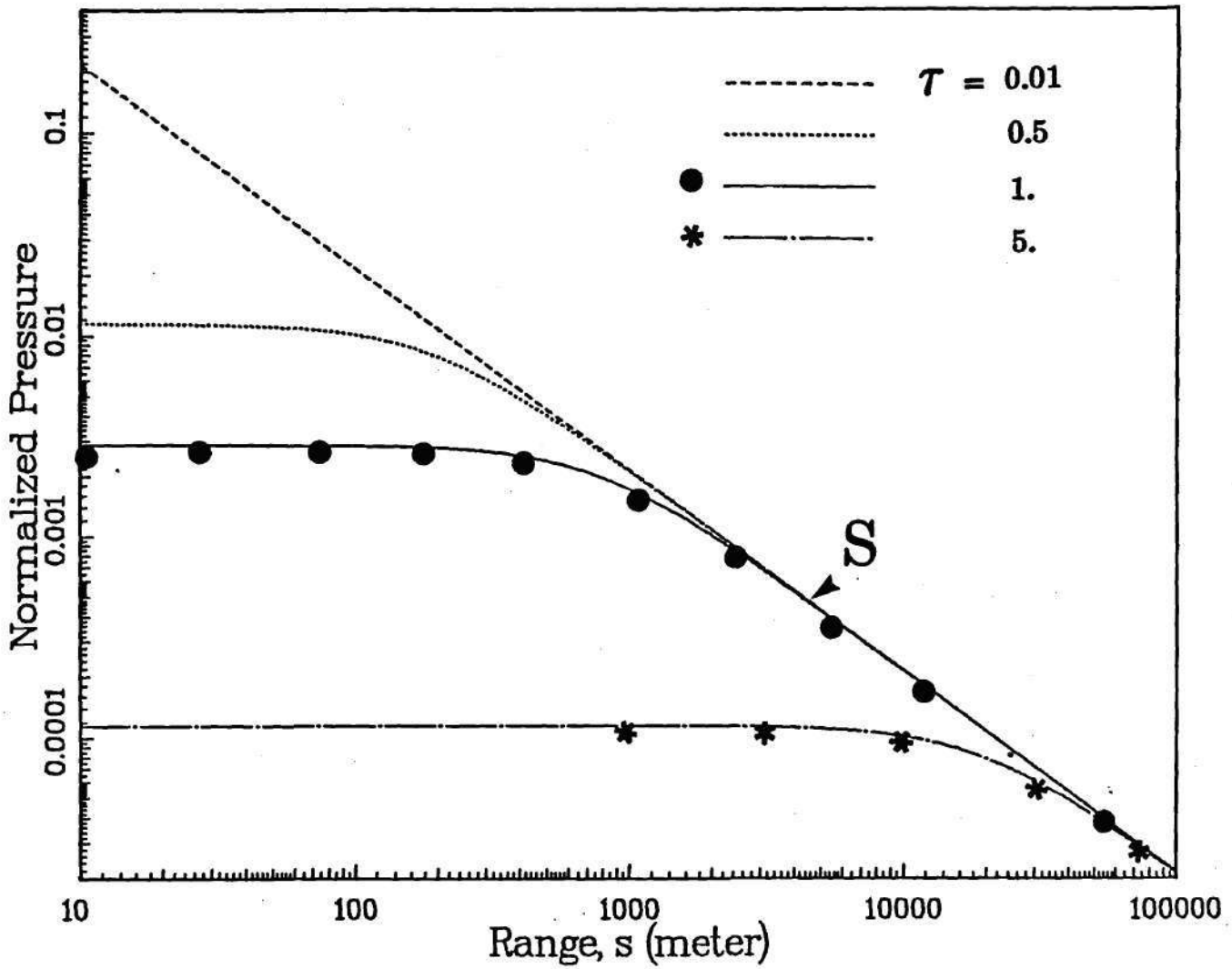

FIGURE 5.4 Logarithmic plot of normalized pressure versus propagation range s along beam axis for various values of τ for cases of $L_y = L_w = \tau L_F$. (Reference pressure is as defined in text.)

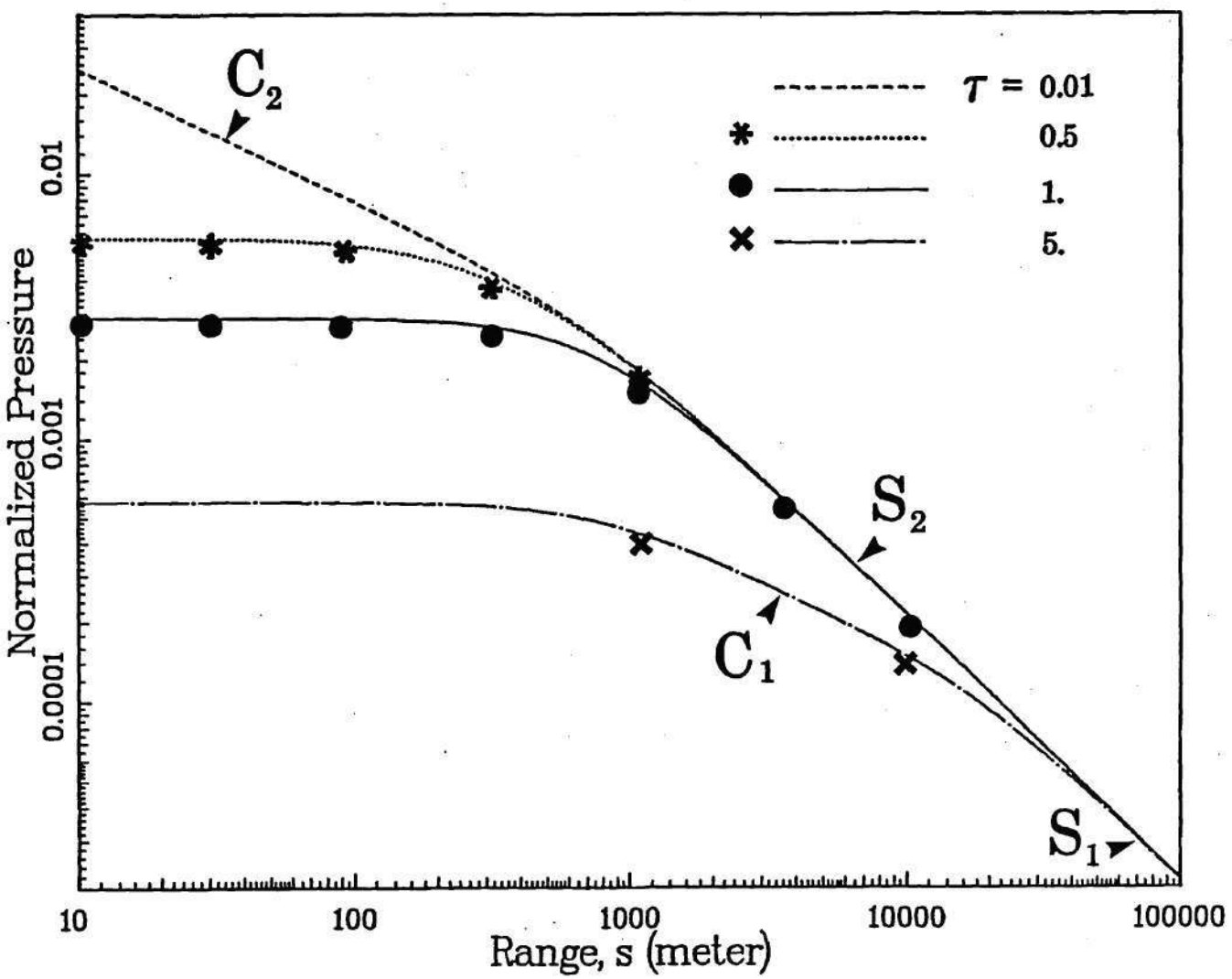

FIGURE 5.5 Logarithmic plot of normalized pressure versus propagation range s along beam axis for various values of τ for cases of $L_w = L_F$ and $L_y = \tau L_F$. (Reference pressure is as defined in text.)

presently chosen frequency.

Figure 5.5 shows a little more information than the previous plot because L_y and L_w are not set equal to each other in most cases. Here, keeping L_w fixed at L_F guarantees that the behavior of the disturbance in the w direction will follow that of the Fresnel region up to the desired beaming distance, s = 1000 meters. Choosing L_y larger than L_F (see τ = 5 curve) will reduce $|p|_s$ proportionally for the reason given earlier. Notice the emergence of the cylindrical spreading zone (indicated in the figure by "C_1"). Finally, as both the dimensions, L_y and L_w, become small compared with $(s/k_B)^{1/2}$, the disturbance spreads spherically (indicated by "S_1"). For cases with smaller values of L_y with respect to L_w (τ = 0.5 and 0.01), similar arguments hold. The cylindrical spreading behavior is not quite prominent in the τ = 0.5 case. For τ = 0.01, since L_y is too small and L_w is reasonably large, the centerline field characteristics immediately exhibit cylindrical spreading (region indicated by "C_2") once leaving the energy deposition zone. As for every other case, the disturbance eventually will turn into a spherical wave (indicated by "S_2").

5.3.2 Limiting Cases Exhibiting Planar, Cylindrical, and Spherical Spreading

From the preceding discussion, it is found that the four parameters, L_y, L_w, k_B, and s, alone are sufficient to describe the sound field characteristics in the center of the beam and at a distance s from the origin. The parameter L_w, not cT, is considered because it includes the factor cT and additional information concerning the angle θ_B. In the situation where θ_B is extremely shallow, the resulting disturbance will not persist as a collimated beam even if the pulse duration time T is made very long.

Based on the results presented in Sec. 5.1, we may heuristically divide the generation of sound with the present system into four categories:

(i) $k_B L_y^2 >> s$, $k_B L_w^2 >> s$ (Planar wave)

$$|p|_s = \frac{c\beta P k_B}{\pi^2 c_p n L_y} D_{near}(\sigma, \theta_B) \qquad (5.3\text{-}1)$$

(ii)$k_B L_y^2 << s$, $k_B L_w^2 >> s$ (Cylindrical wave)

$$|p|_s = \frac{c\beta P k_B}{\pi^2 c_p n (2s/k_B)^{1/2}} \; D_{near}(\sigma,\theta_B) \tag{5.3-2}$$

(iii) $k_B L_y^2 >> s$, $k_B L_w^2 << s$ (Cylindrical wave)

$$|p|_s = \frac{c^2\beta E k_B}{\pi^{5/2} c_p n L_y (2s/k_B)^{1/2}} \; D_{far}(\sigma,\theta_B) \tag{5.3-3}$$

(iv) $k_B L_y^2 << s$, $k_B L_w^2 << s$ (Spherical wave)

$$|p|_s = \frac{c^2\beta E k_B}{\pi^{5/2} c_p n (2s/k_B)} \; D_{far}(\sigma,\theta_B) \tag{5.3-4}$$

Here, the directionally dependent multiplicative functions D_{near} and D_{far} are defined previously in Eqs. (5.2-9c) and (5.2-10c), respectively.

In all the above cases, we assume that k_B and s are fixed parameters (when the signal frequency and the desired range to beam the sound are chosen) while L_y and L_w can be varied so that the field characteristics nearby the listener's point can be controlled. The effect of varying L_y and L_w is not simply L_y determining how far one spreads the laser power and L_w determining what length of time one adds heat to the water.

Inspection of Cases (i) and (ii) shows that, as long as one can keep L_w sufficiently large, the funtion D_p stays in the form of D_{near}. By varying the size of L_y, the actual factor $|\xi_y| = |[L_y^2 + i(2s/k_B)]^{1/2}|$ appearing in the denominator of $|p|_s$ changes from L_y, where $k_B L_y^2 >> s$, to $(2s/k_B)^{1/2}$, as $L_y \to 0$. Notice that when L_y is increased beyond a value (such as the one previously suggested for the Fresnel-region concept), the disturbance stays planar within the beam, i.e. there is no significant beam spreading. However, the amplitude $|p|_s$ decreases at the same rate that L_y is increased. On the other hand, $|p|_s$ in the beam center increases if L_y is gradually decreased from the aboved-mentioned value and remains stationary at a

peak value once L_y becomes much smaller than $(s/k_B)^{1/2}$. Therefore, letting L_y tend to zero does not indefinitely increase the signal amplitude at s, but only widen the resulting sound beam.

From Cases (iii) and (iv), it is found that whenever s is much greater than $k_B L_w^2$, the function D_p reduces to D_{far} as given by Eq. (5.2-10c). Three factors may cause this situation to happen: (a) θ_B is very close to zero, (b) T is extremely short, and (c) s is extremely large. Regardless which of the three is/are responsible for the case $k_B L_w^2 << s$, we learn from the two expressions, Eq. (5.3-3) and (5.3-4), that the pumping effect indeed exists. The fact that $|p|_s$ is directly proportional to the total laser energy E suggests that $|p|_s$ can be increased by simply lengthening the radiation time T. If the above condition (a) is dominating, L_w stays small until T becomes really large. This result is consistent with the fact that if θ_B is small, the previously created signal needs a longer time to leave the surface and hence more energy can be pumped into this signal. If the condition (b) is true while (a) is not, then one can further pump up the pressure amplitude by simply extending the duration T. However, not much later, the pumping mechanism will cease to function because L_w no longer satisfies the criterion for Cases (iii) and (iv). In fact, as the heating process is further prolongated, the condition on L_w in Cases (i) and (ii) will be met and the result is the extension of the area of effective radiation (characterized by L_w and L_y).

Figure 5.6 exemplifies the effect of the pumping mechanism in one circumstance for which the receiver is located in direction θ_B and at distance 1000 meters from the origin. Here, the normalized pressure [using Eq. (5.2-8)] is plotted against the length of the heating duration T (normalized with respect to $k_B c$). Both theoretical and the numerical predictions are provided in this plot. We assume that the laser track is always centered about the origin regardless of the length of T. The linearly increasing peak pressure amplitude with T at small values of T implies that the pressure is pumped up with the increase in heat radiation duration. When T increases beyond a certain value, the peak pressure amplitude ceases to be enhanced

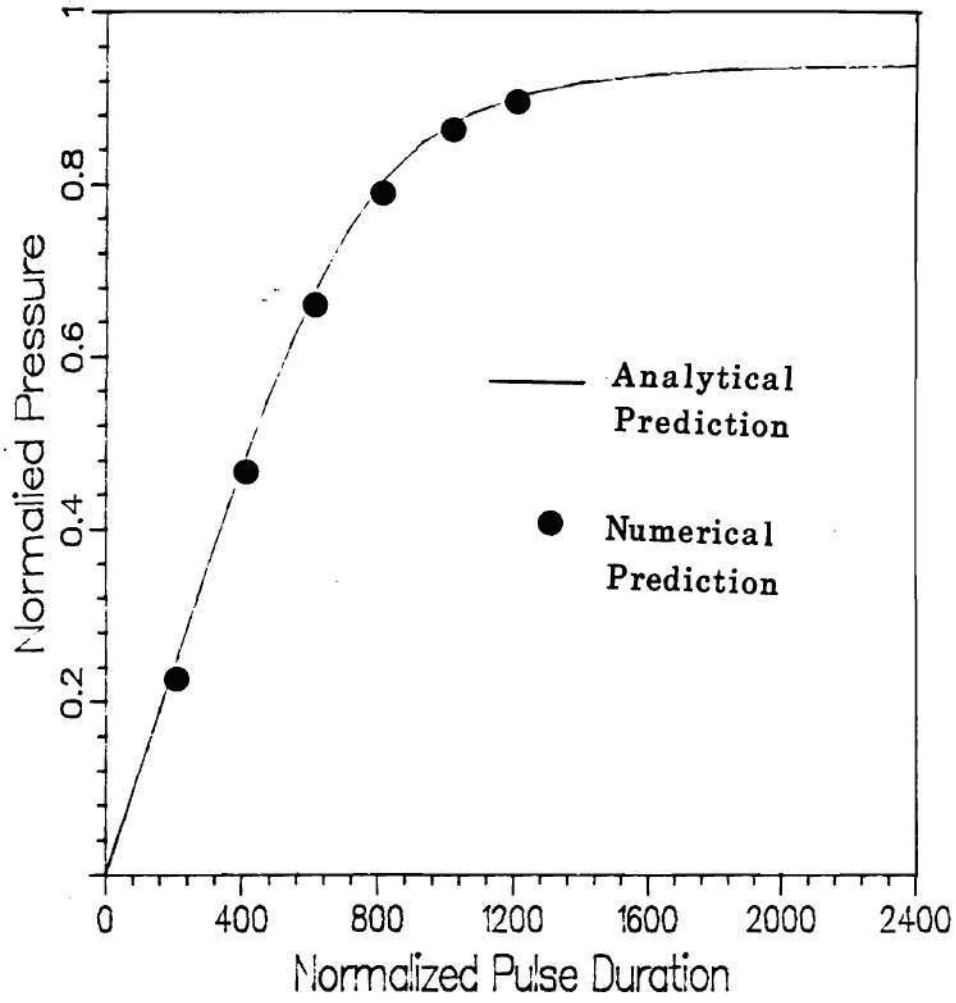

FIGURE 5.6 Plot of normalized pressure p^* versus duration time T of heat energy deposition.

for any further elongation of the radiation duration.

In summary, the role played by the pumping mechanism in the entire sound generation process is only significant in the initial stage (the length of this stage depends on the angle θ_B), and this mechanism gradually converts the directionally dependent multiplicative function for $|p|_s$ from D_{far} to D_{near}.

5.3.3 Finite Pulse Duration Effects on Peak Pressure Amplitude Factor D_p

In sec. 3.4.4, we discussed the pressure-amplitude directionally dependent multiplicative function $D_p(\sigma,\theta_B)$ resulting from the two-dimensional steady-state model. The result (see Fig. 3.7) showed that the peak value of D_p can be reached when θ_B is equal to zero. This expression for D_p also predicts that the above-mentioned peak value would grow indefinitely as the value of σ approaches zero. This, however, assumes that no restriction is placed on the length of the radiation time T in the model.

Based on our large-L_y large-T model for the heating configuration and the former discussion in Sec. 5.2.1, we are able to reconsider the behavior of the function D_p. In the context of the present model, the definition can be extracted from Eqs. (5.2-2) and (5.2-7). [Equation (5.2-7) for the spreading factor SF is involved in defining D_p because L_w and ξ_w are θ_B dependent.]. Because L_y and ξ_y do not depend on θ_B, we can consequently disregard their existence in SF. Combining the above information, we arrive at a modified expression for D_p given by

$$D_p(\sigma,\theta_B,T) = \frac{\sin\theta_B\cos\theta_B}{[\tan^4\theta_B+(2s/k_Bc^2T^2)^2]^{1/4}\,[\sigma^2+\sin^2 2\theta_B]^{1/2}} \qquad (5.3\text{-}5)$$

It is clear from Eq. (5.3-5) that the expression for D_p reduces to the one studied in Chapter III in the limit $T\to\infty$. Notice also that the new version of D_p is range dependent.

Figure 5.7 exemplifies the variation of D_p as a function of θ_B for the cases where T, s, and k_B are held fixed. These three parameters are chosen such that L_w =

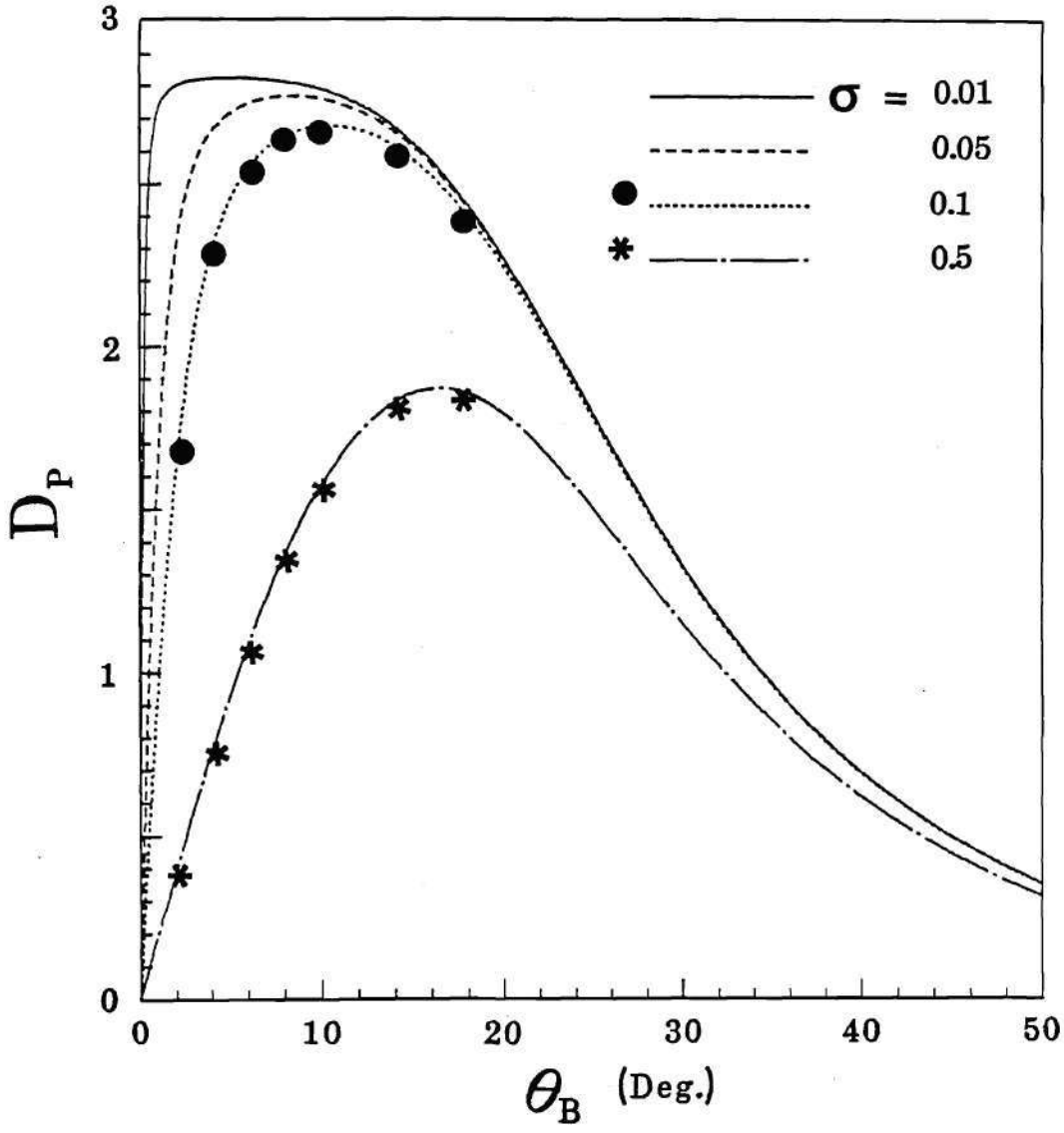

FIGURE 5.7 Plot of function D_p versus beaming angle θ_B for various values of $\sigma = \mu / k_B$.

$cT\tan\theta_B = (1.5s/k_B)^{1/2}$ [i.e., the criterion Eq. (3.4-7) for Fresnel-region beaming] is true when $\theta_B = 20°$. The plot is made for four values of σ(equal to 0.01, 0.05, 0.1, and 0.5). The trend of the curves for σ=0.1 and 0.5 is spot checked using points generated from the numerical integration program. [These numerical results are generated based on the assumptions L_y=6 m, r=1000 m (on beam axis), f_B=10 kHz, T=0.0108 s, and σ=0.1 or 0.5, and follow by a normalization operation for the resulting pressure using the formula $D_p = (\pi^2 n c_p/\beta c)|\xi_y|$ p.]

The major difference between the set of curves in the present figure and the set in Fig. 3.7 for D_p is that all curves are forced to zero when θ_B is zero in the former. This observation is always true regardless of the value of σ as long as T is finite. When $\theta_B = 0$, no matter how far one moves the heating configuration, D_p is always given by D_{far} [see Eqs. (5.2-10c), (5.3-3), and (5.3-4), and the accompanying discussion] which is invaribly equal to zero at $\theta_B = 0$. Notice that the curves peak bluntly at some small values of θ_B as σ becomes smaller. It would seem that the bluntness of these peaks could only be sharpened by increasing the radiation time T.

In Fig. 5.8, the function D_p is once again plotted against the angle θ_B, but now the varied parameter is the pulse duration time T of the heat addition. The value of σ is taken as 0.05 for all cases. The solid curve is for $T = T_o$, where T_o satisfies the above-mentioned criterion, $cT_o\tan 20° = (1.5s/k_B)^{1/2}$, for given values of s and k_B. The other three curves, namely the dashed, dotted, and chain-dotted lines, are for $T = \tau T_o$ with τ = 2, 3, and 4, respectively, for the same given values of s and k_B. The plot shows how prolonged adding of laser energy to the water could help to increase the pressure amplitude at some relatively shallow beaming angle θ_B. Although the present model is not fully applicable to predict the entire sound field when the angle θ_B is extremely small (result only correct on the beam axis), it suggests that the pumping principle can generate large amplitude signals in directions corresponding to small values of θ_B.

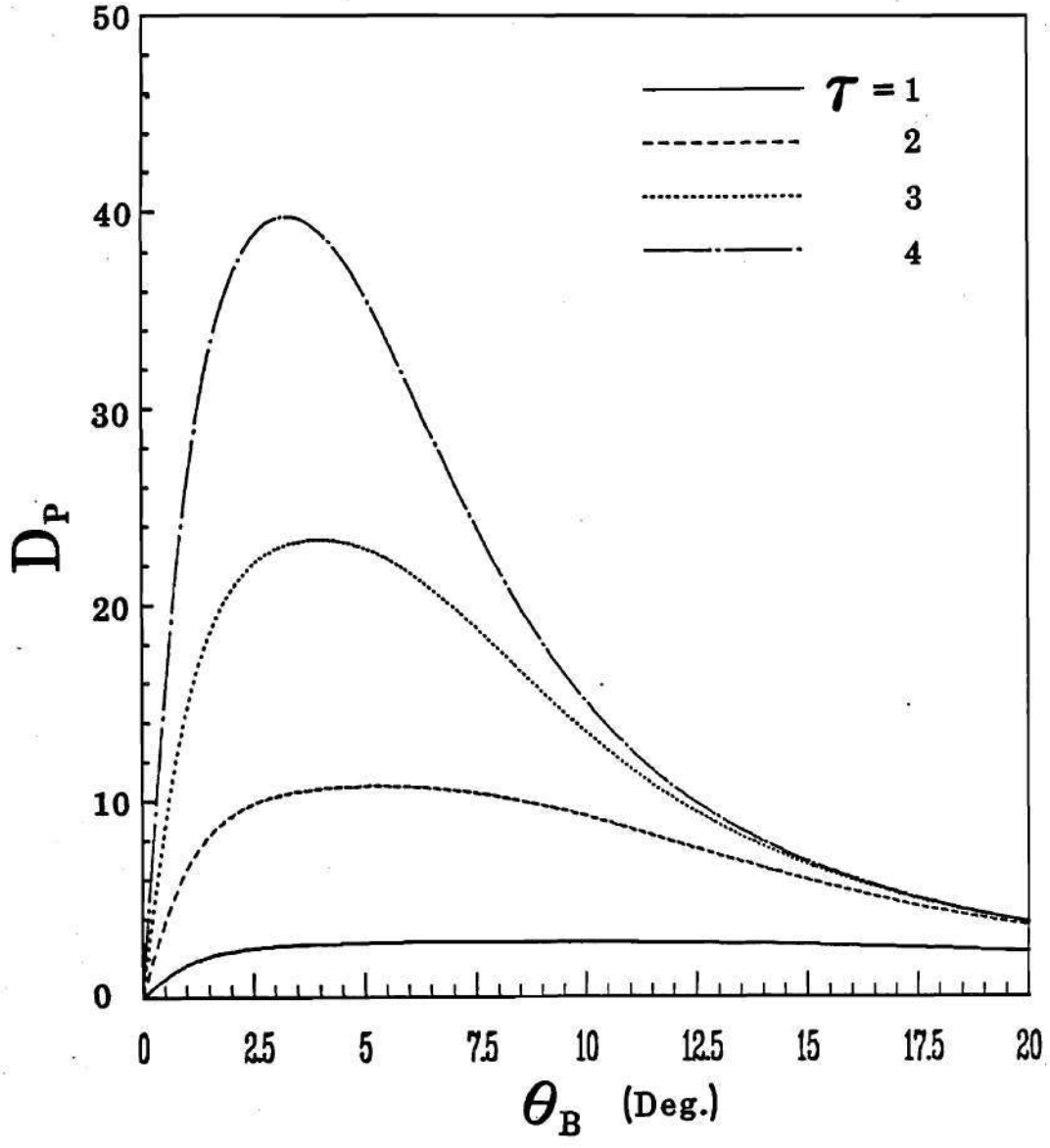

FIGURE 5.8 Plot of function D_p versus beaming angle θ_B for various values of τ for the case of $T = \tau T_o$. The value of $\sigma = \mu/k_B$ is 0.05.

5.4 Numerical Estimates Relating to Overall System Performance

Using expressions for the beam-center peak pressure amplitude [Eqs. (5.2-1)–(5.2-7) with PWF = PE = BE = 1] for the large-L_y large-T case, we proceed to make some numerical estimates regarding the performace of the proposed laser-induced sound system.

5.4.1 The Apparent Source Level

One method to quantify the magnitude of an acoustic signal other than using the pressure amplitude is to discribe the wave by the apparent source level. The latter is computed from the former as 20 times the logarithm, base 10, of the ratio of propagation distance, s, times rms acoustic pressure acoustic pressure amplitude and a standard reference value, 10^{-6} pascal-meters. Figure 5.9 displays the apparent maximum (on beam-axis) source levels (solid lines) received in the "far field" based on the Fresnel-region beaming of sound to a range of 2000 meters from the origin. The horizontal axis represents the power output from the laser. The parameters used are n = 10 cycles, θ_B = 20°, and μ = 13.7 m^{-1}. The thermodynamic properties of water are evaluated at a water temperature of 20°C. The dashed lines are previous predictions (Muir, Culbertson, and Clynch 1976) for cases when the laser beam is stationary and modulated sinusoidally in time. The advantages of using the present method for generating sound should be apparent.

5.4.2 Required Laser Parameters

Based on the refined model derived in Chapter IV, we are able to check the previous estimates regarding the required laser parameters for the generation of easily detectable long range signals. The ambient noise analyses discussed in Sec. 3.4.2 are used again to define the required pressure amplitude, $|p|_s$, at range s in direction θ_B. Expressions corresponding to Eqs. (3.4-12) for $P_{required}$, $2T_{required}$, and $E_{required}$ for the refined model are cumbersome and therefore are not listed here. The estimates of these parameters for the refined model are illustrated in Figs. 5.10

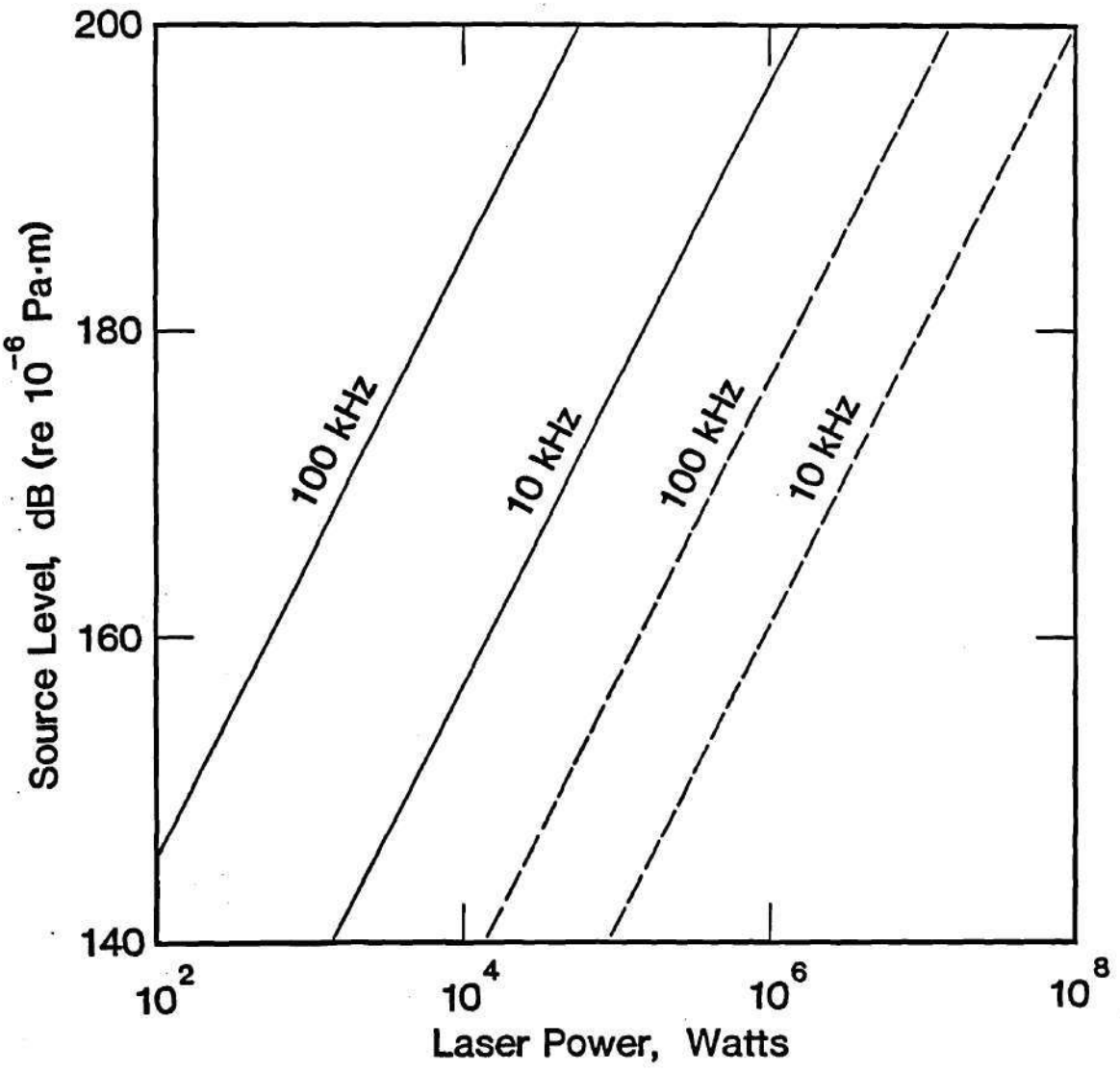

FIGURE 5.9 Predicted apparent maximum source levels for underwater acoustic signal received at a range of 2 km from a surface region where laser-generated heat is added. Dashed lines are predictions of Muir, Culbertson, and Clynch (1975) for stationary modulated laser beams; solid

and 5.11. The lengths, L_y and L_w, are both taken to be equal to $L_F = (1.5s/k_B)^{1/2}$ in accordance with Freedman's result [Eq. (3.3-7)]. Once again, the signal amplitude $|p|_s$ is required to be five times the noise amplitude. We also assumed that one can beam the sound accurately to the target such that all estimates can be made based on the information related to the beam-center pressure amplitude. The values of the environmental parameters used here are identical to the previous values: temperature = 20°C, salinity = 35 parts per thousand, c = 1526 m/s, c_p = 3993 J/kg°K and $\beta = 2.44(10)^{-4}°K^{-1}$. The acoustic absorption coefficient, α, is again computed from the semi-empirical formulas in the reference by Fisher and Simmons (1977). The three controlled parameters, θ_B, n, and μ, are taken to be 20°, 10 cycles, and 13.7 m^{-1}, respectively.

The results presented in Fig. 5.10 and 5.11 show good agreement with the estimates in chapter III. The estimation is done by assuming that the dependency between $P_{required}$ and $E_{required}$ is determined by a third parameter, $T_{required}$, such that $E = \pi^{1/2}TP$. In the present study, $T_{required}$ is calculated prior to the estimation of the former two parameters by using the formula, $2T_{required} = (1.5s/k_B)^{1/2}/(c \tan\theta_B)$, from Eq. (3.4-12b).

In choosing among alternative lasers, the following points should be considered. For Fresnel-region sound generation, the power capability of the laser is important, since the pressure amplitude at the receiving point varies with the laser power. The laser pulse duration T is of minor importance with regard to the establishment of the peak pressure amplitudes.

For very shallow-angle beaming of sound (i.e. $\theta_B \simeq 0$), the laser power becomes of secondary importance to laser pulse energy. The benefits of having smaller μ (longer penetration depths) are more percerpible at small θ_B because such enables the pumping to be maintained longer.

The Laser Focus/Electro-Optics Buyers' Guide (1986) tabulates physical parameters and capabilities for an extensive (but presumably still not exhaustive) list

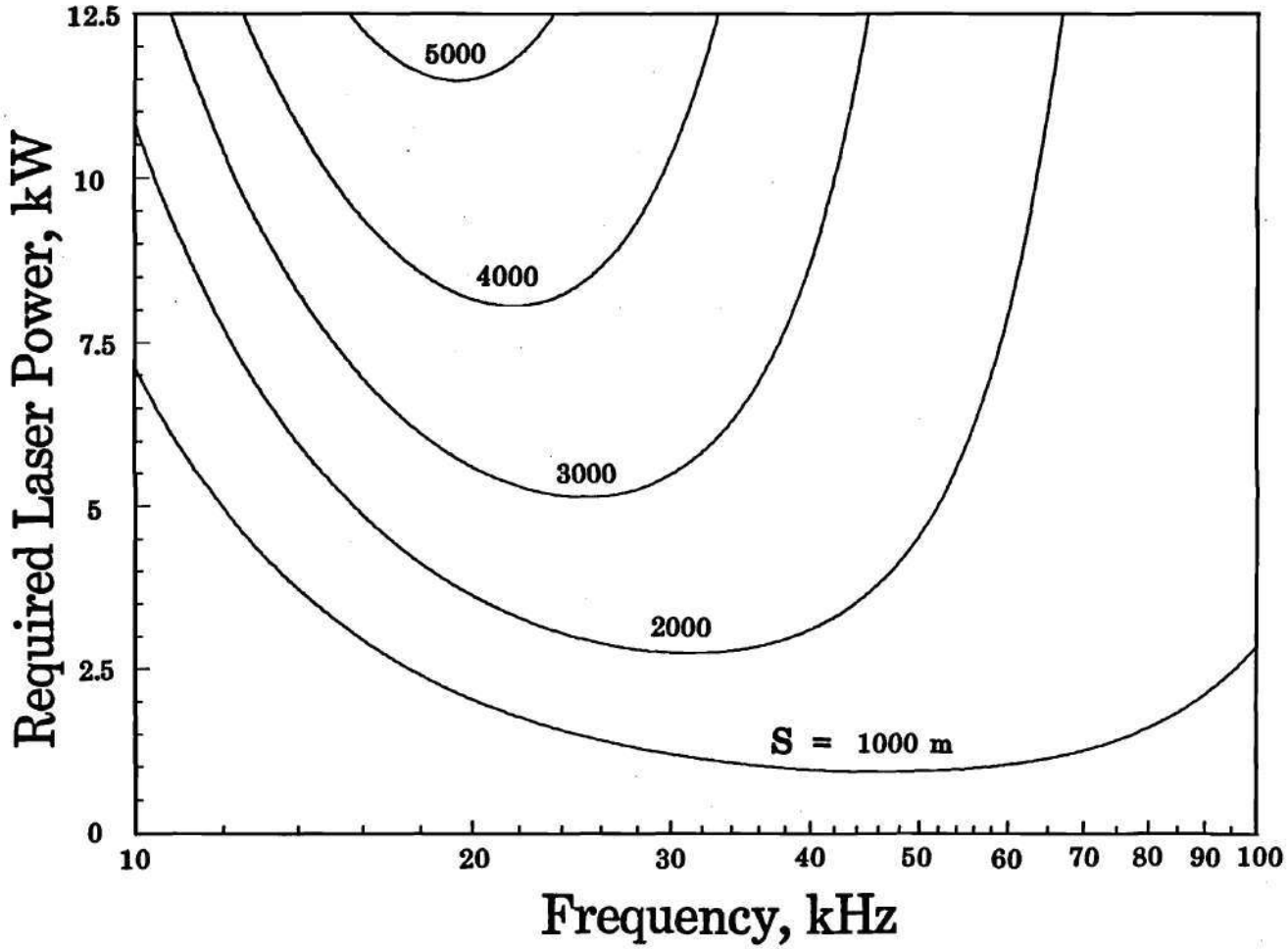

FIGURE 5.10 Estimates of required laser power to generate easily detectable acoustic pulses of specified frequency at given range s along the beam axis. Calculations are based on 3-D transient model described in text; θ_B is 20°.

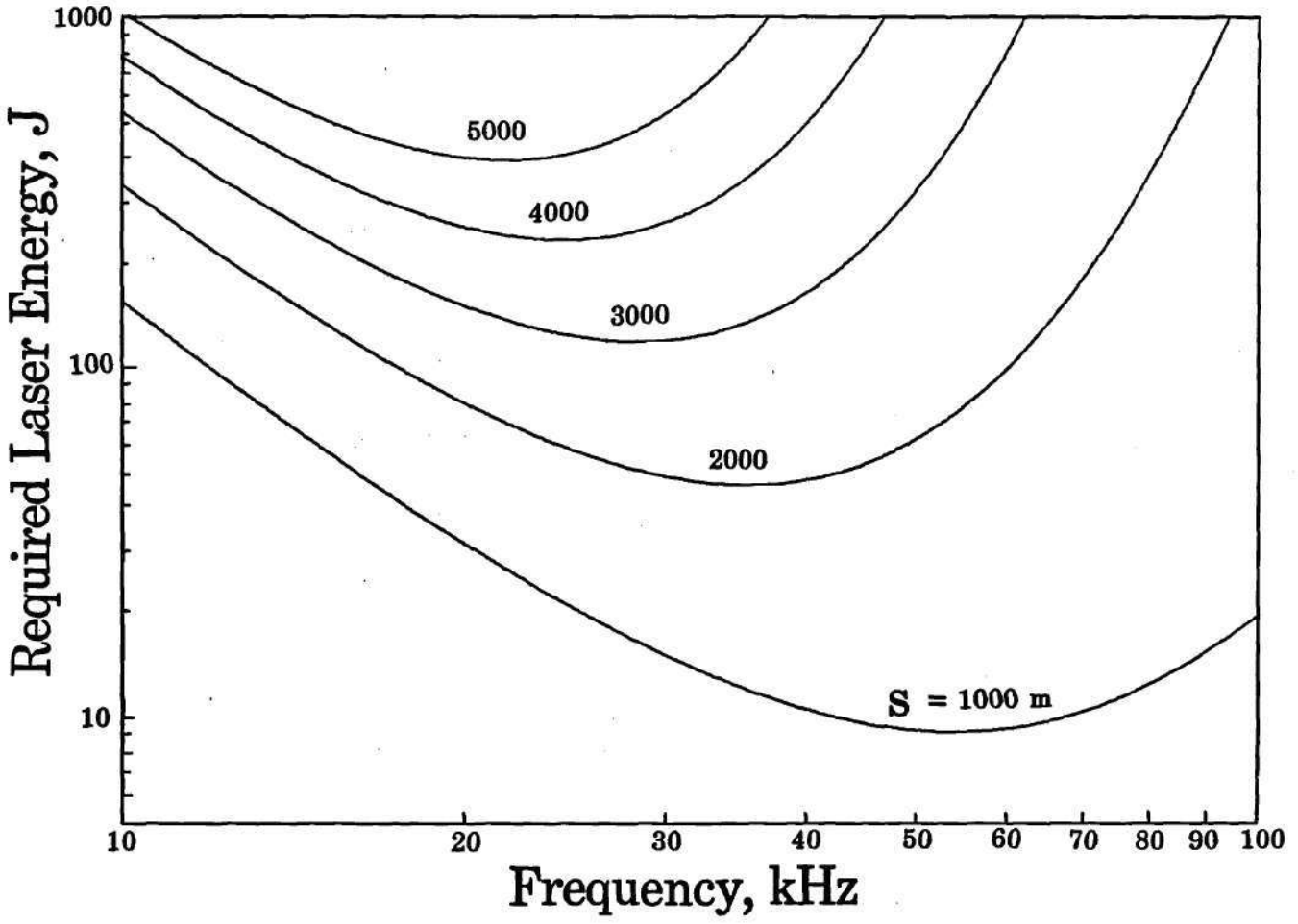

FIGURE 5.11 Estimates of required laser pulsed energy to generate easily detectable acoustic pulses of specified frequency at given range s along the beam axis. Calculations are based on 3-D transient model described in text; θ_B is 20°.

of currently available lasers. Among the examples which tend to meet requirements such as suggested by the numbers in Figs. 5.7 and 5.8 are:

(1) A pulsed solid state laser of the Nd:YAG variety (1.06 micron optical wavelength) that emits pulses of 400 J energy with pulse lengths varying from 0.125 to 10 ms (laser power varying upwards from 40 kW).

(2) A pulsed solid state laser of the Nd:Glass variety (1.06 micron optical wavelength) with pulse energies between 150 and 400 J and a pulse duration of 2 ms (laser power ranging up to 200 kW).

(3) A pulsed solid state ruby laser (0.69 micron optical wavelength) with pulse energies also between 150 and 400 J and a pulse duration of 2 ms (laser power ranging up to 200 kW).

A news item in the September 27, 1982 issue of Aviation Week and Space Technology reported that the DOD had given 20M dollars to Rockwell International, TRW, and Bell Aerospace Textron to develop a supersonic oxygen iodine chemical laser. The program will be managed by the Air Force Weapons Laboratory, Kirtland AFB and should produce a high energy, shorter wavelength (1.3 micron) chemically pumped laser. Comparable lasers mentioned in Aviation Week and Space Technology and in Laser Focus are hydrogen fluoride lasers (2.7 micron) and deuterium fluoride lasers (3.8 micron), both of which have been developed to the point where they yield 10 kW of continuous power.

5.5 Transduction Efficiency Analysis

To analyze the energy transduction efficiency η for the refined model, we consider the less complicated cases for which the lengths L_y and L_w are large compared with the acoustic wavelength. The control volume that has been set up in Sec. 3.4.5 (see Fig. 3.8) is re-used in the present discussion. The expressions for the pressure disturbance given by Eqs. (5.2-9) are taken into consideration. We assume that the beaming angle θ_B is not extremely small so one can assume SF $\simeq$ 1 in Eq.

(5.2-7). Also, we assume the resulting pressure disturbances near point A in Fig. 3.8 as being a planar wave of constant frequency.

Using such an approximation, we obtain the intensity vector **I** which is equal to $(p^2/\rho c)\mathbf{n}_B$ and is time dependent. Following our approach for the previous model, we evaluate the energy I_z radiated per unit time per unit area of the control volume's bottom surface (whose unit outward normal vector is $\mathbf{e}_z$) as $I_z = \mathbf{I}\cdot\mathbf{e}_z$. Then, we can estimate the total acoustic energy, E_{ac}, radiated from the source by integrating the function I_z over the bottom surface of the control volume (an infinitely-large horizontal surface at depth z), and then over all time. In doing so, we get

$$E_{ac} = \frac{1}{2\rho c}\left(\frac{c\beta P}{\pi L_x L_y c_p}\right)^2 \frac{\sin\theta_B \cos^2\theta_B}{[\sigma^2 + \sin^2 2\theta_B]^{1/2}}\ I_o \qquad (5.5\text{-}1)$$

where

$$I_o \simeq \int_{-\infty}^{\infty}\int_{-\infty}^{\infty}\int_{-\infty}^{\infty} e^{-2w^2/L_w^2}\, e^{-2y^2/L_y^2}\, e^{-2(s-ct)^2/L_s^2}\, dx\, dy\, dt \qquad (5.5\text{-}2a)$$

$$= (\pi/2)^{3/2} L_x L_y T \qquad (5.5\text{-}2b)$$

Here, the approximate expression on the right side of Eq. (5.5-2a) is stated consistently with the condition $L_s/c >> 1/\omega_B$, which is equivalent to the initially assumed condition, $k_x L_x >> 1$, for the refined model.

Dividing the expression for E_{ac} in Eq. (5.5-1) by the total optical energy input $\pi^{1/2}PT$, yields the transduction efficiency η_{MHC} associated with the moving heating configuration (MHC) as

$$\eta_{MHC} = \frac{1}{2^{5/2}\pi^2}\frac{c}{\rho}\left(\frac{\beta}{c_p}\right)^2 \frac{Pk_B}{nL_y}\ D_\eta(\sigma,\theta_B) \qquad (5.5\text{-}3a)$$

$$D_\eta = \frac{\sin\theta_B \cos^3\theta_B}{[\sigma^2 + \sin^2 2\theta_B]} \qquad (5.5\text{-}3b)$$

Notice that the expression D_η in Eq. (5.5-3b) is identical to the previously derived

Eq. (3.4-24) (with all θ_S replaced by θ_B) in Chapter III.

The efficiency η_{MHC} for the k_xL_y, $k_xL_w >> 1$ case is scaled by the laser power. The effect of the pumping mechanism ceases at some finite propagation time when the sound beam reaches depths below the heating configuration extent. However, the benefit of the early stage pumping of the laser energy is embedded in the function D_{MHC} which is the primary constituent of the presently obtained D_η (note that $D_\eta = D_{MHC}^2 \sin\theta_B \cos\theta_B$). Dividing η_{MHC} in Eq. (5.5-3a) by η_{SMLB} in Eq. (2-20) yields the following ratio

$$\eta_{MHC}/\eta_{SMLB} = \frac{1}{2^{1/2}\pi n L_y k_B F(\sigma)} D_\eta(\sigma,\theta_B) \qquad (5.5\text{-}4)$$

where $F(\sigma)$ is previously defined in Eq. (2.6-7).

It can be seen that the enhancement of the ratio relies partially on the minimization of the parameters, n, L_y, and k_B. To calibrate one's thinking regarding the magnitude of the ratio given by Eq. (5.5-4), one might take $n = 10$ cycles and $L_y = (10/k_B)^{1/2}$. For the case where k_B is in the kilohertz range and μ is of the order of one, the ratio demonstrates no marked improvement in η_{MHC} over η_{SMLB} for the angle of interest, $0 < \theta_B < 50°$. In fact, the value of η_{MHC} for such circumstances are roughly two to three orders of magnitude lower than those of η_{SMLB}. The situation when a blue-green laser ($\mu \simeq 0.1$ m^{-1}) is used is different. Fig. 5.12 illustrates the ratio plotted against θ_B for three frequencies (f_B = 10, 30, 50 kHz) with μ taken as 0.1 m^{-1}. Only the range of very small values of θ_B are shown. One concludes that, when using the classes of heating configuration discussed in this thesis, one cannot substantially exceed the peak efficiency predicted in Chapter II.

5.6 Numerical Study on the Effect of $\theta_S \neq \theta_S$ on Pressure Amplitude and Beam Shape

In Sec. 3.2.3, we have assessed the effects in pressure amplitude due to the deviation of θ_S from θ_B based on the simplified two-dimensional heat model. Here, our intention is to verify the trends shown in such result using the developed general

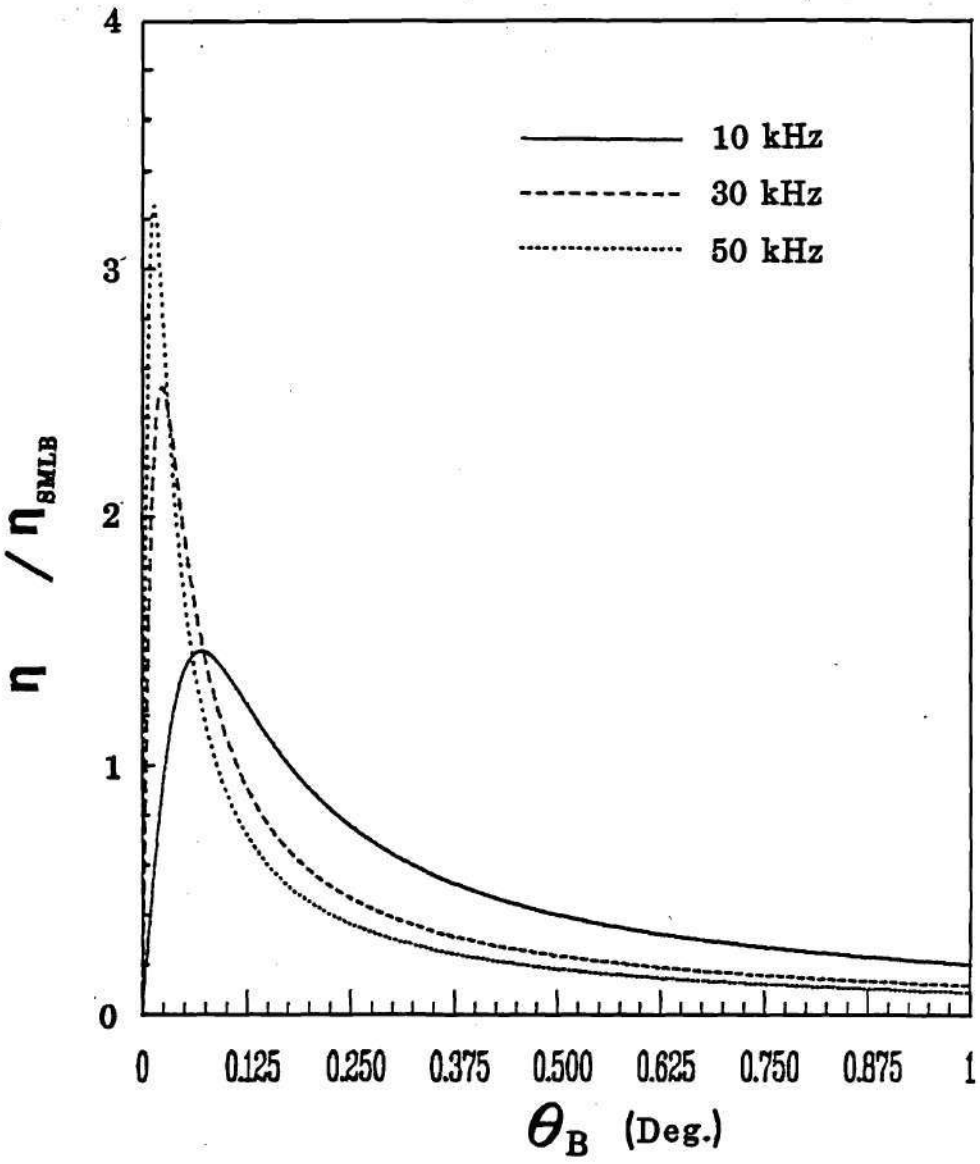

FIGURE 5.12 Plot of ratio η_{MHC}/η_{SMLB} versus beaming angle θ_B for various frequencies and for $\mu=0.1$ m^{-1}.

numerical codes with the heating function taken as the more refined transient model posed in Sec. 4.1.

In Figure 5.13, the peak pressure amplitude is plotted against the slant angle θ_S for various values of σ (0.01, 0,1, 1.0, and 10.0) where $\sigma=\mu/k_B$. The numerical inputs are P=1 watt, $\beta=2.44(10)^{-4}$ $°K^{-1}$, $c_p=3993$ J/kg°K, $\theta_B=20°$, $L_y=6$ m , $L_w=0.6$ m, r=1000 m, $f_B=10$ kHz, and n=10 cycles. The trends of these curves are nearly the same as those predicted by the two-dimensional del (see Fig. 3.3). The conclusion that can be drawn from Fig. 5.13 regarding the sensitivity of the $\theta_S \neq \theta_B$ effect on the peak pressure amplitude is consequently invariant from that drawn earlier from Eq. (3.2-11) and Fig. 3.3.

Another concern regarding the deviation of θ_S from θ_B would be the influences it has on the resulting beam shape when μ/k_B is small compared to unity. Since we assume that the beam penetration directions are always perpendicular to the y direction, one expects that any possible influence on the beam shape would be in the w direction.

For $\sigma=0.05$ (which is quite small compared with unity), the resulting Fresnel region is evaluated for two cases: (i) $\theta_S=\theta_B=20°$ and (ii) $\theta_B=20°$ but $\theta_S=25°$ (see Fig. 5.14). The numerical inputs for various parameters are P=1 watt, $\beta=2.44(10)^{-4}$ $°K^{-1}$, $c_p=3993$ J/kg°K, $L_y=L_w=6$ m, S=1000 m, $f_B=10$ kHz, and n=10 cycles. The penalty for not having $\theta_S=\theta_B$ is shown in Fig. 5.14. This amplitude reduction effect of $\theta_S \neq \theta_B$ is typical in the case $\sigma << 1$, and one should be very cautious in picking the suitable laser when the range of possible values k_B is specified. The shape of the created sound beam in the w direction, on the other hand, does not receive much influence from the deviation of θ_S from θ_B.

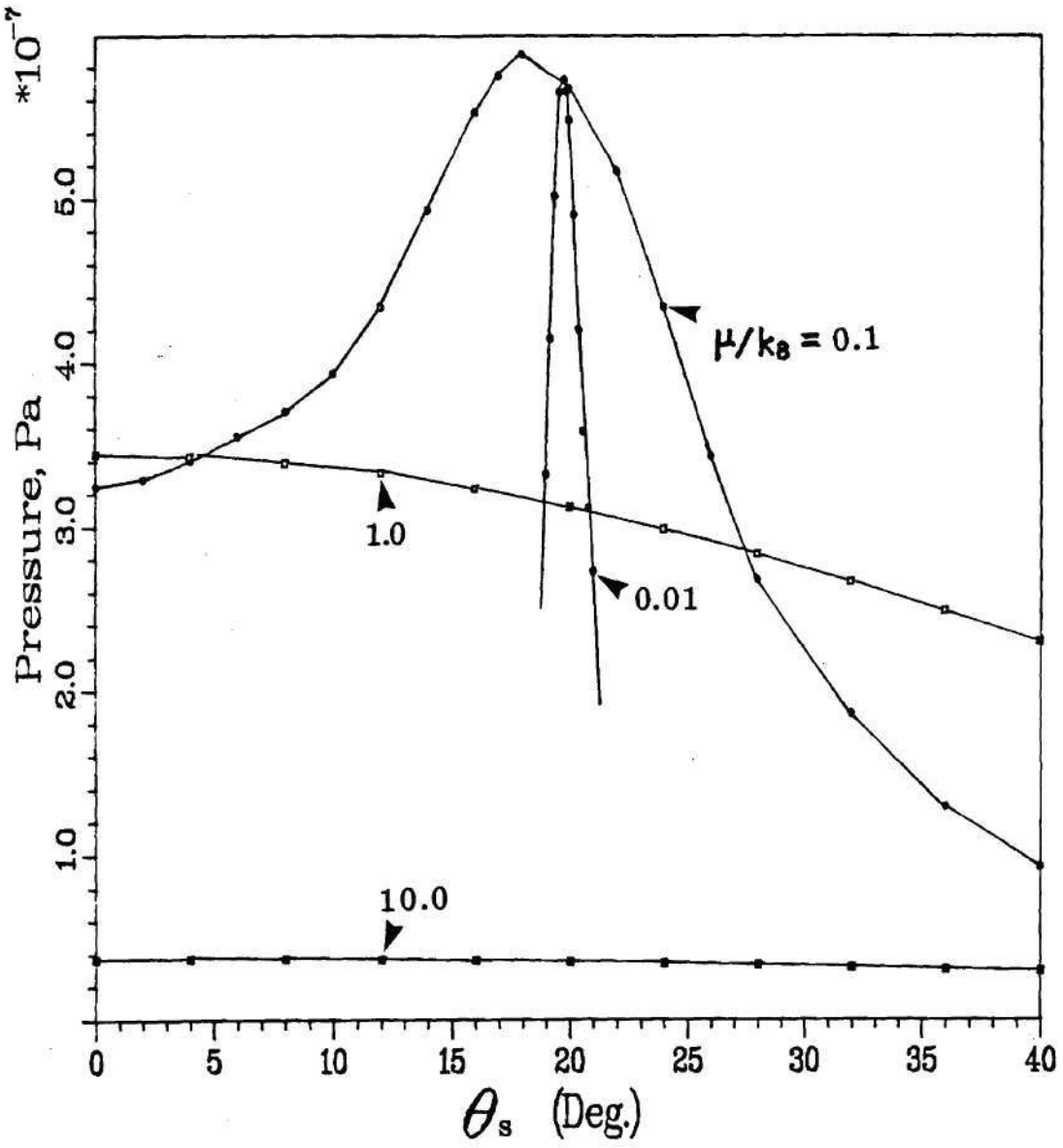

FIGURE 5.13 Peak pressure amplitude in beam versus slant angle θ_S. Computations are based on triple integral solution of inhomogeneous wave euqation. The angle θ_B is 20°.

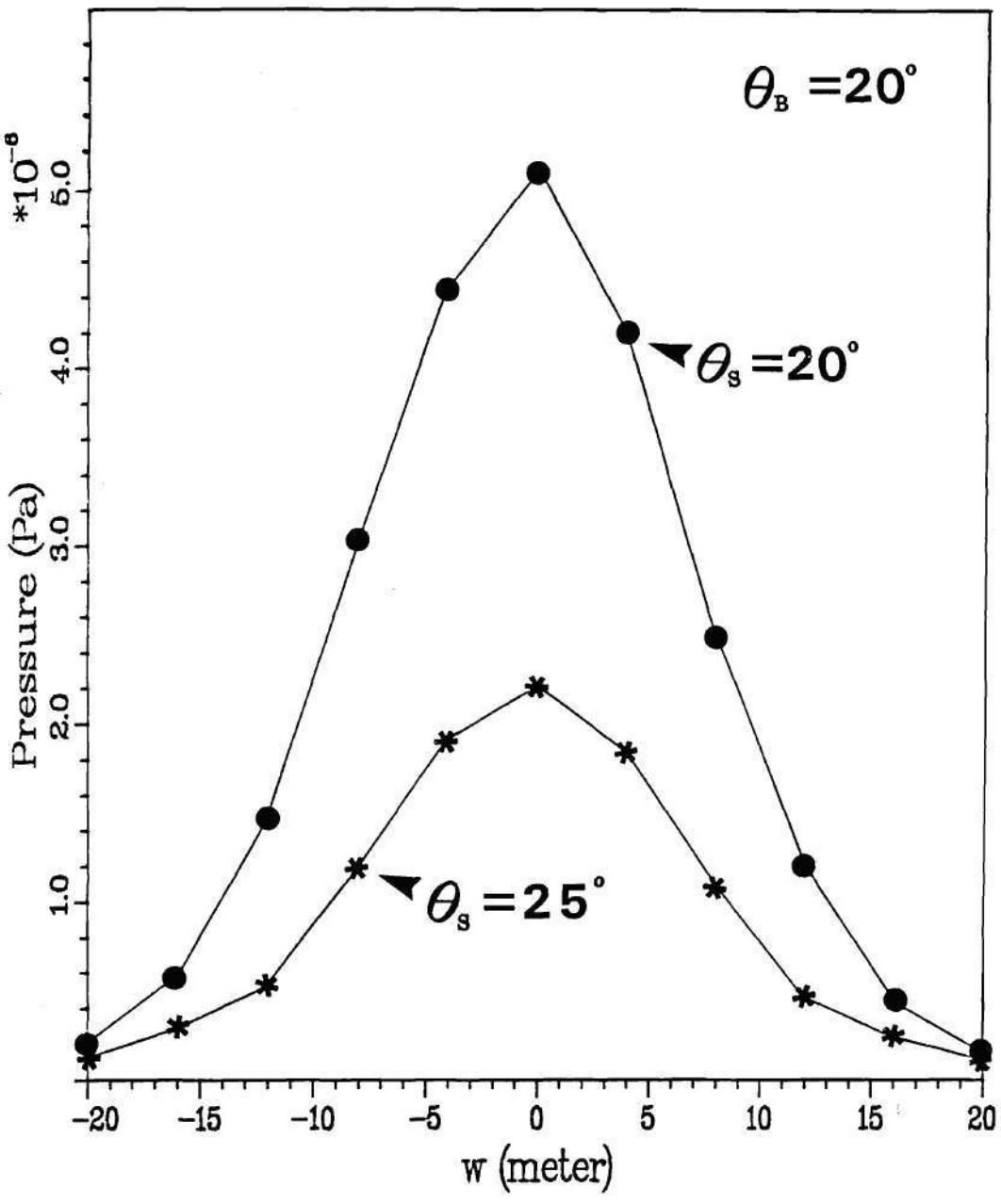

FIGURE 5.14 Effect of $\theta_S \neq \theta_B$ on the beam shape in w direction. Calculations are based on direct numerical integration of triple integral solution of inhomogeneous wave equation.

CHAPTER VI

MODIFICATIONS, EXTENSIONS, AND ADDITIONAL DISCUSSION OF THE ANALYTICAL MODEL

The present chapter is concerned with extending the analytical model of Chapters IV and V to less restrictive situations. A reinterpretation of the previously derived asymptotic solution as being a solution of the parabolic wave equation (or parabolic equation) allows one to identify more closely the cause-effect relations between the parameters describing the heating configuration and the farfield acoustic disturbance. It also leads to a different, but closely related, analytical approximation for the sound radiated at very shallow angles. The parabolic equation is closely akin to geometrical acoustics, and a geometrical acoustics interpretation of the Fresnel region aolution allows one to learn how to predict acoustic fields for heating configurations where the envelopes are not Gaussian shaped and where the velocity of the configuration over the water surface varies with position.

In the latter part of the chapter, the effects of water waves on sound generation is briefly considered, with a consequent demonstration of the criterion that the laser radiation should be such that $1/\mu$ is substantially larger than the mean water wave height if the pumping principle is to be effectively exploited. It is also argued that the value of μ/k_B should substantially exceed the rms slope of the water surface.

6.1 Parabolic Approximation

6.1.1 Derivation of the Parabolic Equation

Consider the homogeneous reduced wave equation for fixed frequency of propagation. The Laplacian operator of this equation is expressed using an

orthogonal coordinate system (s,y,w) as

$$(\partial^2/\partial s^2 + \partial^2/\partial y^2 + \partial^2/\partial w^2 + k_B^2)\, p = 0 \qquad (6.1\text{-}1)$$

The coordinates s and w are defined in reference to the same two coordinates introduced earlier in Sec. 5.2. One may consider these two directions being the result of rotating the x (horizontal) and z (depth) directions about the y axis through an angle of $\frac{1}{2}\pi - \theta_B$ in the clockwise direction. Here we seek a solution of the form

$$p = f(s,y,w)\, e^{ik_B s} \qquad (6.1\text{-}2)$$

where the function $f(s,y,w)$ is regarded as slowly varying in s over scales that are large relative to an acoustic wavelength. Substitution of Eq. (6.1-2) into (6.1-1) with neglect of the term containing $\partial^2 f/\partial s^2$ yields a simple form of the parabolic equation (Tappert 1977):

$$(2ik_B)\, \partial f/\partial s + \partial^2 f/\partial y^2 + \partial^2 f/\partial w^2 = 0 \qquad (6.1\text{-}3)$$

The nature of Eq. (6.1-3) is that, if an "initial condition" $f(0, y, w)$ is specified, then one can uniquely determine $f(s, y, w)$ for all $s > 0$. The solution f can be expressed (Carslaw and Jaeger 1959, pp. 50-56) in terms of the superposition of a particular solution (i.e. the Green's function) of Eq. (6.1-3), this Green's function being

$$G(s, y-y_o, w-w_o) = -(ik_B/2\pi s) \exp\{ (ik_B/2s)[(y-y_o)^2 + (w-w_o)^2] \} \qquad (6.1\text{-}4)$$

and the superposition integral being

$$f(s,y,w) = \int_{-\infty}^{\infty} \int_{-\infty}^{\infty} f(0, y_o, w_o)\, G(s, y-y_o, w-w_o)\, dy_o\, dw_o \qquad (6.1\text{-}5)$$

The expression Eq. (6.1-4) for the Green's function resembles, as $s \to 0$, a two-dimensional delta function $\delta(y-y_o, w-w_o)$, located at $y_o = y$ and $w_o = w$, so one can

verify that the integral expression of f given by Eq. (6.1-3) satisfies the prescribed "initial condition" at s=0.

6.1.2 Gaussian Beam Solution of Parabolic Equation

The solution f satisfying the parabolic equation (6.1-3) for those circumstances the when "initial condition" is of the doubly Gaussian form,

$$f(0, y, w) = A_o\, e^{-y^2/L_y^2}\, e^{-w^2/L_w^2} \tag{6.1-6}$$

can be obtained if the multiplicative factor A_o is assumed to be indpendent of s, y, and w. Using Eqs. (6.1-4) and (6.1-6) in (6.1-5), one finds that the integrals over y_o and w_o can be evaluated independently. The integral over y_o is

$$\int_{-\infty}^{\infty} e^{-y_o^2/L_y^2}\, e^{-(k_B/2is)(y_o-y)^2}\, dy_o \tag{6.1-7}$$

which is subsequently found to be

$$\frac{(2is\pi/k_B)^{1/2}\, L_y}{[L_y^2+2is/k_B]^{1/2}}\; e^{-y^2/[L_y^2+2is/k_B]} \tag{6.1-8}$$

The integral over w_o is nearly identical to that over y_o; the result of that integration is

$$\frac{(2is\pi/k_B)^{1/2}\, L_w}{[L_w^2+2is/k_B]^{1/2}}\; e^{-w^2/[L_w^2+2is/k_B]} \tag{6.1-9}$$

Putting together everything, we obtain

$$f(s, y, w) = A(s)\, e^{-y^2/[\xi_y(s)]^2}\, e^{-w^2/[\xi_w(s)]^2} \tag{6.1-10}$$

where

$$A(s) = A_o \frac{L_y\, L_w}{\xi_y(s)\, \xi_w(s)} \tag{6.1-11a}$$

$$\xi_y(s) = [L_y^2 + 2is/k]^{1/2} \tag{6.1-11b}$$

$$\xi_w(s) = [L_w^2 + 2is/k]^{1/2} \tag{6.1-11c}$$

From Eq. (6.1-2), the expression for the pressure is then identified as

$$p = A_o \frac{L_y L_w}{\xi_y \xi_w} e^{-y^2/\xi_y^2} e^{-w^2/\xi_w^2} e^{ik_B s} \tag{6.1-12}$$

6.1.3 Reinterpretation of Previously Derived Results

A comparison of the expressions (5.2-1)-(5.2-7) with the above Gaussian beam solution shows that what results for the pressure disturbance (in both the Fresnel and the farfield regions) in the high frequency and wide laser track limits is an approximate solution of the parabolic equation described in Sec. 6.1.1. A minor difference between the two cases is that one is a steady-state monochromatic disturbance and the other is a finite pulse of nearly constant frequency enclosed within the envelope factor PE [Eq. (5.2-4)]. The appropriate identification of the factor A_o would be two times the factor "Const." given in Eq. (5.2-2). Equivalently, one may regard the radiation problem posed in Chapter IV, with a heating pattern q defined by Eq. (4.1-1), as being the solution of the parabolic equation with prescribed initial conditions that depend on controllable parameters such as E, L_y, T, n, θ_B, and k_B.

The parabolic approximation is a helpful tool for understanding certain aspects of the propagation which are not necessarily associated with the assumed form for the heating configuration. One learns, for example, how the beam shape in the w direction is associated with the laser pulse shape function $E_T(t)$. (This is further discussed in Sec. 6.6.)

6.2 Disturbance for Extremely Shallow Beaming Angle

6.2.1 Inhomogeneous Parabolic Equation Model

For a rudimentary understanding of the nature of the acoustic disturbance when the angle θ_B is very small, it is sufficient to consider the idealized case

$\theta_B = \theta_S = 0$, $L_y = \infty$, with $k_B L_x$ and $k_B cT$ being finite but large. The two-dimensional version of the inhomogeneous wave equation (3.2-1) is written as

$$\partial^2 p/\partial x^2 + \partial^2 p/\partial z^2 - c^{-2}\, \partial^2 p/\partial t^2 = -(\beta/c_p)\, \partial q/\partial t \qquad (6.2\text{-}1)$$

where, given that $\omega_B T$ is substantially larger than unity, the quantity $\partial q/\partial t$ can be approximated by

$$\partial q/\partial t = K\omega_B\, e^{-\mu|z|}\, \mathrm{sign}(z)\, \cos[k_B(x - ct)]\, e^{-(x-ct)^2/L_x^2}\, e^{-t^2/T^2} \qquad (6.2\text{-}2)$$

Since the wave disturbance as well as the heat source is moving with speed c in the x direction, it is appropriate to introduce a new variable $x^* = x - ct$, so that

$$(\partial/\partial t)_{\text{fixed } x} = (\partial/\partial t)_{\text{fixed } x^*} - c\,(\partial/\partial x^*) \qquad (6.2\text{-}3)$$

Such a substitution allows one to rewrite Eq. (6.2-1) as

$$(2/c)(\partial/\partial x^*)\, \partial p/\partial t + \partial^2 p/\partial z^2 - c^{-2}\, \partial^2 p/\partial t^2 = -(\beta/c_p)\, \partial q/\partial t \qquad (6.2\text{-}4)$$

and to transform $\partial q/\partial t$ from the version of Eq. (6.2-2) to

$$\partial q/\partial t = K\omega_B\, e^{-\mu|z|}\, \mathrm{sign}(z)\, \cos(k_B x^*)\, e^{-x^{*2}/L_x^2}\, e^{-t^2/T^2} \qquad (6.2\text{-}5)$$

The desire here is to describe the principal part of the acoustic pulse at large values of x. Equivalently, one desires p when t is very large (much larger than T, for example) and $|x^*|$ is comparable or smaller than L_x. For these circumstances, given that $k_B L_x >> 1$, the pressure pulse should have the approximate form

$$p = -(K\omega_B \beta/c_p)\, e^{-x^{*2}/L_x^2}\, \mathrm{Re}\,[\, F\, e^{ik_B x^*}\,] \qquad (6.2\text{-}6)$$

where $F(z,t)$ depends on z and t, but has negligible dependence on x^*. Substitution of (6.2-6) into (6.2-4) with application of the assumption $k_B L_x >> 1$ subsequently yields

$$(2ik_B/c)\ \partial F/\partial t + \partial^2 F/\partial z^2 - c^{-2}\ \partial^2 F/\partial t^2 = \text{sign}(z)\ e^{-\mu|z|}\ e^{-t^2/T^2} \quad (6.2\text{-}7)$$

which is approximated to the inhomogeneous parabolic equation

$$(2ik_B/c)\ \partial F/\partial t + \partial^2 F/\partial z^2 = \text{sign}(z)\ e^{-\mu|z|}\ e^{-t^2/T^2} \quad (6.2\text{-}7a)$$

The reason for the neglect of the second derivative with respect to t term is that F is expected to vary slowly with t over time intervals of $1/ck_B$; the principal time variation of p is already taken care of by the factor $e^{ik_B x^*}$ in Eq. (6.2-6).

To solve the inhomogeneous parabolic equation above, one introduces the Fourier integral representation for F,

$$F = \int_{-\infty+i\epsilon}^{\infty+i\epsilon} \psi(z,\omega)\ e^{-i\omega t}\ d\omega \quad (6.2\text{-}8)$$

and consequently finds the ordinary differential equation which the Fourier transform ψ should satisfy

$$d^2\psi/dz^2 + l_o^2\ \psi = Q(z) \quad (6.2\text{-}9)$$

Here

$$l_o^2 = (2k_B\omega/c) \quad (6.2\text{-}10a)$$

$$Q = (1/2\pi)\ e^{-\mu|z|}\ \text{sign}(z) \int_{-\infty}^{\infty} e^{-t^2/T^2}\ e^{i\omega t}\ dt$$

$$= (T/2\pi^{1/2})\ e^{-\mu|z|}\ \text{sign}(z)\ e^{-\frac{1}{4}T^2\omega^2} \quad (6.2\text{-}10b)$$

Solution of (6.2-9) results with application of the Green's function technique used in Secs. 3.2 and 4.2.4. The appropriate Green's function here that conforms to the causality condition of going to zero as $\omega \to i\infty$ is

$$g(z\,|\,z_o) = \frac{1}{2il_o}\ e^{il_o|z-z_o|} \quad (6.2\text{-}11)$$

Consequently, we can write ψ in terms of the Green's function integral as

$$\psi(z,\omega) = \int_{-\infty}^{\infty} Q(z_o)\, g(z\,|\,z_o)\, dz_o \tag{6.2-12}$$

which can then be further evaluated in a closed form as

$$\psi(z,\omega) = (T/2\pi^{1/2})\, e^{-\frac{1}{4}T^2\omega^2}\, \frac{e^{-\mu z} - e^{il_o z}}{\mu^2 + (2k_B/c)\omega} \tag{6.2-13}$$

6.2.2 Analytical Solution for Large Times

When the above solution for ψ is inserted into the Fourier integral representation (6.2-8) for F, it is convenient to break the integral into two parts, one from $-\infty$ to 0, the other from 0 to ∞ and to change the integration variable to ξ, where $\omega t = \xi^2$, and with $\xi = t^{1/2}\omega^{1/2}$ defined as being analytic in the upper half of the ω-plane. Then

$$l_o = (2k_B/ct)^{1/2}\xi \tag{6.2-14}$$

and

$$F = (T/\pi^{1/2}) \int_C \frac{e^{-\xi^4 T^2/4t^2}\, e^{-i\xi^2}\, [e^{-\mu z} - e^{i(2k_B z^2/ct)^{1/2}\xi}]}{\mu^2 t + 2k_B\xi^2/c}\, \xi\, d\xi \tag{6.2-15}$$

Here the integration contour C lies entirely within the first quadrant of the ξ-plane and proceeds from $i\infty$ to the vicinity of the origin to ∞. [One may note that the apparent pole on the positive imaginary axis is cancelled by a coincident zero of the numerator.]

For $t >> T$, the two terms comprising (6.2-15) can each be evaluated by the saddle point approximation. For the first term, the saddle point is at $\xi = 0$ and the path of steepest descents is in the $-\pi/4$ direction near the saddle point. For the second term, the saddle point is approximately at

$$\xi_{sp} \simeq (k_B z^2/2ct)^{1/2} \tag{6.2-16}$$

and the path of the steepest descents is also approximately in the $-\pi/4$ direction near the saddle point. The first term gives minor contribution at large t and is accordingly discarded, so we get

$$F \simeq -\frac{T\,(k_B z^2/2ct)^{1/2}}{\mu^2\, t + (k_B^2 z^2/c^2 t)}\; e^{ik_B z^2/2ct}\; e^{-i\pi/4} \tag{6.2-17}$$

Since the above derivation presumes $|x^*|$ to be finite and t to be large, one may equivalently replace ct by x in the above. Also, since z is presumed small compared with x, one can replace z/ct by θ, the polar angle reckoned downward from the horizontal. Such substitutions yield

$$F \simeq -\frac{T}{(2k_B x)^{1/2}}\frac{c}{k_B}\;\frac{\theta}{\theta^2 + (\mu/k_B)^2}\; e^{i\frac{1}{2}k_B x\theta^2}\; e^{-i\pi/4} \tag{6.2-18}$$

so Eq. (6.2-6) becomes

$$p \simeq \frac{Kc^2\beta}{c_p}\;\frac{T\, e^{-(x-ct)^2/L_x^2}}{(2k_B x)^{1/2}}\;\frac{\theta}{\theta^2 + (\mu/k_B)^2}\cos\{k_B(x-ct) + \tfrac{1}{2}k_B x\theta^2 - \tfrac{1}{4}\pi\} \tag{6.2-19}$$

6.2.3 Discussion of Solution

The above describes a cylindrically spreading radiation pattern with one (possibly very narrow) lobe that points obliquely downwards into the water. The pressure vanishes at the free surface ($\theta = 0$) as it should and has a peak amplitude at $\theta = \mu/k_B$ (assuming that μ/k_B is somewhat smaller than unity). The lobe has half power points where

$$\frac{\theta_{half}}{\theta_{half}^2 + (\mu/k_B)^2} = (2)^{-1/2}\,(k_B/2\mu) \tag{6.2-20}$$

or such that

$$\theta_{half} = (2^{1/2} \pm 1)\,\mu/k_B \tag{6.2-21}$$

The beam width is consequently $2\mu/k_B$.

A heuristic correction to Eq. (6.2-19) to take into account the finite value of L_y is easily provided by noting that the pressure disturbance should spread in y with increasing propagation distance x in the same manner as for a Gaussian beam, so with reference to Eqs. (4.3-27)–(4.3-28), we see that a factor

$$(L_y/\xi_1)\, e^{y^2/\xi_1^2} \qquad \text{with} \quad \xi_1^2 = L_y^2 + i2x/k_B \tag{6.2-22}$$

should be included. Thus one obtains

$$p \simeq \frac{Kc^2\beta}{c_p} \frac{T\, e^{-(x-ct)^2/L_x^2}}{(2k_Bx)^{1/2}} \frac{\theta}{\theta^2 + (\mu/k_B)^2} L_y\, Re\{\frac{e^{-y^2/\xi_1^2}\, e^{i\Phi}}{\xi_1}\} \tag{6.2-23}$$

as the result, where

$$\Phi = k_B(x - ct) + k_Bx\theta^2/2 - \pi/4$$

$$= k_B(s - ct) - \pi/4 \tag{6.2-24}$$

is the phase function. Here we recognize that

$$x + x\theta^2/2 = x + z^2/2x \simeq [x^2 + z^2]^{1/2} = s \tag{6.2-25}$$

is the distance along a line from the origin. The multiplicative factor K, according to Eq. (4.1-7), with $\theta_B = 0$, is

$$K = \frac{\mu E}{\pi^{3/2} L_x L_y T} \tag{6.2-26}$$

Note that the factors of T cancel, so the amplitude of the generated sound is proportional to the energy E of the laser pulse in this limit, given that $x >> cT$.

One may anticipate that the above results match (in some sense) those results for the moderate θ_B case that are given in Sec. 5.2.1. If one lets θ_B be small in Eqs. (5.2-1)–(5.2-7) and assumes $2s >> k_B L_w^2$, then the solution of Sec. 5.2.1 reduces along

the center of the beam (w=0) to

$$p = \frac{Kc^2\beta}{c_p} \frac{T\, e^{-(x-ct)^2/L_x^2}}{(2k_B x)^{1/2}} \mathrm{Re}\{\frac{L_y}{\xi_1} e^{-y^2/\xi_1^2} e^{i\Phi} \frac{\theta_B}{2\theta_B + i(\mu/k_B)} \frac{k_B}{\mu}\} \quad (6.2\text{-}27)$$

In contrast, Eq. (6.2-23) reduces at the beam peak, where $\theta = \mu/k_B$, to

$$p = \frac{Kc^2\beta}{c_p} \frac{T\, e^{-(x-ct)^2/L_x^2}}{(2k_B x)^{1/2}} \mathrm{Re}\{\frac{L_y}{\xi_1} e^{-y^2/\xi_1^2} e^{i\Phi} \frac{1}{2} \frac{k_B}{\mu}\} \quad (6.2\text{-}28)$$

This, however, is the same as (6.2-27) in the limit $\theta_B >> \mu/k_B$. One should bear in mind that the result (6.2-23) is applicable only for small θ, so its prediction of the peak value in the beam applies only if μ/k_B is substantially smalller than unity. One may note that, in all other aspects, the two solutions agree. Thus, the moderate θ_B solution is substantiated down to relatively small values of θ_B if μ/k_B is small. This conclusion could also apply for larger μ/k_B, but the present analysis does not give any information in this respect.

6.3 Theory for General Models of Heat Deposition

The present section outlines an approximate theory for predicting the acoustic field when the heat deposition is of a somewhat more general form than described in Sec. 4.1. Here we take

$$\partial q/\partial t = \mathrm{Re}\{ K(x,y,t)\, e^{-\mu_T|z|}\, \mathrm{sign}(z)\, e^{i\Phi}\} \quad (6.3\text{-}1)$$

where K(x,y,t) is a real function that varies slowly with its arguments x, y, and t over distances of the order of a representative acoustic wavelength or over times of the order of a representative wave period.

The coefficient $\mu_T(x,y,t)$ is possibly complex and a slowly varying function of x, y, and t. The phase function $\Phi(x,y,t)$ is real and varies primarily with x and t, but possibly also varies slowly with y. The phase Φ should appear nearly constant to

someone moving at a supersonic speed V(x,y,t) in the x direction over the surface. The structure of Φ is assumed quasi-linear in both x and t, such that the quantities

$$k_x(x,y,t) = \partial\Phi/\partial x \tag{6.3-2a}$$

$$\omega_B(x,y,t) = -\partial\Phi/\partial t \tag{6.3-2b}$$

are both slowly varying functions of their arguments. The speed V(x,y,t) is identified as

$$V(x,y,t) = \omega_B/k_x \tag{6.3-3}$$

One also identifies

$$k_y(x,y,t) = \partial\Phi/\partial y \tag{6.3-4}$$

but this is regarded as much smaller than k_x. Both ω_B and k_x are assumed positive, and V is greater than c. The generated sound wave can be expected to propagate at an angle θ_B with the horizontal where

$$\cos\theta_B = (c/\omega_B)\,[k_x^2 + k_y^2]^{1/2} \tag{6.3-5}$$

is also a function of x, y, and t.

At distances of the order of $1/\mu_T$ or less below the water surface, the perturbed pressure disturbance should locally be proportional to K, so one can set

$$p \simeq (\beta/c_p)\,\mathrm{Re}\{\,I\,K\,e^{i\Phi}\} \tag{6.3-6}$$

where I(x,y,z,t) is slowly varying with x, y, and t, but perhaps rapidly varying with z. Substitution of this and Eq. (6.3-1) into the inhomogeneous wave equation (3.2-1) with appropriate approximations consequently yields

$$d^2I/dz^2 + [k_B^2 \sin^2\theta_B]\, I = -\, e^{-\mu_T|z|}\, \mathrm{sign}(z) \tag{6.3-7}$$

where

$$k_B^2 = \omega_B^2/c^2 \tag{6.3-8}$$

is the wave number of the plane wave in the direction of propagation.

The appropriate solution of the ordinary differential equation (6.3-7), as discussed in the earlier Sec. 3.2 of this thesis, is

$$I = \frac{e^{ik_B z \sin\theta_B} - e^{-\mu_T z}}{\mu_T^2 + k_B^2 \sin^2\theta_B} \tag{6.3-9}$$

for $z>0$ (below the water surface). Here, in contrast to what was assumed in previous sections, the quantities k_B, θ_B, and μ_T are all assumed to be slowly varying functions of x, y, and t. [The above is the same in Eq. (3.2-8), with the identification $\mu_T = \mu_c - ik_x \tan\theta_S$.]

6.4 Geometrical Acoustics Theory

The simplest model which ensues from the equations presented above is that of geometrical acoustics, whereby the sound propagates obliquely downwards along rays without appreciable diffraction effects. Such a model should be applicable in the Fresnel region and may also retain some applicability in the far field, especially near the center of the beam of sound or if ray tube spreading dominates over spreading due to diffraction.

To introduce the geometrical acoustics theory into the present problem, one sets

$$p = -(\beta/c_p)\, \mathrm{Re}\{ \frac{K\, e^{-\mu_T z}\, e^{i\Phi}}{\mu_T^2 + k_B^2 \sin^2\theta_B} \} + (\beta/c_p)\, \mathrm{Re}\{ \Psi\, e^{iW} \} \tag{6.4-1}$$

where Ψ and W remain to be determined. Comparison with Eqs. (6.3-6) and (6.3-9) indicates that Ψ and W should reduce to

$$\Psi \rightarrow \frac{K}{\mu_T^2 + k_B^2 \sin^2\theta_B} \qquad \text{as} \quad z \rightarrow 0 \qquad (6.4\text{-}2a)$$

$$W \rightarrow \Phi + k_B z \sin\theta_B \qquad \text{as} \quad z \rightarrow 0 \qquad (6.4\text{-}2b)$$

Furthermore, the method of construction which led to Eq. (6.3-9) suggests that Ψe^{iW} can, to a very good approximation, be regarded as a solution of the homogeneous wave equation. Such would be especially so, for example, if K, μ_T, k_B, and θ_B were slowly varying over distances larger than $1/|\mu_T|$.

If one adheres to the spirit of the geometrical acoustics approximation, then the phase W should appear constant to someone moving along a ray with speed c. Let such a ray leave a point x_o, y_o on the water surface at time t_o. The ray is a straight line and is in the direction of (k_x,k_y,k_z) where k_x and k_y are evaluated at x_o, y_o, t_o, and where $k_z = k_B \sin\theta_B$. Thus one has

$$W(x,y,z,t) = \Phi(x_o,y_o,t_o) \qquad (6.4\text{-}3a)$$

$$x = x_o + c(t-t_o)k_x/k_B \qquad (6.4\text{-}3b)$$

$$y = y_o + c(t-t_o)k_y/k_B \qquad (6.4\text{-}3c)$$

$$z = c(t-t_o)\sin\theta_B \qquad (6.4\text{-}3d)$$

This can be regarded as a parametric description of the phase function W(x,y,z,t). One can, in principle, solve Eqs. (6.4-3b,c,d) for x_o, y_o, and t_o in terms of x, y, z, and t; then one substitutes into the arguments of $\Phi(x_o,y_o,t_o)$ on the right side of Eq. (6.4-3a). What results must be a solution of the first order partial differential equation

$$c^{-2}(\partial W/\partial t)^2 = (\nabla W)^2 \tag{6.4-4}$$

In accord with the approximate theory of Sommerfeld and Runge (1911, described by Pierce, 1981, pp. 396-400), the amplitude function Ψ should vary along a ray as

$$\Psi(x,y,z,t) = \{\frac{S_I\, S_{II}}{[S_I + c(t-t_o)]^{1/2}\,[S_{II} + c(t-t_o)]^{1/2}}\}\,\{\frac{K}{\mu_T^2 + k_B^2 \sin^2\theta_B}\}_o \tag{6.4-5}$$

where the subscript "o" refers to the arguments x_o, y_o, and t_o, while S_I and S_{II} are principal radii of curvature of the wavefront at x_x, y_o, and t_o. The latter two quantities are determined from the requirement that the mapping $(x_o,y_o,0,t_o)$ to (x,y,z,t) for fixed t, according to the ray tracing equations (6.4-3), should predict that two adjacent rays simultaneously intersect. This implies that the differential relations

$$\begin{bmatrix} dx \\ dy \\ dz \end{bmatrix} = \begin{bmatrix} 1-(\partial n_x/\partial x_o)s & -(\partial n_x/\partial y_o)s & -(\partial n_x/\partial t_o)s - cn_x \\ -(\partial n_y/\partial x_o)s & 1-(\partial n_y/\partial y_o)s & -(\partial n_y/\partial t_o)s - cn_y \\ -(\partial n_z/\partial x_o)s & -(\partial n_z/\partial y_o)s & -(\partial n_z/\partial t_o)s - cn_z \end{bmatrix} \begin{bmatrix} dx_o \\ dy_o \\ dt_o \end{bmatrix} \tag{6.4-6}$$

where $s = -c(t-t_o)$, should have a result where $dx=0$, $dy=0$, $dz=0$ for some nonzero vector dx_o, dy_o, dz_o. [In the above equation, $\mathbf{n} = n_x\mathbf{e}_x + n_y\mathbf{e}_y + n_z\mathbf{e}_z$ is the unit vector in the direction of the ray passing through x_o, y_o, z_o, at time t_o.] This will be so if the determinant of the coefficient matrix vanishes, so

$$\begin{Vmatrix} 1-(\partial n_x/\partial x_o)s & -(\partial n_x/\partial y_o)s & -(\partial n_x/\partial t_o)s - cn_x \\ -(\partial n_y/\partial x_o)s & 1-(\partial n_y/\partial y_o)s & -(\partial n_y/\partial t_o)s - cn_y \\ -(\partial n_z/\partial x_o)s & -(\partial n_z/\partial y_o)s & -(\partial n_z/\partial t_o)s - cn_z \end{Vmatrix} = 0 \tag{6.4-7}$$

Using the various properties of determinants, plus the fact that $n_x^2 + n_y^2 + n_z^2 = 1$, one arrives at the equivalent condition

$$\begin{Vmatrix} 1-(\partial n_x/\partial x_o)s & -(\partial n_x/\partial y_o)s & -c^{-1}(\partial n_x/\partial t_o)s-n_x \\ -(\partial n_y/\partial x_o)s & 1-(\partial n_y/\partial y_o)s & -c^{-1}(\partial n_y/\partial t_o)s-n_y \\ n_x & n_y & -1 \end{Vmatrix} = 0 \qquad (6.4\text{-}8)$$

Then, since $n_x=-c\Phi_x/\Phi_t$ and $n_y=-c\Phi_y/\Phi_t$ (with subscripts on Φ denoting partial derivatives evaluated at x_o, y_o, and t_o) one derives

$$\begin{Vmatrix} \Phi_t^2+(\Phi_{xx}\Phi_t-\Phi_x\Phi_{xt})cs & (\Phi_{xy}\Phi_t-\Phi_x\Phi_{yt})cs & c\Phi_x\Phi_t(\Phi_{xt}\Phi_t-\Phi_x\Phi_{tt})s \\ (\Phi_{yx}\Phi_t-\Phi_y\Phi_{xt})cs & \Phi_t^2+(\Phi_{yy}\Phi_t-\Phi_y\Phi_{yt})cs & c\Phi_y\Phi_t(\Phi_{yt}\Phi_t-\Phi_y\Phi_{tt})s \\ c\Phi_x & c\Phi_y & \Phi_t \end{Vmatrix} = 0 \qquad (6.4\text{-}9)$$

This is readily seen to be a quadratic equation for s. The two roots correspond to S_I and S_{II}, respectively.

6.5 Beam Generated by Heat Deposition with Variable Velocity

As a special case of the theory outlined in the previous section, one can consider the case when the phase function Φ depends on x and t only, such that

$$\Phi = \omega_B \int_0^x V^{-1}(\xi)\, d\xi - \omega_B t \qquad (6.5\text{-}1)$$

Here, ω_B is assumed to be a constant and V is a slowly varying function in x over the representative distance between two adjacent light-slabs. The fact that Φ is independent of y means that, in the absence of diffraction, the resulting sound beam will have no spreading in the y direction. From Eq. (6.3-2a), the wave number of the heating ripples on the water surface is identified to be

$$k_x(x) = \omega_B/V(x) \qquad (6.5\text{-}2)$$

This would be true for the case where the spacings between light-slabs are constantly adjusted such that the ω_B can be held fixed while velocity is being varied .

To apply the geometrical acoustics theory developed in the previous section, we proceed by evaluating the derivatives of Φ with respect to x, y, and t. Equation (6.5-1) enables one to obtain

$$\Phi_x = \omega_B/V \; ; \qquad \Phi_{xx} = -\omega_B V^{-2}(dV/dx) \tag{6.5-3a}$$

$$\Phi_t = -\omega_B \; ; \qquad \Phi_{tt} = \Phi_{xt} = 0 \tag{6.5-3b}$$

$$\Phi_y = \Phi_{yy} = \Phi_{xy} = \Phi_{yt} = 0 \tag{6.5-3c}$$

Substituting Eq. (6.5-3) into the condition given by Eq. (6.4-9), we obtain the equation (linear rather than quadratic) which S_I should satify; this equation predicts

$$S_I = \frac{1 - M^2}{dM/dx} \tag{6.5-4}$$

where $M=V(x)/c$ is the Mach number of the moving heating pattern. The second principal radius S_{II} associated with the y direction, which does not emerge from the condition (6.4-9), is known in advance to be equal to ∞ .

Since S_I is positive for a diverging ray tube and $1-M^2<0$ for V being supersonic, one way to create a diverging sound beam (and thereby broadening the beam-width) is to choose

$$dM/dx < 0 \tag{6.5-5}$$

which means that the heating pattern decelerates as it is moved along the $+x$ direction. The amplitude factor along a ray under such circumstance is identified from Eq. (6.4-5) as

$$\frac{p(x,y,z,t)}{p(x_o,y_o,0,t_o)} = \left[\frac{S_I}{S_I + c(t-t_o)}\right]^{1/2}$$

$$= \left[1 + \left(\frac{dM/dx}{1-M^2}\right) c(t-t_o)\right]^{-1/2} \tag{6.5-6}$$

which resembles cylindrical spreading when $c(t-t_0)$ is large. [Note that $c(t-t_o)$ is the propagation distance s.]

The directions covered by the generated sound beam can be found with Eq. (6.3-5); in the present context θ_B is such that

$$\cos\theta_B = ck_x/\omega_B = c/V(x) \tag{6.5-7}$$

Consequently, we conclude that the beam width is

$$[\text{Beamwidth}] = \cos^{-1}(c/V_{max}) - \cos^{-1}(c/V_{min}) \tag{6.5-8}$$

where V_{max} and V_{min} represent the maximum (initial) and the minimum (final) velocity of the heating pattern.

In the event that one wishes to have k_x fixed (independent of x) while varying V, the simplest case would be

$$\Phi = k_x x - k_x \int_0^t V(\tau)\, d\tau \tag{6.5-9}$$

Here, it is convenient to define the velocity V(t) as a function of time elapsed. Following the same approach described above, we find

$$S_I = \frac{cM(1-M^2)}{dM/dt} \tag{6.5-10}$$

A similar condition, $dM/dt<0$, is required for the sound beam to diverge; the amplitude factor would be

$$[\text{Amplitude Factor}] = [1 + (\frac{dM/dt}{cM(1-M^2)})\, c(t-t_o)\,]^{-1/2} \tag{6.5-11}$$

The relation $\cos\theta_B=c/V(t)$ indicates that Eq. (6.5-8) is still valid for the description of the resulting beamwidth. For the constant k_x model, listeners located within the sound beam in various ray directions should receive acoustic signals of

slightly different frequencies.

6.6 Theory for Heat-Deposition Patterns with Non-Gaussian Envelopes

The angular distribution of the resulting sound beam and the envelope shape of the pulsed acoustic signal can be approximately predicted using the geometrical acoustic theory discussed in Sec. 6.4. Here, we consider the phase function as being of the form

$$\Phi = k_x x - \omega_B t \tag{6.6-1}$$

The simplified model for Φ predicts no spreading in both the y and w directions. [This can be shown by substituting the derivatives of Φ with respect to x, y, and t into condition (6.4-9) and subsequently deducing that $S_I = S_{II} = \infty$.] Neverless, the model suffices to explain how non-Gaussian envelopes affect the resulting acoustic disturbance.

For the general classes of sound generation described in Chapters IV and V, we find that the description of the sound beam is simplified with the use of the coordinates s and w (rather than x and z). Thus, we proceed to develop mapping equations analogous to those given in Eqs. (6.4-3), which will map a point (x_o,y_o) at time t_o on the surface to a point (s,w,y) that lies on the same ray at time t.

In Fig. 6.1, we can identify that $\underline{AC} = \underline{OD} = w$, $\underline{OC} = \underline{AD} = s$, $\underline{OB} = w/\sin\theta_B$, and $\underline{DB} = w\cot\theta_B$. Consequently, we can write

$$x_o = \underline{OB} = w/\sin\theta_B \tag{6.6-2a}$$

$$y_o = y \tag{6.6-2b}$$

$$t_o = t - \underline{AB}/c = t - (s - w\cot\theta_B)/c \tag{6.6-2c}$$

Because $S_I = S_{II} = 0$, the amplitude factor is equal to unity. Therefore, one concludes

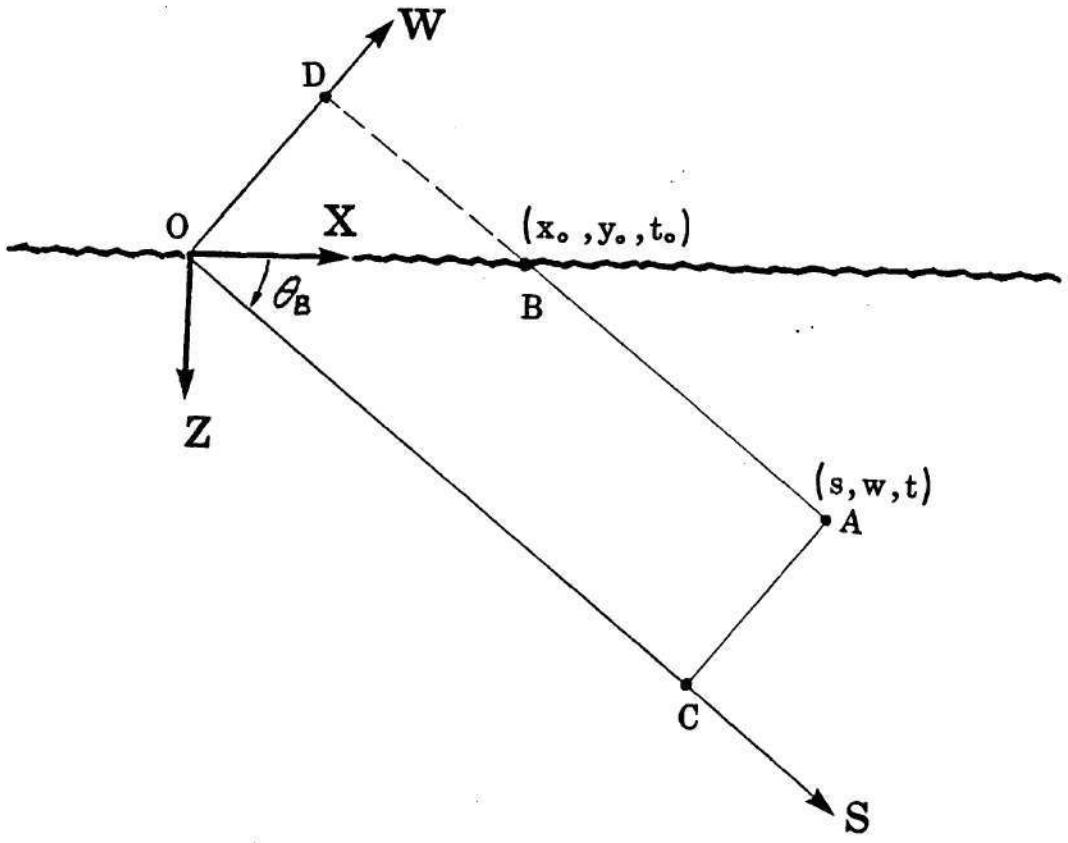

FIGURE 6.1 Geometry used in the discussion of sound generation by a heat-deposition pattern with non-Gaussian envelope functions.

from Eq. (6.4-5) that

$$\Psi(x,w,y,t) = \frac{K(x_o,y_o,t_o)}{\mu_T^2 + k_B^2 \sin^2\theta_B} \tag{6.6-3a}$$

$$K(x_o,y_o,t_o) = K(w/\sin\theta_B,\ y,\ t - \frac{s + w\cot\theta_B}{c}) \tag{6.6-3b}$$

Here, Eq. (6.6-3b) results directly from the mapping equations (6.6-2).

Let us also assume, for simplicity, that $K(x_o,y_o,t_o)$ is made up of the product of three envelope factors $E_T(t_o)$, $E_x(x_o - Vt_o)$, and $E_y(y_o)$. The product of the latter two factors is referred to as the moving envelope function $E_M(x_o - Vt_o, y_o)$ in Sec. 4.1. The product of these envelope factors should be such that they posess the properties of the $K(x_o,y_o,t_o)$ prescribed in the beginning of Sec 6.3. Using the mapping relations Eq. (6.6-2) and the identity $V = c/\cos\theta_B$, we rewrite the argument of E_x as

$$\begin{aligned} x_o - Vt_o &= w/\sin\theta_B - c(t - c^{-1}s)/\cos\theta_B - w\cot\theta_B/\cos\theta_B \\ &= (s - ct)/\cos\theta_B \end{aligned} \tag{6.6-4}$$

With the three envelope factors inserted into Eq. (6.6-3a) to describe the resulting sound beam, one recognizes that

$$E_x(\frac{s - ct}{\cos\theta_B}), \quad E_y(y), \quad \text{and} \quad E_T(t.c^{-1}s + c^{-1}w\cot\theta_B) \tag{6.6-5}$$

govern the pulse shape, and the beam shapes in the y and w directions, respectively. This identification may be used to explain results obtained in Sec. 5.2.1: (i) the acoustic pulse length is associated with the parameter L_x and (ii) the beam shapes in the y and w directions are scaled by the parameters L_y and T, respectively.

To test the above theory, we consider the case for which

$$K(x_o,y_o,t_o) = K_o\, e^{-(x_o - Vt_o)^2/L_x^2}\, e^{-y_o^2/L_y^2}\, E_T(t_o) \tag{6.6-6a}$$

$$E_T(t) = 8.16\,(1 + t/T)\,e^{-3(1+t/T)} \qquad \text{for } t > -T$$

$$= 0 \qquad \text{otherwise} \qquad (6.6\text{-}6b)$$

and compare the above inferences with explicitly calculated numerical results based on the triple integral of Eq. (4.1-8). The parameter K_o is the same as the K defined previously in Eq. (4.1-7). We study the resulting beam shape in the w direction of the sound beam at some propagation distance s within the Fresnel region, so the functions, E_x and E_y, retain the definitions used in Chapters IV and V. The function $E_T(t)$ [see Fig. 6.2(a)] given by Eq. (6.6-6b) is a mathematical curve-fit to the intensity versus time relation of a typical laser pulse reported in experimental works by Muir, Culbertson, and Clynch (1976) and Berthelot (1985) (see also Fig. 1.1).

Figure 6.2(b) gives numerical results for the pressure amplitude along the w direction with Eq. (6.6-6c) taken as describing the laser pulse shape. The computation is for $s=ct$ and $y=0$, so the two factors E_x and E_y in Eq. (6.6-5) are each unity. The numerical inputs are $\theta_B=\theta_S=20°$, $L_y=6$ m, $n=10$ cycles, $T=0.0108$ s, $s=100$ m, $\mu=13.7$ m^{-1}, and $f_B=10$ kHz. The dashed line is the prediction using the described heuristic theory [or Eq. (6.4-1)] and the dots (connected with solid straight lines) are results obtained from the direct numerical integration. (The portion of the program that describes this particular heating function, named the "alternate heating function," is listed in a comment block near the end of the program listing in the Appendix.) The ripples exhibited by the numerical results for the triple integration that appear on left side (–w side) of the curves is a diffraction effect associated with the abrupt beginning of the function E_T [see Eq. (6.6-6c) and Fig. 6.2(a)]. Geometrical acoustics theory, on the other hand, assumes that K(x,y,t) is smoothly varying with its arguments, and consequently tacitly eliminates diffraction effects. Apart from the diffraction anomalies, the two results show reasonably good agreement.

The theory given above should be an appropriate rough approximation for

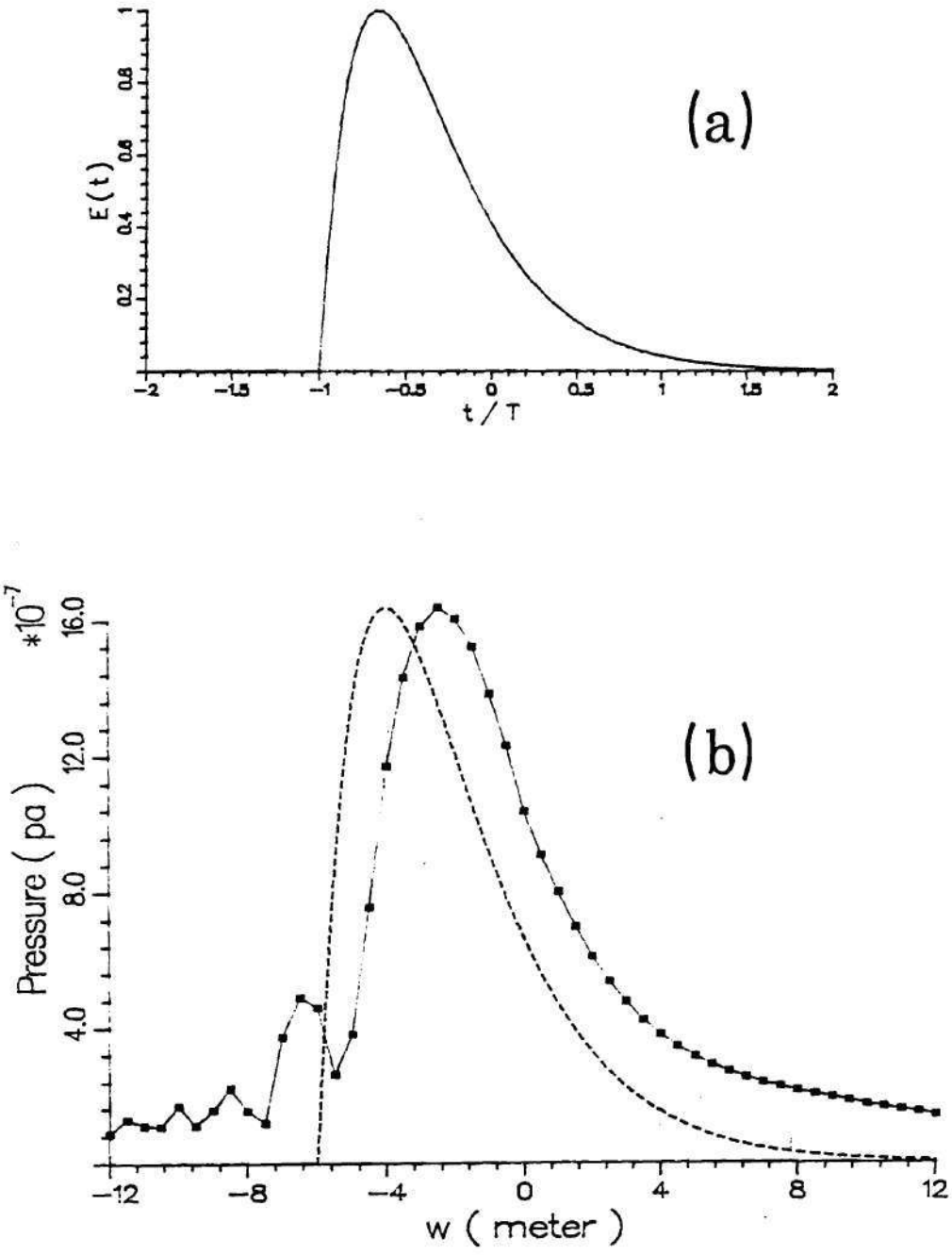

FIGURE 6.2 Comparison of two predictions of beam shape, giving pressure amplitude versus transverse coordinate w. Indicated points correspond to direct numerical interagtion of triple integral; the dashed line corresponds to a simple theoretical model based on geometrical acoustics.

propagation distances s up to the outer extent of the Fresnel region. Although the simplest (without diffraction spreading) theory breaks down in the farfield where s is large compared with k_B^2cT, the beam shapes in the y and w directions can be predicted using the parabolic equation described in Sec. 6.1. For given slowly varying functions $E_T(t)$ and $E_y(y)$, one used the geometrical acoustics theory to predict $f(0,y,w)$ (i.e., the "initial condition" mentioned in Sec. 6.1.1). This prediction is then used along with Eqs. (6.1-4) and (6.1-5). Beam shapes for any $s>0$ can be determined from Eq. (6.1-5). One notes that in the limit $k_Bs\rightarrow\infty$, the expression (6.1-5) has the asymptotic form

$$f(s\rightarrow\infty,y,w) = -(ik_B/2\pi s)\, e^{i(k_B/2s)(y^2+w^2)}\, F(0, k_By/s, k_Bw/s) \qquad (6.6\text{-}7)$$

where

$$F(0,\alpha_y,\alpha_w) = \iint f(0,y_o,w_o)\, e^{i\alpha_y y_o}\, e^{i\alpha_w w_o}\, dy_o\, dw_o \qquad (6.6\text{-}8)$$

is the Fourier transform of f. Therefore, it is concluded that the farfield beam pattern (given the restricted types of heating configurations considered here) is closely related to the Fourier transform of its nearfield beam pattern.

6.7 Effect of Water Waves on Sound Generation

A detailed analysis of the effects of water waves (or ocean waves) on the generation of laser-induced sound is outside the scope of the present thesis; the discussion here is confined to the identification of the basic mechanisms and to the development of simple analytical models for quantitatively determining whether water waves could have an important influence on system performance.

Water wave influences are discussed in a number of previous papers [e.g. Bozhkov, Bunkin, and Gyrdev (1976); Kasoev and Lyamshev (1977); Lyamshev and Sedov (1977); Bozhkov and Gyrdev (1978); and Kasoev et al. (1979)]. In these

papers, for the most part, the laser beam is stationary and the principal effect considered is the scattering of the sound from the rippled pressure-release surface. The general heating configurations discussed in this thesis, however, are also subject to another water wave effect because the sound source is horizontally extended. The surface height fluctuations with horizontal displacement could cause a loss of phase coherence so that there would be large fluctuations in the farfield sound at great distances. It is this mechanism that is examined here.

6.7.1 Heating Configuration Model with Water Waves

To display the governing physical principles with a minimum of mathematical complications, one may take the water surface height above ambient to be given by

$$\eta = h_w \cos(k_w x - \omega_w t) \tag{6.7-1}$$

where k_w and ω_w are related by the deep-water dispersion relation relation

$$\omega_w^2 = g\, k_w \tag{6.7-2}$$

with g being the acceleration due to gravity. One may regard ω_w as being much less than the frequency of the generated sound and $2\pi/k_w$ as being much longer than the wavelength of the generated sound. However, the water wave height h_w may be comparable to the acoustic wavelength. For the laser-heat deposition, one may, for an initial exploratory study, use that discribed by Eq. (3.2-2), with z taken as distance below the true surface. Thus one has

$$q = K\, e^{-\mu_e(z+\eta)}\ \{1 + \sin(\omega_B t + k_x[x + (z+\eta)\tan\theta_S])\} \tag{6.7-3}$$

This is the same as Eq. (3.2-2), only $z+\eta$ replaces z, with η given by Eq. (6.7-1).

One effect that should be taken into account is that θ_S is affected by the nonzero slope of the surface when a water wave is present. This effect may be

important if the value of μ/k_B is small and if the angle of incidence is intended to cause $\theta_S = \theta_B$. With reference to Eqs. (3.2-9), (3.2-10), (3.2-11), and (3.2-13), one finds that $\delta\theta_S$ is at most of the order of the water wave slopt and that the change in D_p will be small if the latter is small compared to σ. Thus, one clear criterion for neglecting water wave effects is that μ/k_B be substantially larger than the rms water slope.

6.7.2 Water Wave Effects on Shallow Angle Propagation

For simplicity and also because the small θ_B case exhibits the essential features of a heating configuration that exploits the acoustic pumping principle, the analysis here is limited to the case when the configuration moves over the surface at a near sonic speed. The task is to modify the analysis of Sec. 6.2 to account for a water wave of the form of Eq. (6.7-1).

One may argue that the analysis leading to Eqs. (6.2-6) and (6.2-7a) is again based on reasonable approximations provided z is replaced by $z+\eta$, so one has

$$p = -(K\omega_B\beta/c_p)\, e^{-x^{*2}/L_x^2}\, \mathrm{Re}\,[\, F\, e^{ik_Bx^*}\,] \tag{6.7-4a}$$

$$(2ik_B/c)\,\partial F/\partial t + \partial^2 F/\partial z^2 = \mathrm{sign}(z+\eta)\, e^{-\mu|z+\eta|}\, e^{-t^2/T^2} \tag{6.7-4b}$$

with $x^* = x - ct$ and $\eta = h_w\cos(k_w[x^*+ct]-\omega_w t)$. Also, since the disturbance is localized near $x^*=0$ and since $\omega_w/k_w << c$, one can approximate

$$\eta = h_w \cos(k_w^* ct) \tag{6.7-5a}$$

$$k_w^* = k_w - \omega_w/c \simeq k_w \tag{6.7-5b}$$

The solution of the parabolic equation (6.7-4b) proceeds as outlined in Sec. 6.2 with the result

$$F = \int_{-\infty+i\epsilon}^{\infty+i\epsilon} \psi(z,\omega)\, e^{-i\omega t}\, d\omega \tag{6.7-6a}$$

$$\psi(z,\omega) = -\int_{-\infty}^{\infty} Q(z_o)\,(2il_o)^{-1}\,e^{il_o|z-z_o|}\,dz_o \tag{6.7-6b}$$

$$l_o^2 = 2k_B\omega/c \tag{6.7-6c}$$

Here, however,

$$Q = (1/2\pi)\int_{-\infty}^{\infty} e^{-\mu|z+\eta|}\,\mathrm{sign}(z+\eta)\,e^{-t^2/T^2}\,e^{i\omega t}\,dt \tag{6.7-7}$$

or, with an approximate power series expansion in η,

$$Q = (1/2\pi)\,e^{-\mu|z|}\,\mathrm{sign}(z)\int_{-\infty}^{\infty} e^{-t^2/T^2}\,e^{i\omega t}\,dt$$

$$+ (1/2\pi)\,[2\delta(z) - \mu e^{-\mu|z|}]\int_{-\infty}^{\infty} \eta e^{-t^2/T^2}\,e^{i\omega t}\,dt \tag{6.7-8a}$$

$$\simeq (T/2\pi^{1/2})\,e^{-\mu|z|}\,\mathrm{sign}(z)\,e^{-\frac{1}{4}T^2\omega^2}$$

$$+ \frac{Th_w}{2\pi^{1/2}}\,(\delta(z) - \tfrac{1}{2}\mu e^{-\mu|z|})\,[e^{-\frac{1}{4}T^2(\omega+k_wc)^2} + e^{-\frac{1}{4}T^2(\omega-k_wc)^2}] \tag{6.7-8b}$$

where $\delta(z)$ denotes the Dirac delta funtion.

Thus, the water-wave induced fluctuation in $\psi(z,\omega)$ is given by

$$\Delta\psi = (Th_w/2\pi^{1/2})\,[e^{-\frac{1}{4}T^2(\omega+k_w^*c)^2} + e^{-\frac{1}{4}T^2(\omega-k_w^*c)^2}]$$

$$\int_{-\infty}^{\infty} (\delta(z_o) - \tfrac{1}{2}\mu e^{-\mu|z_o|})\,\frac{e^{il_o|z-z_o|}}{2il_o}\,dz_o$$

$$= -(Th_w/2\pi^{1/2})\,[e^{-\frac{1}{4}T^2(\omega+k_w^*c)^2} + e^{-\frac{1}{4}T^2(\omega-k_w^*c)^2}]$$

$$\cdot\,[\frac{\mu e^{-\mu z} + il_o e^{il_o z}}{2(\mu^2 + l_o^2)}] \tag{6.7-9}$$

The corresponding fluctuation ΔF in the inverse Fourier transform F of ψ can be expressed as an integral over $\xi = t^{1/2}\omega^{1/2}$ in a manner analogous to that described in

Sec. 6.2.2. The resulting contour integral is

$$\Delta F = -\frac{Th_w}{\pi^{1/2}} \int_C E(\xi) \frac{[\mu e^{-\mu z} + i(2k_B/ct)^{1/2}\xi e^{i(2k_B z^2/ct)^{1/2}\xi}]}{\mu^2 t + 2k_B\xi^2/c} \xi \, d\xi \quad (6.7\text{-}10)$$

with

$$E(\xi) = \tfrac{1}{2}[e^{-\frac{1}{4}(T/t)^2(\xi^2 + k_w^* ct)^2} + e^{-\frac{1}{4}(T/t)^2(\xi^2 - k_w^* ct)^2}] e^{-i\xi^2} \quad (6.7\text{-}11)$$

and where the contour C is as described previously. The method of steepest descents can again be used to evaluate the integral with the result

$$\Delta F \simeq -\frac{T}{(2k_B ct)^{1/2}} \frac{c}{k_B} k_B h_w \frac{(z/ct)}{(z/ct)^2 + (\mu/k_B)^2} e^{i\pi/4} e^{i(k_B ct/2)(z/ct)^2}$$

$$\cdot \tfrac{1}{2}\{1 + e^{-(k_B cT/4)^2[(z/ct)^2 - 2k_w/k_B]^2}\}$$

$$\simeq -\frac{T}{(2k_B x)^{1/2}} \frac{c}{k_B} k_B h_w \frac{\theta^2}{\theta^2 + (\mu/k_B)^2} e^{i\pi/4} e^{ik_B x\theta^2/2}$$

$$\cdot \tfrac{1}{2}[1 + e^{-(k_B cT/4)^2(\theta^2 - 2k_w/k_B)^2}] \quad (6.7\text{-}12)$$

The resulting pressure deviation Δp that should be added to Eq. (6.2-23) is then

$$\Delta p \simeq \frac{Kc^2\beta}{2c_p} TL_y k_B h_w \frac{e^{-(x-ct)^2/L_x^2}}{(2k_B x)^{1/2}} \frac{\theta^2}{\theta^2 + (\mu/k_B)^2}$$

$$\cdot [1 + e^{-(k_B cT/4)^2(\theta^2 - 2k_w/k_B)^2}] \, \mathrm{Re}\{\frac{e^{-y^2/\xi_1^2} e^{i\Phi}}{\xi_1}\} \quad (6.7\text{-}13)$$

where the phase Φ is defined earlier in Eq. (6.2-24).

One may note from the above that the time averages of $(\Delta p)^2$ and p^2 are in the ratio

$$\frac{<(\Delta p)^2>_{av}}{<p^2>_{av}} = [\text{Factor of order of unity}]\,(h_w k_B)^2\,(z/x)^2 \qquad (6.7\text{-}14)$$

Since this is independent of the water wave frequency and wavelength, one may infer that one can replace

$$h_w^2 \rightarrow <\eta^2> \qquad (6.7\text{-}15)$$

where $<\eta^2>$ is the mean-squared water wave height.

Although $h_w k_B$, which is 2π times the ratio of water wave height to an acoustic wavelength, is not necessarily small, the water wave fluctuating height effect on the acoustic signal will be small if

$$(h_w k_B)^2\,(\mu/k_B)^2 = (h_w \mu)^2 << 1 \qquad (6.7\text{-}16)$$

This is because the value of θ for which p achieves its maximum is μ/k_B. This criterion, that $h_w\mu$ be small, states that the penetration depth $1/\mu$ of the laser beam into the water should be much larger than the rms water wave height. This criterion confirms to the notion that small changes in the length or portion of an antenna should not have substantial effects on its radiation. Consequently, one would expect such a criterion to also apply for more complicated models. The rms height of the water waves places an upper limit on the absorption coefficient μ of the laser radiation that can be used to generate sound.

If one simultaneously applies the criterion (6.7-16) in conjunction with that mentioned previously, of the slope being small compared with μ/k_B, then one has

$$1/h_w k_B >> \mu/k_B >> h_w k_w \qquad (6.7\text{-}16a)$$

or

$$1/(k_B h_w k_w) >> 1/\mu >> h_w \qquad (6.7\text{-}16b)$$

These two criteria are compatible provided

$$h_w k_w << (k_w/k_B)^{1/2} \simeq (c/c_w)^{1/2} \tag{6.7-17}$$

where c_w is the speed of the water wave. Since the sound speed is much larger than the water wave speed, there is reason to believe that an appropriate value for μ exists.

CHAPTER VII

CONCLUSIONS AND RECOMMENDATIONS

7.1 Conclusions

The studies reported in this thesis lead to a number of conclusions.

The analysis in Chapter II shows that the linear acoustic equations with the heat source term included have an energy corollary in which the acoustic energy added per unit time and volume can be explicitly identified in terms of acoustic variables, thermodynamic quantities, and the heat q added to the fluid per unit time and volume. In particular, this acoustic energy source term contains the product of the acoustic pressure p and q. This fact allows a constructive method of thinking about how one might add laser-produced heat to a fluid to efficiently generate sound. In particular, it demonstrates that there may be merit in placing the heat within the fluid in such a way that a traveling pressure disturbance is continually pumped in amplitude.

A previously unpublished formula for the energy transduction efficiency for the special case of a stationary modulated laser beam normally incident on water is derived in Chapter II and this shows that, in such cases the greatest efficiency, for a given modulation frequency, is obtained when ka is small and μ/k is of the order of 0.5. This maximized efficiency is proportional to laser power and the square of the frequency of the acoustic disturbance. Although this result is derived with the assumption that ka is small, the fact that an earlier published derivation for large ka yields a lower efficiency leads to the tentative conclusion that the peak efficiency derived here is as high as one can expect for the case of a stationary modulated laser beam. In fact, the detailed calculations presented in later chapters of the thesis suggest that one cannot substantially exceed the peak efficiency predicted in Chapter II. This is implied, for example, by Fig. 5.12. On the other hand, the aggregate results

and analyses in the present thesis show that one can simultaneously achieve comparable efficiencies and yet produce sound beams that have controllable radiation properties by exploiting the acoustic pumping principle.

The analysis contained in Chapter III shows that one can make meaningful estimates of some principal features of the sound produced by moving laser-induced heating configurations with a relatively simple two-dimensional model. The model in turn confirms that one should in principle be able to place heat into a fluid in such a manner that the pumping principle is exploited. In particular, the dependence of the generated pressure wave amplitude demonstrates that the sound field may have a sensitive dependence on (i) the angle θ_B in which one desires the sound to be beamed, (ii) the angle θ_S that the entering light beams make with the vertical, and (iii) the ratio μ/k_B of the absorption coefficient of light to the acoustic wave number. In particular, the sound amplitude is very sensitive to the deviation of θ_S from θ_B when μ/k_B is much less than one but not especially sensitive to this deviation when μ/k_B is of the order of unity or larger. The acoustic amplitude does increase with decreasing μ/k_B when θ_S equals θ_B (which could be the situation for largest pressure amplitude) but there is very little change when μ/k_B decreases below the value of $2\sin\theta_B$. Thus, for beaming obliquely downwards at moderate angles with the horizontal, one need not place great importance on the value of μ for the laser light, provided $1/\mu$ is of the order of the desired acoustic wavelength or greater. Choosing the laser such that μ/k_B is small could have an adverse effect because then the acoustic amplitude is much more sensitive to deviations of θ_S from θ_B. This analysis, however, is not necessarily applicable when the angle θ_B is small, although results derived using other models in other chapters suggest that the analysis based on the simple two-dimensional model can apply in many circumstances for the pressure amplitude in the center of the beam when the angle θ_B is less than 1°.

The analysis in Chapter IV demonstrates that it is possible to obtain a relatively simple asymptotic analytical solution for the generated sound field, both in

the Fresnel region and at ranges further out, for a less idealized three-dimensional model for the moving heating configuration. Versions of this solution are obtainable using Green's function and complex variable techniques for both the limiting cases of the heat deposition width L_y being very small or large compared with an acoustic wavelength. The latter solution has a near field resembling the plane wave solution found in Chapter III, but also shows how diffraction tends to broaden the sound beam and eventually, at large ranges, lead to spherical spreading. Thus one can predict the eventual farfield radiation pattern of the acoustic field.

Although the exact limitations on the analytical theory of Chapter IV are unwieldy to succinctly describe, some criteria are given in Chapter V that confirm that the analytical results are valid for circumstances discussed in the thesis. Also, direct numerical evaluation of the triple integral solution of the inhomogeneous equation substantiates that the analytical results have a wide domain of applicability. This is indicated by the comparisons shown in a number of figures in Chapter V. The analytical theory consequently allows one to make refined statements (improving and substantiating those of Chapter III) concerning the feasibility of beaming sound to distances of the order of a kilometer or more. In particular, one can estimate what requirements should be placed on laser power, laser pulse energy, or laser pulse duration to generate easily detectable signals at a given fixed range, taking into account the ambient noise in the ocean and the absorption of sound with propagation distance. The results indicate that such is possible up to ranges of as much as 5 km with existing laser systems.

The model of the heating configuration used in the development of the results of Chapters IV and V has certain intrinsic idealizations including Gaussian envelope shapes and constant heating configuration velocity over the surface. Also the analytical theory did not apply when the configuration sweep velocity was very close to the speed of sound, such that the value of θ_B is zero. The development in Chapter VI, however, allows one to conclude that analytical theories that apply for less

restricted circumstances are not difficult to derive. In particular, the analytical results of Chapter IV are shown to have viable interpretations in terms of the parabolic equation and geometrical acoustics. With this recognition, one can develop a model that applies when the envelope functions are not Gaussian. Also, the geometrical acoustics model applied to the case when the configuration velocity varies with position shows that one can control the angular beamwidth of the generated far field sound pattern with choices for the initial and final velocities during a sweep. This removes the inherent dependence on diffraction effects for the broadening of the beam and should be of significance when designing systems for communicating or interrogating targets whose positions are imprecisely known.

The model developed for near surface propagation using the parabolic equation assuming a laser-induced heat deposition of finite duration yields further insight concerning the applications of the pumping principle. In the asymptotic limit of large propagation range, the resulting sound pulse is an unsymmetrically shaped beam that is tilted obliquely downwards, with an angular width of the order of μ/k_B in radians. The peak acoustic amplitude in this beam at a given farfield range tends to be proportional to the total heat energy deposited by the laser and therefore to depend on laser power and pulse duration only through their product. Also, although the shape of the beam is affected by the value of μ, the peak sound amplitude tends to be independent of μ in the limit of small μ. Thus, one is again led to the conclusion that there is relatively no advantage to using lasers that generate light with extremely small μ.

Although the effect of water waves are only briefly considered in this thesis, the analysis in the latter part of Chapter VI leads one to the tentative conclusion that the rms height of the water waves may be an important parameter to consider when designing laser induced sound systems that make use of spatially extended moving heating configurations. In particular, the analysis suggests that the value of $1/\mu$ should substantially exceed the greatest expected rms water wave height and that

μ/k_B should exceed the rms water-wave induced surface slope. The method of analysis does not tell one, however, over what range, if any, of wavelengths of the water waves should these requirements be imposed.

7.2 Recommendations for Further Study

The present thesis is entirely analytical, so all of the new concepts and analytical results presented here are as yet unconfirmed by experiment. While the basic physical principles that have used in the development here are certainly well established, there is always some possibility that one has not considered all the relevant physics. One needs experiments to check whether the implementation of some of the basic ideas advanced in this thesis is feasible. Also, one needs to learn whether the considered approximations apply for those situations that can be measured in a laboratory setting. As a start, one should attempt experiments with a laser beam split into several parallel beams by a diffraction grating, all of which are simultaneously reflected by a rotating mirror onto a water surface. This could be an extension of the types of experiments that were reported by Berthelot (1985) in his Ph. D. thesis. The mirror could also be curved in such a manner that the split beam would broaden in the transverse direction (which is referred to as the y direction in the present thesis). Also, curving of the mirror could cause the laser beam to travel along the surface at a decelerating velocity.

Additional analytical work could be done to merge the two analytical models developed here for the cases of zero θ_B and finite θ_B into one which is uniformly valid at large propagation ranges. The analysis in Chapter VI suggests that such is highly feasible although possibly intricate. Such a development was omitted in the present thesis because it would have unduly lengthened the presentation and would have postponed the reporting of the present results.

The effect of water waves on system performance still is largely unanswered. The analysis in Chapter VI is only cursory; a thorough analysis must take into

account the random character of the water waves and use techniques of stochastic processes. In addition to theoretical work on this problem, it would seem that much can be learned by laboratory experiments in which carefully controlled water waves are generated during the generation of underwater sound.

The optical design of systems that achieve heating configurations such as assumed to be possible in the present thesis is another area that should be given detailed study. One should seek to learn what factors affect the achievement of such a configuration and seek novel optical methods that might be employed. A thorough feasibility study should be followed by a fabrication of a possible operational system with laboratory tests.

APPENDIX

SOURCE CODE FOR EVALUATION OF TRIPLE INTEGRAL

The following listing is in VAX FORTRAN and has been used on a VAX/11 750 minicomputer with VMS operating system. The program evaluates the triple integral given by Eq. (4.1-8) in the text.

```
      PROGRAM NUMERICAL_INTEGRATION
      REAL LX,Ly,Kx,KB,MUe,MU,LAMDAB,LAMDAZ,ANS(20)
      COMMON XL,YL,ZL,c,Kx,V,Lx,Ly,CAPT,MUe,time,THETAB

      PI = 3.14159265
***********************************************
*  INPUT TEMPERATURE AND PROPERTIES OF WATER  **
***********************************************
      TEMP   = 20.
      BETA   = (16.3 + .81*(TEMP-10.))*1E-5
      Cp     = 3988. + .54*(TEMP-10.)
      c      = 1490. + 3.6*(TEMP-10.)

************************************************
**  INPUT:                                    **
**    FREQ -- frequency (Hz)                  **
**  ANGLEB -- oblique beaming angle (deg)     **
**    NEFF -- number of cycles                **
**      MU -- 1/"penetration depth" (per meter) **
**      Ly -- configuration half-width (meter)  **
**    CAPT -- laser pulse half-duration (sec)   **
************************************************
      FREQ = 10000.
      ANGLEB = 20.
      NEFF = 10
      MU = 13.7
      Ly = 6.
      CAPT = .0108
***************************************
**  OR USE:                          **
**      Lw = 6.                      **
**      CAPT = Lw / c / TAN(THETAB)  **
***************************************

      THETAB = ANGLEB * PI / 180.
      V = c / COS(THETAB)
      MUe = MU / COS(THETAB)
      LAMDAB = c / FREQ
      KB = 2. * PI / LAMDAB
      Kx = KB * COS(THETAB)
      Lx = PI * NEFF / Kx

****************************
**  Enter LASER POWER     **
****************************
      POWER  = 1.
      CONST = (MUe*POWER/Lx/Ly/PI) * (BETA/4./PI/Cp)

*****************************************************
**  Input NUMBER OF POINTS per cycle in x, y,      **
**  and z directions                               **
*****************************************************
      NXPECYC = 4
      NYPECYC = 2
      NZPECYC = 4

******************************
**  Determining NX and NZ   **
******************************
      IF (THETAB .NE. 0.) THEN
```

```
        LAMDAZ = 2.*PI/(KB*SIN(THETAB))
        ZRATIO = (1./MUe)/LAMDAZ
        NZ = NZPECYC*ZRATIO
      ENDIF

      IF (NZ.LT.4) NZ = 4
      VT = V * CAPT
      RATIO = VT/Lx
      NX = 2. * FLOAT(NEFF) * (1.+RATIO) * NXPECYC
      XA = -2.*(1.+RATIO)
      XB = 2.*(1.+RATIO)
      IF (NX .GT. 20000) THEN
         PRINT*,'NX = ',NX,'SORRY, TOO MANY POINTS'
         STOP
      ENDIF

************************************************************
**************    CHOICE I:  for Ly >> Lamda  **************
************************************************************
**  input LOCATION (XL,YL,ZL) of the listener               **
************************************************************
      READ*,SL
      READ*,THETA
      READ*,YL
      XL = SL * COS(THETA)
      ZL = SL * SIN(THETA)

************************
**  Determining NY    **
************************
      RY = SQRT(SL*SL + 4.*Ly*Ly)
      YRATIO = (RY-SL)/LAMDAB
      NY = NYPECYC*YRATIO
      IF (NY.LT.4) NY = 4

************************************************************
**************   CHOICE II:  for Ly << Lamda  **************
************************************************************
**  Input LOCATION (RL,THETA,PHI) of the listener           **
************************************************************
*      READ*,RL                                            *
*      READ*,PHI                                           *
*      THETA = THETAB                                      *
*      XL    = RL * COS(THETA)                             *
*      YL    = RL * SIN(THETA) * SIN(PHI)                  *
*      ZL    = RL * SIN(THETA) * COS(PHI)                  *
*      NY    = 4                                           *
************************************************************

************************************************************
**  Searching PEAK PRESSURE AMPLITUDE                       **
**  Calculating pressure values within a one-half peak-cycle**
************************************************************
      Tcenter = RL/c
      PERIOD = 1./FREQ
      TA = Tcenter - .25*PERIOD
      TB = Tcenter + .25*PERIOD
      TDEL = (TB-TA)/10.
      PRESMAX = 0.
```

```
      DO 500 I= 1, 11
      IF (I .GT. 3) THEN
         ST1 = ABS(ANS(I-3))
         ST2 = ABS(ANS(I-2))
         ST3 = ABS(ANS(I-1))
         CALL FINDMAX(ST1, ST2, ST3, VALUE, PRESMAX)
         IF (ABS(VALUE).LE.1 .AND. PRESMAX.GE.ST2) THEN
           GO TO 1000
         ENDIF
      ENDIF
      time = TA + (I-1)*TDEL
      CALL QUADRAT (NX, NY, NZ, XA, XB, -2., 2., 0., 4., ANS(I))
      ANS(I) = 2. * ABS(ANS(I)) * CONST
  500 CONTINUE
 1000 CONTINUE
      WRITE(17,*)PRESMAX
      PRINT*,CHAR(7)

      STOP
      END

*****************************************************************
***  Numerical intergration using a 21-point scheme          ***
*****************************************************************
      SUBROUTINE QUADRAT (NX,NY,NZ,XA,XB,YA,YB,ZA,ZB,ANS)
      REAL Lx,Ly,Kx,KB,MUe,MU
      COMMON XL,YL,ZL,c,Kx,V,Lx,Ly,CAPT,MUe,time,THETAB

      X2H = (XB-XA)/FLOAT(NX)
      Y2H = (YB-YA)/FLOAT(NY)
      Z2H = (ZB-ZA)/FLOAT(NZ)
      XH = X2H/2.
      YH = Y2H/2.
      ZH = Z2H/2.
      XHF = X2H/4.
      YHF = Y2H/4.
      ZHF = Z2H/4.

****************** SUM VERTICE ********************
************************************************
** SUM VERTICE AT VERTICE
      SUMVV = F(XA,YA,ZA) + F(XA,YA,ZB) + F(XA,YB,ZA) + F(XA,YB,ZB)
     !      + F(XB,YA,ZA) + F(XB,YA,ZB) + F(XB,YB,ZA) + F(XB,YB,ZB)
** SUM VERTICE ON EDGE
      SUMVE = 0.
      DO 210 I = 1, NX-1
      X = XA + I*X2H
  210 SUMVE = SUMVE + F(X,YA,ZA) + F(X,YA,ZB) + F(X,YB,ZA) + F(X,YB,ZB)
      DO 211 J = 1, NY-1
      Y = YA + J*Y2H
  211 SUMVE = SUMVE + F(XA,Y,ZA) + F(XA,Y,ZB) + F(XB,Y,ZA) + F(XB,Y,ZB)
      DO 212 K = 1, NZ-1
      Z = ZA + K*Z2H
  212 SUMVE = SUMVE + F(XA,YA,Z) + F(XA,YB,Z) + F(XB,YA,Z) + F(XB,YB,Z)
** SUM VERTICE ON FACE
      SUMVF = 0.
      DO 220 I = 1, NX-1
      DO 220 J = 1, NY-1
      X = XA + I*X2H
      Y = YA + J*Y2H
```

```
  220 SUMVF = SUMVF + F(X,Y,ZA) + F(X,Y,ZB)
      DO 221 I = 1, NX-1
      DO 221 K = 1, NZ-1
      X = XA + I*X2H
      Z = ZA + K*Z2H
  221 SUMVF = SUMVF + F(X,YA,Z) + F(X,YB,Z)
      DO 222 J = 1, NY-1
      DO 222 K = 1, NZ-1
      Y = YA + J*Y2H
      Z = ZA + K*Z2H
  222 SUMVF = SUMVF + F(XA,Y,Z) + F(XB,Y,Z)
** SUM VERTICE OF INTERIOR **
      SUMVI = 0.
      DO 230 I = 1, NX-1
      DO 230 J = 1, NY-1
      DO 230 K = 1, NZ-1
      X = XA + I*X2H
      Y = YA + J*Y2H
      Z = ZA + K*Z2H
  230 SUMVI = SUMVI + F(X,Y,Z)
      SUMV = SUMVV + 2.*SUMVE + 4.*SUMVF + 8.*SUMVI

***************** SUM FACE ******************
*********************************************
** SUM FACE ON FACE **
      SUMFF = 0.
      DO 240 I = 1, NX
      DO 240 J = 1, NY
      X = XA + XH + (I-1)*X2H
      Y = YA + YH + (J-1)*Y2H
  240 SUMFF = SUMFF + F(X,Y,ZA) - F(X,Y,ZB)
      DO 241 I = 1, NX
      DO 241 K = 1, NZ
      X = XA + XH + (I-1)*X2H
      Z = ZA + ZH + (K-1)*Z2H
  241 SUMFF = SUMFF + F(X,YA,Z) - F(X,YB,Z)
      DO 242 J = 1, NY
      DO 242 K = 1, NZ
      Y = YA + YH + (J-1)*Y2H
      Z = ZA + ZH + (K-1)*Z2H
  242 SUMFF = SUMFF + F(XA,Y,Z) - F(XB,Y,Z)
** SUM FACE OF INTERIOR **
      SUMFI = 0.
      DO 250 I = 1, NX
      DO 250 J = 1, NY
      DO 250 K = 1, NZ
      X = XA + XH + (I-1)*X2H
      Y = YA + YH + (J-1)*Y2H
      Z = ZA + ZH + (K-1)*Z2H
  250 SUMFI = SUMFI + F(X+XH,Y,Z) + F(X,Y+YH,Z) + F(X,Y,Z+ZH)
      SUMF = SUMFF + 2.*SUMFI
***************** SUM INTERIOR ******************
*************************************************
** SUM INTERIOR POINTS IN A CUBE **
      SUMIC = 0.
      SUMIH = 0.
      DO 260 I = 1, NX
      DO 260 J = 1, NY
      DO 260 K = 1, NZ
      X = XA + XH + (I-1)*X2H
```

```
      Y = YA + YH + (J-1)*Y2H
      Z = ZA + ZH + (K-1)*Z2H
      SUMIC = SUMIC + F(X,Y,Z)
  260 SUMIH = SUMIH + F(X,Y,Z-ZHF) + F(X,Y,Z+ZHF) + F(X,Y-YHF,Z)
     !              + F(X,Y+YHF,Z) + F(X-XHF,Y,Z) + F(X+XHF,Y,Z)

      SUM = 5.*SUMV + 8.*SUMF + 128.*SUMIH - 496.*SUMIC
      XH  = XH*Lx
      YH  = YH*Ly
      ZH  = ZH/MUe
      ANS = (8.*XH*YH*ZH) * SUM/360.
      RETURN
      END

*********************************************************************
** Subroutine to find peak value using a quadratic curve fitting **
** F1, F2, and F3 are three ordinate values difined at three     **
** equally-spaced abscissa values. If |XX| < 1, peak lies within **
** domain defined by abscissa values; iteration is completed.    **
*********************************************************************
      SUBROUTINE FINDMAX(F1, F2, F3, XX, FMAX)
      AA = .5*F3 + .5*F1 - F2
      BB = .5*(F3 - F1)
      CC = F2
      XX = -BB/2./AA
      FMAX = AA*XX**2 + BB*XX + CC
      RETURN
      END

*********************************************************************
** Subroutine defining HEATING CONFIGURATION, dq(x,y,z,t)/dt **
*********************************************************************
      FUNCTION F(XOS, YOS, ZOS)
      REAL NP,NM
      REAL Lx,Ly,Kx,KB,MUe,MU
      COMMON XL,YL,ZL,c,Kx,V,Lx,Ly,CAPT,MUe,time,THETAB
      XO = XOS * Lx
      YO = YOS * Ly
      ZO = ZOS / MUe
      RP = SQRT ((XL-XO)**2 + (YL-YO)**2 + (ZL-ZO)**2)
      RM = SQRT ((XL-XO)**2 + (YL-YO)**2 + (ZL+ZO)**2)
      TRETP = time - RP/c
      TRETM = time - RM/c
      NP = XO + ZO*TAN(THETAB) - V*TRETP
      NM = XO + ZO*TAN(THETAB) - V*TRETM
      AKXNP = Kx * NP
      AKXNM = Kx * NM
      FACP = Kx*V*SIN(AKXNP)
     !       + 2.*(1.+COS(AKXNP))*(V*NP/Lx**2-TRETP/CAPT**2)
      FACM = Kx*V*SIN(AKXNM)
     !       + 2.*(1.+COS(AKXNM))*(V*NM/Lx**2-TRETM/CAPT**2)
      EXPONP = -ZOS -YOS**2 - (NP/Lx)**2 -(TRETP/CAPT)**2
      EXPONM = -ZOS -YOS**2 - (NM/Lx)**2 -(TRETM/CAPT)**2
*********************************************************************
********  Alternate HEATING CONFIGURATION, q(x,y,z,t)  ********
*********************************************************************
*      TBARP = TRETP/CAPT                                           *
*      TBARM = TRETM/CAPT                                           *
*      IF (TRETP.GT.0) THEN                                         *
*      FACP = Kx*V*SIN(AKXNP)*(.406+.406*TBARP)                     *
```

```
*     |  +(1.+COS(AKXNP)) * (-(.813+1.219*TBARP)/CAPT+          *
*     |   2.*V*NP/Lx**2*(.406+.406*TBARP))                      *
*      ELSE                                                     *
*      FACP = 0.                                                *
*      ENDIF                                                    *
*      IF (TRETM.GT.0) THEN                                     *
*      FACM = Kx*V*SIN(AKXNM)*(.406+.406*TBARM)                 *
*     |  +(1.+COS(AKXNM)) * (-(.813+1.219*TBARM)/CAPT+          *
*     |   2.*V*NM/Lx**2*(.406+.406*TBARM))                      *
*      ELSE                                                     *
*      FACM = 0.                                                *
*      ENDIF                                                    *
*      EXPONP = -ZOS -YOS**2 - (NP/Lx)**2 -TBARP*3.             *
*      EXPONM = -ZOS -YOS**2 - (NM/Lx)**2 -TBARM*3.             *
*************************************************************
      IF (EXPONP .LT. -30.) THEN
         TERMP = 0.
      ELSE
        TERMP = FACP*EXP(EXPONP)/RP
      ENDIF
      IF (EXPONM .LT. -30.) THEN
         TERMM = 0.
      ELSE
         TERMM = FACM*EXP(EXPONM)/RM
      ENDIF
      F = TERMP - TERMM
      RETURN
      END
*************************************************************
*-------------------------  THE END  -------------------------*
*************************************************************
```

REFERENCES

M. Abramowitz and I. A. StegunHandbood of Mathematical Functions, Chap. 25, 895, Dover publications, Inc., New York, (1972).

AIP (American Institute of Physics) Handbook, 3rd ed., edited by D. E. Gray, McGraw-Hill Book Co., (1972).

G. A. Askar'yan, A. M. Prokhorov, G. F. Chanturiya, and G. P. Shipulo, "The Effects of a Laser Beam in a Liquid," JETP (USSR) **44**, 2180-2182, June, (1963) [Sov. Physics JETP **17**(6), 1463-1465, Dec., (1963)].

M. Bath, Mathematical Aspects of Seismology, Elservier Publishing Co., New York, (1968).

A. G. Bell, "On the Production and Reproduction of Sound by Light," Proc. Amer. Assoc. Advan. Sci. 29, 115-136 (1881); "Upon the Production of Sound by Radiant Energy," Phil. Mag. (5)**11**, 510-528 (1881).

C. M. Bender and S. A. Orszag, Advanced Mathematical Methods for Scientists and Engineers , Chap. 6, McGraw Hill Co., New York, (1978).

Y. H. Berthelot, "Generation of Underwater Sound by a Moving High-Power Laser Source," Doctoral Thesis, The University of Texas, Austin, Texas, (1985).

Y. H. Berthelot and I. J. Busch-Vishniac, "Laser-Induced Thermoacoustic Radiation," J. Acoust. Soc. of Am. **78**(6), 2074-2082, Dec., (1985).

Y. H. Berthelot and I. J. Busch-Vishniac, "Thermoacoustic Radiation of Sound by a Moving Laser Source," submitted to J. Acoust. Soc. Am., (1987a).

Y. H. Berthelot and I. J. Busch-Vishniac, "The Doppler Shift of an Acoustic Source Moving at Transonic Velocity," submitted to J. Acoust. Soc. Am., (1987b).

N. Bleistein and R. A. Handelsman, Asymptotic Expansions of Intrgrals, Holt, Rinehart, and Winston, (1975).

N. Bleistein, Mathematical Methods for Wave Phenomena, Academic Press, Inc., (1984).

M. Born and E. Wolf, Principles of Optics, 6th ed., Pergamon Press, 13-14 or 125, (1980).

R. Bullough and J. J. Gilman, "Elastic Explosion in Solids Caused by Radiation," J. Appl. Physics **37**(6), 2283-2287, (1966).

A. I. Bozhkov and F. V. Bunkin, "Generation of Sound in a Liquid as a Result of Absorption of Modulated Laser Radiation," Kvantovaya Elektronika (Moscow) **2**, 1763-1776, Aug., (1975) [Sov. J. Quant. Elect. **5**(8), 956-964, (1975)].

A. I. Bozhkov, F. V. Bunkin, and L. L. Gyrdev, "Influence of Perturbation of the Surface of a Liquid on the Acoustic Field Excited in the Liquid by Q-Switched Laser Radiation," Kvantovaya Elektronika (Moscow) **3**, 1494-1500, July, (1976) [Sov. J. Quant. Elect. **6**(7), 809-8112, July, (1976)].

A. I. Bozhkov, F. V. Bunkin, and Al. A. Kolomenskii, "Investigation of the Acoustic

Field (Focusing) of a Supersonic Optoacoustic Antenna," Kvant. Elekt. (Moscow) **4**, 942-943, Apr., (1977) [Sov. J. Quant. Elect. **7**(4), 536-537, Apr., (1977)].

A. I. Bozhkov, F. V. Bunkin, and Al. A. Kolomenskii, "Optoacoustic Sound Generation with Finite Tracks," Pis'ma v Zh. Tekh. Fiz. **4**, 1283-1286, 12 Nov., (1978) [Sov. Tech. Phys. Lett. **4**(11), 516-517, Nov., (1978)].

A. I. Bozhkov, F. V. Bunkin, and Al. A. Kolomenskii, "Doppler Thermooptical Source of Ultrasound," Akust. Zh. **25**, 786-788, Sept.-Oct., (1979) [Sov. Phys. Acoust. **25**(5), 443-445, Sept.-Oct., (1979)].

A. I. Bozhkov, F. V. Bunkin, and V. V. Savranskii, "Generation of Sound in a Liquid by Irradiating Its Surface with a Modulated Laser," Pis'ma Zh. Tekh. Fiz. **1**, 435-439,(1975) [Sov. Tech. Phys. Lett. **1**(5), 203-204, (1975)].

A. I. Bozhkov and L. L. Gyrdev, "Statistical Characteristic of a Floating Optoacoustic Antenna," Kvantovaya Elektronika (Moscow) **5**, 1019-1027, May, (1978) [Sov. J. Quant. Elect. **8**(5), 583-588, May, (1978)].

A. I. Bozhkov and Al. A. Kolomenskii, "Acoustic Field of an Optoacoustic Antenna Moving at Subsonic or Supersonic Velocity," Kvant. Elekt. (Moscow) **5**, 2577-2586, Dec., (1978) [Sov. J. Quant. Elect. **8**(12), 1449-1454, Dec., (1978)].

F. V. Bunkin, N. V. Karlov, V. M. Komissarov, and G. P. Kuz'min, "Excitation of Sound when a Surface Layer of a Liquid Absorbs a Laser Pulse," ZhETF Pis. Red.**13**(9), 479-483 [JETP Lett. **13**, 341-343, (1971)].

F. V. Bunkin and V. M. Komissarov, "Optical Excitation of Sound Waves," Akust. Zh. **19**, 305-320, May-June, (1973) [Sov. Phys. Acoust. **19**(3), 203-211, Nov.-Dec., (1973)].

F. V. Bunkin, A. I. Malyarovskii, V. G. Mikhalevich, and G. P. Shipulo, "Experimental Investigation of the Acoustic Field of a Moving Optoacoustic Antenna," Kvantovaya Elektronika (Moscow) **5**, 457-459, Feb., (1978) [Sov. J. Quant. Elect. **8**(2), 270-271, Feb., (1978)].

F. V. Bunkin, A. I. Malyarovskii, and V. G. Mikhalevich, "Experimental Study of Pulsed Sound Fields Excited by Moving Laser Thermooptical Sources," Akust. Zh. **27**, 179-186, Mar.-Apr., (1981) [Sov. Phys. Acoust. **27**(2), 98-102, Mar.-Apr.,(1981)].

L. V. Burmistrova, A. A. Karabutov, A. I. Portnyagin, O. V. Rudenko, and E. B. Cherepetskaya, "Method of Transfer Functions in Problems of Thermooptical Sound Generation," Akust. Zh. **24**, 655-663, Sept.-Oct., (1978) [Sov. Phys. Acoust. **24**(5), 369-374, Sept.-Oct., (1978)].

E. F. Carome, N. A. Clark, and C. E. Moeller, "Generation of Acoustic Signals in Liquids by Ruby Laser-Induced Thermal Stress Transients," Appl. Phys. Lett. **4**(6), 95-97, Mar., (1964).

G. F. Carrier, M. Krook, and C. E. Pearson, Functions of a Complex Variable, McGraw-Hill, New York, (1966).

H. S. Carslaw and J. C. Jaeger, Conduction of Heat in Solids, 2nd ed., Oxford at the Clarendon Press, (1959).

B. T. Chu, "Pressure Waves Generated by Addition of Heat in a Gaseous Medium," NACA Technical Note 3411, Washington, June, (1955).

C. S. Clay, and H. Medwin, Acoustical Oceanography, John wiley and Sons, New York, (1977).

N. G. DeBruijn, Asymptotic Methods in Analysis, Chap. 5,, Dover Pub., Inc., New York, (1981).

T. A. Dunina, S. V. Egerev, L. M. Lyamshev, and K. A. Naugol'nykh, "Near Field of a Pulsed Thermoacoustic Array," Akust. Zh. **25**, 60-64, Jan.-Feb., (1979a) [Sov. Phys. Acoust. **25**(1), 32-34, Jan.-Feb., (1979a)].

T. A. Dunina, S. V. Egerev, L. M. Lyamshev, and K. A. Naugol'nykh, "Thermooptical Excitation of Sound by Nanosecond Laser Pulses," Pis'ma v Zh. Tekh. Fiz. **5**, 986-989, 26 Aug., (1979b) [Sov. Tech. Phys. Lett. **5**(8), 411-412, Aug., (1979b)].

S. V. Egerev, I. B. Esipov, L. M. Lysmahev, and K. A. Naugol'nykh, "Sound Generation by Long Laser Pulses," Akust. Zh. **25**, 220-226, Mar.-Apr., (1979) [Sov. Phys. Acoust. **25**(2), 119-122, Mar.-Apr., (1979)].

D. H. Ezrow, "Measurement of the Thermal-Noise Spectrum of Water," J. Acoust. Soc. Am. **34**, 550-554, (1962).

F. H. Fisher and V. P. Simmons, "Sound Absorption in Sea Water," J. Acoust. Soc. Am. **62**, 558-564, (1977).

A. Freedman, "Sound Field of a Rectangular Piston," J. Acoust. Soc. Am. **32**, 197-209,(1960).

V. S. Gorodetskii, S. V. Egerev, I. B. Esipov, and K. A. Naugol'nykh, "Generation of Sound by Laser Pulses," Kvantovaya Elektronika (Moscow) **5**, 2396-2401, Nov., (1978) [Sov. J. Quant. Elect. **8**(11), 1345-1347, Nov., (1978)].

L. S. Gournay, "Conversion of Electromagnetic to Acoustic Energy by Surface Heating," J. Acoust. Soc. Am. **40**(6), 1322-1330, June, (1966).

H. A. Hsieh and A. D. Pierce, "Some Possible Novel Configurations for Optico-Acoustic Transducer Arrays Created by Controlled Motion of Laser Beams across Water Surfaces," J. Acoust. Soc. Am. Suppl. 1 **75**, S16, Spring, (1984a).

H. A. Hsieh and A. D. Pierce, "Transduction Efficiency for Sound Waves Systematically Pumped by Controlled Motion of Laser Beams across Water Surfaces," J. Acoust. Soc. Am. Suppl. 1 **76**, S23-S24, Fall, (1984b).

H. A. Hsieh and A. D. Pierce, "Asymptotic Analysis of Diffraction Effects in the Radiation of Underwater Sound by Interesting Configurations of Laser-Generated Heat Deposition," J. Acoust. Soc. Am. Suppl. 1 **78**, S27, Fall, (1985).

H. A. Hsieh and A. D. Pierce, "Fresnel Zone Radiation of Underwater Sound Created by Transient Moving Spatially Modulated Patterns of Laser-Generated Heat Deposition," J. Acoust. Soc. Am. Suppl. 1 **79**, S84, Spring, (1986).

C. L. Hu, "Spherical Model of an Acoustical Wave Generated by Rapid Laser

Heating in a Liquid," J. Acoust. Soc. Am. **46**(3(II)), 728-736, Oct., (1968).

S. D. Hunter, W. V. Jones, and D. J. Malbrough, "Nonthermal Acoustic Signals from a Cylinderical Laser Beam in Water," J. Acoustic Soc. Am. **69**(6), 1563-1567, (1981).

S. D. Hunter, W. V. Jones, D. J. Malbrough, A. L. Van Buren, A. Liboff, T. Bowen, J. J. Jones, J. G. Learned, H. Bradner, L. Pfeffer, R. March, and U. Camerini, "Acoustic Signals of Nonthermal Origin from High Energy Protons in Water," J. Acoust. Soc. Am. **69**(6), 1557-1562, (1981).

U. Ingard, "Acoustics," in Handbook of Phvsics, edited by E. U. Condon and H. Odishaw, Chap. 8, McGraw-Hill, New York, (1958).

J. D. Jackson, Classical Electrodynamics, 2nd ed., John Wiley and Sons, New York, 290-292, (1965).

S. G. Kasoev, M. G. Lisovskaya, L. M. Lyamshev, and L. V. Sedov, "Laser Generation of Sound in a Fluid Half-Space with Two Types of Boundary Roughness," Akust. Zh. **25**, 401-407, May-June, (1979) [Sov. Phys. Acoust. **25**(3), 228-231, May-June, (1979)].

S. G. Kasoev and L. M. Lyamshev, "Sound Generation by the Absorption of Modulated Laser Radiation in a Fluid Half-Space with Large-Scale Irregularities of the Boundary," Akust. Zh. **23**, 265-272, Mar.-Apr., (1977a) [Sov. Phys. Acoust. **23**(2), 149-153, Mar.-Apr., (1977a)].

S. G. Kasoev and L. M. Lyamshev, "Theory of Laser-Pulse Generation of Sound in a Liquid," Akust. Zh. **23**, 890-898, Nov.-Dec., (1977b) [Sov. Phys. Acoust. **23**(6), 510-514, Nov.-Dec., (1977b)].

S. G. Kasoev and L. M. Lyamshev, "Sound Generation in a Liquid by Laser Pulses of Arbitrary Shape," Akust. Zh. **24**, 534-539, July-Aug., (1978) [Sov. Phys. Acoust. **24**(4), 302-305, July-Aug., (1978)].

Laser Focus/Electro-Optics Buyers' Guide, 21st ed., PennWell Publishing Company, Massachusett, (1986).

L. M. Lyamshev, "Optoacoustic Sources of Sound," Akust. Zh. **24**, 637-669, (1981) [Sov. Phys. Acoust. **24**(12), 977-995. (1981)].

L. M. Lyamshev, V. G. Mikhalevich, and G. P. Shipulo, "Thermal Excitation of Acoustic Waves in Absorbing Media by a Periodic Sequence of Short Laser Pulses," Akust. Zh. **25**, 146-148, Jan.-Feb., (1979) [Sov. Phys. Acoust. **25**(1), 80-81, Jan.-Feb., (1979)].

L. M. Lyamshev, V. G. Mikhalevich, and G. P. Shipulo, "Thermooptical Excitation of Acoustic Fields in a Liquid by a Periodic Train of Laser Pulses," Akust. Zh. **26**, 230-236, Mar.-Apr., (1980) [Sov. Phys. Acoust. **26**(2), 126-130, Mar.-Apr., (1980)].

L. M. Lyamshev and K. A. Naugol'nykh, "Sound Generation by Thermal Sources," Akust. Zh. **22**, 625-627, July-Aug., (1976) [Sov. Phys. Acoust. **22**(4), 354-355, July-Aug., (1976)].

L. M. Lyamshev and K. A. Naugol'nykh, "Optical Generation of Sound: Nonlinear Effects (Review)" Akust. Zh. **27**, 641-668, Sept.-Oct., (1981) [Sov. Phys. Acoust.

27(5), 357-371, Sept.-Oct., (1981)].

L. M. Lyamshev and L. V. Sedov, "Theory of Sound Generation by Absorption of Intensity-Modulated Laser Radiation in a Fluid Half-Space with Irregular Boundary," Akust. Zh. **23**, 411-419, May-June, (1977a) [Sov. Phys. Acoust. **23**(3), 229-233, May-June, (1977a)].

L. M. Lyamshev and L. V. Sedov, "Theory of Sound Generation by Absorption of Intensity-Modulated Laser Radiation in a Fluid Half-Space with Irregular Boundary," Akust. Zh. **23**, 411-419, May-June, (1977b) [Sov. Phys. Acoust. **23**(3), 229-233, May-June, (1977b)].

L. M. Lyamshev and L. V. Sedov, "Excitation of Sound by a Moving Opticoacoustic Source which Emits Pulses of Arbitrary Shape," Pis'ma v Zh. Tekh. Fiz. **5**, 970-972, 26 Aug., (1979a) [Sov. Tech. Phys. Lett. **5**(8), 403-404, Aug., (1979a)].

L. M. Lyamshev and L. V. Sedov, "Generation of Sound by a Moving Pulsed Optoacoustic Source," Akust. Zh. **25**, 906-915, Nov.-Dec., (1979b) [Sov. Phys. Acoust. **25**(6), 510-514, Nov.-Dec., (1979b)].

L. M. Lyamshev and L. V. Sedov, "Optical Generation of Sound in a Liquid: Thermal Mechanism (Review)," Akust. Zh. **27**, 5-29, Jan.-Feb., (1981) [Sov. Phys. Acoust. **27**(1), 4-18, Jan.-Feb., (1981)].

J. Mathews and R. L. Walker, Mathematical Methods of Physics, W. A. Benjamin, Inc., New York, (1965).

R. W. Mellen, "The Thermal-Noise Limit in the Detection of Underwater Sound Signals," J. Acoust. Soc. Am. **24**, 478-480, (1952).

T. G. Muir, C. R. Culbertson, and J. R. Clynch, "Experiments on Thermoacoustic Arrays with Laser Excitation," J. Acous. Soc. Am. **59**(4), 735-743, Apr., (1976).

J. P. Mutschlecner, D. K. Burge, and E. Regelson, "Sea Water Attenuation Measurements with a Ruby Laser," Appl. Opt. **2**(11), 1202-1203, Nov., (1963).

C. B. Officer, Introduction to the Theory of Sound Transmission, McGraw Hill, (1958).

A. D. Pierce, J. W. Posey, and E. F. Iliff, "Variation of Nuclear Explosion Generated Acoustic-Gravity Waveforms with Burst Height and with Energy Yield," J. Geophys. Res. **76**, 5025-5042, (1971).

A. D. Pierce, Acoustics : An Introduction to Its Physical Principles and Applications, 1st ed., McGraw-Hill, (1981).

A. D. Pierce, "Waveform Shape near Mach Cone Arrival for the Pressure Perturbation Created by a Modulated Laser Beam Moving over a Water Surface at Supersonic Speed," J. Acoust. Soc. Am. Suppl. 1 **71**, S13, (1982a).

A. D. Pierce, "Nonlinear Thermoacoustics and Electrostriction Explanations of Acoustic Signatures in 4°C Water Caused by Laser Pulses and Proton Beams," J. Acoust. Soc. Am. Suppl. 1 **72**, S13, (1982b).

A. D. Pierce, "Underwater Sound Pulse Generated by a Highly Attenuating Laser Beam Moving over the Surface," J. Acoust. Soc. Am. Suppl. 1 **73**, S68-69, (1983a).

A. D. Pierce, "Irreversible Thermodynamics Formulation of Multiple Relaxation Processes, with Application to Laser-Generated Sound in 4°C Water," J. Acoust. Soc. Am. Suppl. 1 **73**, S50, (1983b).

A. D. Pierce, "Energy Partitioning and Optical-to-Acoustic Conversion Efficiency during Laser Generation of Underwater Sound," J. Acoust. Soc. Am. Suppl. 1 **74**, S78, Fall (1983c).

A. D. Pierce, "The Inhomogeneous Wave Equation of Thermoacoustics," Unsteady Fluid Motion, edited by G. E. A., Meier, and F., Obermeier, 92-100, Springer-Verlag, Berlin, (1985).

A. D. Pierce and H. A. Hsieh, "Multi-Dimensional Acoustic Transients Created by Laser Beams Moving over Water Surfaces at Supersonic Speeds," Multi-Dimensional Fluid Transients, edited by M. H. Chaudhry and C. S. Martin, 69-75, American Society of Mechanical Engineers, New York, (1984).

A. D. Pierce and H. A. Hsieh, "Radiation of Sound Induced by Laser Beams Incident on Water Surfaces: A Tutorial Survey of the World Literature," J. Acoust. Soc. Am. Suppl. 1 **77**, S103, Spring, (1985a).

A. D. Pierce and H. A. Hsieh, "Achievement of Substantially Higher Source Levels for Airborne-Laser-Induced Underwater Sound," J. Acoust. Soc. Am. Suppl. 1 **77**, S104, Spring, (1985b).

A. D. Pierce and H. A. Hsieh, "Underwater Soundbeams Created by Airborne Laser Systems," ICA Congress Symposium on Underwater Acoustics, Halifax, Nova Scotia, Canada, July, (1986).

A. D. Pierce and H. A. Hsieh, "Structural Relaxation and Irreversible Thermodynamics Theory of Laser Pulse Generation of Sound in 4°C Water," J. Acoust. Soc. of Am., (under revision).

A. A. Putnam and W. R. Dennis, "A Study of Burner Oscillations of the Organ-pipe," Trans. ASME **75**, 15-28, Jan. (1953).

W. C. Roentgen, "On Tones Produced by the Intermittent Irradiation of a Gas," Philosophical Magazine, S. 5, **11**(68), 308-311, Apr. (1881).

W. C. Strahle, "On Combustion Generated Noise," J. of Fluid Mechanics **49**, 399-414, Sept., (1971).

A. C. Tam, "Photoacoustics: Spectroscopy and other applications," in Ultrasensitive Laser Spectroscopy, edited by Kliger D. S., Chap. 1, Academic Press, New York, (1983).

F. D. Tappert, "The Parabolic Approximation Method," Wave Propagation and Underwater Acoustics, Edited by J. B. Keller and J. S. Papadakis, 224-287, Springer-Verlag, (1977).

I. Tolstoy and C. S. Clay, Ocean Acoustics, McGraw-Hill Book Co., New York, (1966).

J. Tyndall, "Action of an Intermittent Beam of Radiant Heat upon Gaseous Matter," Proc. Royal Soc. of London, **31**, 307-317, (1881).

P. J. Westervelt and R. S. Larson, "Laser-Excited Broadside Array," J. Acoust. Soc.

Am. **54**(1), 121-122, July, (1973).

V. M. Zolotarev, B. A. Mikhailov, L. I. Alperovich, and S. I. Popov, "Dispersion and Absorption of Liquid Water in the Infrared and Radio Regions of the Spectrum," Opt. Spectrosc. **27**, 430-433, (1969).

VITA

Hsiao-An Hsieh was born on April 25, 1961 in Taipei, Taiwan, the son of Professor and Mrs. Yun-Fei Hsieh. In 1967 the Hsieh family moved to Singapore. After Mr. Hsieh had finished his elementary and high school education, he came to the United States in August 1978 to attend Louisiana State University. He majored in mechanical engineering and graduated in June 1981. After graduation, he continued with graduate study at Louisiana State University. Six months later, he transferred to the School of Mechanical Engineering at the Georgia Institute of Technology, where he received the degree of Master of Science in Mechanical Engineering. His MS thesis work was in conduction heat transfer and was carried out under the supervision of Professor William Z. Black. He enrolled in the doctoral program at Georgia Tech in January 1984 and initiated research on the generation of sound by lasers. On August 19, 1984, Hsiao-an Hsieh married Wei Du, who was also born in Taiwan and who is presently a doctoral student in statistics at the University of Georgia. With the completion of this thesis, Dr. Hsieh will be employed as an acoustical engineer by the Digital Equipment Corporation in Maynard, Massachusetts.